CANADIAN THESES ON MICROFICHE

THÈSES CANADIENNES SUR MICROFICHE

National Library of Canada
Collections Development Branch

Canadian Theses on
Microfiche Service

Ottawa, Canada
K1A 0N4

Bibliothèque nationale du Canada
Direction du développement des collections

Service des thèses canadiennes
sur microfiche

NOTICE

The quality of this microfiche is heavily dependent upon the quality of the original thesis submitted for microfilming. Every effort has been made to ensure the highest quality of reproduction possible.

If pages are missing, contact the university which granted the degree.

Some pages may have indistinct print especially if the original pages were typed with a poor typewriter ribbon or if the university sent us an inferior photocopy.

Previously copyrighted materials (journal articles, published tests, etc.) are not filmed.

Reproduction in full or in part of this film is governed by the Canadian Copyright Act, R.S.C. 1970, c. C-30. Please read the authorization forms which accompany this thesis.

AVIS

La qualité de cette microfiche dépend grandement de la qualité de la thèse soumise au microfilmage. Nous avons tout fait pour assurer une qualité supérieure de reproduction.

S'il manque des pages, veuillez communiquer avec l'université qui a conféré le grade.

La qualité d'impression de certaines pages peut laisser à désirer, surtout si les pages originales ont été dactylographiées à l'aide d'un ruban usé ou si l'université nous a fait parvenir une photocopie de qualité inférieure.

Les documents qui font déjà l'objet d'un droit d'auteur (articles de revue, examens publiés, etc.) ne sont pas microfilmés.

La reproduction, même partielle, de ce microfilm est soumise à la Loi canadienne sur le droit d'auteur, SRC 1970, c. C-30. Veuillez prendre connaissance des formules d'autorisation qui accompagnent cette thèse.

THIS DISSERTATION
HAS BEEN MICROFILMED
EXACTLY AS RECEIVED

LA THÈSE A ÉTÉ
MICROFILMÉE TELLE QUE
NOUS L'AVONS REÇUE

Canada

NL 339 (r. 85/09)

National Library of Canada
Bibliothèque nationale du Canada

Ottawa, Canada
K1A 0N4

139

TC –

ISBN 0-315-21333-7

CANADIAN THESES ON MICROFICHE SERVICE – SERVICE DES THÈSES CANADIENNES SUR MICROFICHE

PERMISION TO MICROFILM – AUTORISATION DE MICROFILMER

• Please print or type – Écrire en lettres moulées ou dactylographier

AUTHOR – AUTEUR

Full Name of Author – Nom complet de l'auteur

BARRY BARA

Date of Birth – Date de naissance

Nov 2 1959

Canadian Citizen – Citoyen canadien

☑ Yes / Oui ☐ No / Non

Country of Birth – Lieu de naissance

CANADA

Permanent Address – Résidence fixe

Box 716
LEDUC, ALBERTA
T9E 2Y4

THESIS – THÈSE

Title of Thesis – Titre de la thèse

Water Channel - Simulation of Concentration Fluctuations from a Ground Level Source

Degree for which thesis was presented
Grade pour lequel cette thèse fut présentée

M.Sc

Year this degree conferred
Année d'obtention de ce grade

Spring 1985

University – Université

University of Alberta

Name of Supervisor – Nom du directeur de thèse

D.J. Wilson

AUTHORIZATION – AUTORISATION

Permission is hereby granted to the NATIONAL LIBRARY OF CANADA to **microfilm** this thesis and to **lend** or **sell copies of the film.**

The author reserves other publication rights, and neither the thesis nor extensive extracts from it may be printed or otherwise reproduced without the author's written permission.

L'autorisation est, par la présente, accordée à la BIBLIOTHÈQUE NATIONALE DU CANADA de **microfilmer** cette thèse et de **prêter** ou de **vendre des exemplaires du film.**

L'auteur se réserve les autres droits de publication; ni la thèse ni de longs extraits de celle-ci ne doivent être imprimés ou autrement reproduits sans l'autorisation écrite de l'auteur.

ATTACH FORM TO THESIS – VEUILLEZ JOINDRE CE FORMULAIRE À LA THÈSE

Signature

Barry Bara

Date

April 22/85

Canada

THE UNIVERSITY OF ALBERTA

WATER CHANNEL SIMULATION OF CONCENTRATION FLUCTUATIONS FROM A GROUND LEVEL SOURCE

by

BARRY BARA

(C)

A THESIS

SUBMITTED TO THE FACULTY OF GRADUATE STUDIES AND RESEARCH

IN PARTIAL FULFILMENT OF THE REQUIREMENTS FOR THE DEGREE

OF MASTER OF SCIENCE

DEPARTMENT OF MECHANICAL ENGINEERING

EDMONTON, ALBERTA

SPRING 1985

THE UNIVERSITY OF ALBERTA

RELEASE FORM

NAME OF AUTHOR BARRY BARA

TITLE OF THESIS WATER CHANNEL SIMULATION OF CONCENTRATION FLUCTUATIONS FROM A GROUND LEVEL SOURCE

DEGREE FOR WHICH THESIS WAS PRESENTED MASTER OF SCIENCE

YEAR THIS DEGREE GRANTED SPRING 1985

Permission is hereby granted to THE UNIVERSITY OF ALBERTA LIBRARY to reproduce single copies of this thesis and to lend or sell such copies for private, scholarly or scientific research purposes only.

The author reserves other publication rights, and neither the thesis nor extensive extracts from it may be printed or otherwise reproduced without the author's written permission.

(SIGNED) ..Barry Bara.....

PERMANENT ADDRESS:

..Box 716.....

..LEDUC, ALBERTA.....

..T9E 2Y4.....

DATED ..APRIL 22.....1985

THE UNIVERSITY OF ALBERTA

FACULTY OF GRADUATE STUDIES AND RESEARCH

The undersigned certify that they have read, and recommend to the Faculty of Graduate Studies and Research, for acceptance, a thesis entitled WATER CHANNEL SIMULATION OF CONCENTRATION FLUCTUATIONS FROM A GROUND LEVEL SOURCE submitted by BARRY BARA in partial fulfilment of the requirements for the degree of MASTER OF SCIENCE.

.....

Supervisor

.....

.....

Date.....April 9, 1985.....

Dedicated to my parents

Abstract

A water channel model was used to simulate concentration fluctuations from a ground release in a neutrally stable atmospheric wind blowing over a forested terrain. Concentration fluctuations of a neutrally buoyant mixture of saltwater and alcohol were measured with a fast response conductivity detector developed for this study. The ability of the detector to follow rapidly varying concentrations was confirmed with an apparatus developed to measure the detector's frequency response.

A well behaved dispersion process was verified in the channel by comparing gradient diffusion theory to the measured mean concentration profiles and rates of plume growth. Also, considering the limitations of the water channel model, it simulates the mean concentration field of a neutrally stable atmosphere reasonably well. A disadvantage of the channel was that it could not simulate the very large scale atmospheric meandering effects in the crosswind direction.

Vertical and crosswind profiles of concentration variance, total fluctuation intensity, "conditional" variance and fluctuation intensity (i.e. "conditional" statistics exclude periods of zero concentration), and intermittency were measured in the water channel. Existing mathematical models for concentration fluctuations from a ground level source were compared to this new set of independent data. The models were adequate in describing

most of the crosswind and vertical profiles of the fluctuation statistics. However, a serious deficiency was detected in the models used to describe the conditional fluctuation intensity and intermittency measurements in the vertical direction.

Acknowledgements

The author wishes to thank Dr. D. J. Wilson for his encouragement, guidance and patience in seeing this thesis to its completion. Assistance in the form of research grants from Imperial Oil Ltd. and the Natural Sciences and Engineering Research Council (NSERC) to D. J. Wilson made this study possible. Thanks are also extended to the Department of Mechanical Engineering and NSERC for personal financial assistance while at the University of Alberta.

I would like to express my sincere gratitude to Brian Zelt who worked with me in setting up the laser doppler velocimeter and then continued on to take majority of the velocity measurements for this project. His enthusiasm and attention to detail in taking experimental data is very much appreciated. I am also grateful to Brian for his assistance in typing the first four chapters of this thesis.

Thanks are also due to Al Muir and his colleagues in the Mechanical Engineering machine shop for their excellent work in the fabrication of many devices for the experimental set up. I would like to express appreciation to Wayne Pittman for his invaluable assistance with the electronic devices used in this study. I am also grateful to the Mechanical Engineering technicians and fellow graduate students who provided assistance throughout this project.

Finally I would like to express a special thanks to some friends who gave generously of their time to assist me in the completion of my thesis. I am especially grateful to

Heather McIntosh who typed the last three chapters of the thesis. I would like to express my appreciation to Eddy Chui for the numerous errands he ran for me while I was at work and unable to get to the campus. Thanks is also extended to Deane Clark who assisted me in the final preparation of the figures.

Table of Contents

Chapter		Page
1.	INTRODUCTION	1
	1.1 Need to Study Concentration Fluctuations	1
	1.2 Concentration Fluctuations in the Atmosphere	2
	1.3 Purpose of a Water Channel Model	4
	1.4 Study Objectives	5
2.	SIMULATING THE ATMOSPHERIC WIND	7
	2.1 Introduction	7
	2.2 Water Channel System	7
	2.3 Velocity Measurements	10
	2.4 Generating Boundary Layer Profiles in the Water Channel	15
	2.5 u_*, Friction Velocity	25
3.	MODELING ATMOSPHERIC DISPERSION IN THE WATER CHANNEL	29
	3.1 Introduction	29
	3.2 Relation of Turbulence to Plume Spread	29
	3.3 Scaling Criteria	33
	3.4 Deficiences of Water Channel Model	34
	3.4.1 Absence of Low Frequency Turbulence in Model	35
	3.4.2 Absence of High Frequency Turbulence in Model	36
	3.4.3 Effect of Molecular Diffusion on Concentration Scales	39
	3.5 Turbulent Flow Structure in Water Channel	42
	3.6 Effect of Tracer Injection on Flow	50
	3.7 Effect of Source Size on Concentration Fluctuations	53

4. MEASUREMENT OF CONCENTRATION FLUCTUATIONS 56

4.1 Introduction 56

4.2 Design of the Conductivity Probe 56

4.3 Creating a Neutrally Buoyant Tracer 59

4.4 Static Calibration of Detector 62

4.5 Dynamic Calibration of Detector 64

4.6 Corrections for Probe Induced Signal Attenuation 73

4.7 Data Aquisition and Analysis Methods 80

4.7.1 Calculating Intermittency 81

5. MEAN CONCENTRATION FIELD 90

5.1 Introduction 90

5.2 Analytical Theory for Mean Concentration Field ..90

5.3 Mean Concentration Profiles in Water Channel and Atmosphere 92

5.4 Rates of Plume Growth in Water Channel 99

5.5 Summary 105

6. FLUCTUATING CONCENTRATION FIELD 106

6.1 Introduction 106

6.2 Crosswind Profiles of Concentration Variance and Total Fluctuation Intensity 108

6.3 Crosswind Profiles of Conditional Fluctuation Intensity and Intermittency 117

6.4 Vertical Profiles of Concentration Fluctuation Statistics 124

6.5 Deficiencies in Modeling Vertical Profiles of Conditional Fluctuation Intensity and Intermittency 134

6.6 Summary 139

7. CONCLUSIONS AND RECOMMENDATIONS 140

References 143

APPENDIX A: LDV System and Data Analysis Procedure 145

APPENDIX B: Measuring Water Velocity with a Pressure Transducer Operating With Air 150

APPENDIX C: Evaluation of Integral for the Ratio of Effective to True Variance 155

APPENDIX D: Measurements of Concentration Fluctuation Statistics at Various Downwind Distances 159

APPENDIX E: Derivation of an Expression for Conditional Fluctuation Intensity in Vertical Direction 168

List of Tables

Table		Page
3.1	Comparison of water channel boundary layer with full scale atmospheric data of Counihan (1975).	44
5.1	Measurement locations of concentration profiles in water channel.	94

List of Figures

Figure		Page
1.1	Typical concentration signal occurring in atmospheric dispersion.	3
2.1	Water channel system, left to right beside channel are: saline tracer supply tank, pressure regulator and rotameter, 1000 Hz low pass filter, fast response conductivity detector, Digital LSI 11/23 data aqusition system.	8
2.2	Schematic of water channel system used for concentration fluctuation measurements.	9
2.3	Comparison of velocity profiles measured on channel centerline with a pitot tube and laser-doppler velocimeter.	12
2.4	LDV system, left to right: 50mW HeNe laser with optics, forward-reverse control for traversing mechanism, T.S.I. tracker processor, direction controller and distance counter for traversing mechanism, Digital LSI 11/23 data aqusition system.	13
2.5	Schematic of LDV system used for measuring velocities in water channel (actual x-y beam crossing plane rotated 90° for illustration).	14
2.6	Measured velocity profiles, at 287.1cm from inlet of water channel, with and without castellated wall boundary trip.	17
2.7	Mean velocity profiles at various downstream distances from source location, x=0, showing fully developed flow.	19
2.8	Measured mean velocity profile across channel showing flow uniformity outside influence of wall boundary layer.	20
2.9	Log law boundary layer profile of equation (2=1) compared to measured mean velocity profile at x/H=9.7	21

Figure Page

2.10 Power law variation of equation (2-3) fitted to measured mean velocity profile at x/H=9.7 24

2.11 Uniformity of friction velocity, u_*, along water channel centerline. 26

2.12 Determination of friction velocity, u_*, and surface roughness, z_o. 27

3.1 Uniformity of vertical proflies of longitudinal turbulence intensity at varying downstream locations. 45

3.2 Vertical profile of longitudinal integral length scale showing scatter in two sets of independent measurements. 47

3.3 Longitudinal turbulence intensity measured across the water channel at z/H=0.5, showing negligible effect of channel sidewalls. 49

3.4 Longitudinal integral lenghth scale of turbulence measured across water channel at z/H=0.5, showing negligible sidewall influence. 51

3.5 Mean velocity profile measured at the injector location, with and without the injector, showing influence of injector on flow. 52

3.6 Effect of injector flow rate on turbulence intensity at 12.7cm, (20 injector diameters), downstream of injector. 54

4.1 Wedge shaped double electrode probe. 57

4.2 Probe immersed in channel for measurement. 57

4.3 Optimizing composition of tracer injection solution to produce a neutrally buoyant mixture. 61

4.4 Steady state calibration curve for conductivity detector showing linear range. 63

Figure Page

4.5 Test apparatus to measure dynamic response of conductivity probe. 67

4.6 Measured response of conductivity probe to a step change in concentration for a probe velocity of 18.0 cm/sec. 69

4.7 Probe response distance, ℓ_p, for varying probe flushing velocities. 72

4.8 Intermittent concentration signal measured in water channel illustrating method used to determine intermittency factor γ. 82

4.9 Signal with no intermittency illustrating continued existence of zeros of derivative. 85

4.10 Setting threshold values to eliminate effect of background noise. 86

4.11 Test of closure for threshold method for determining intermittency. 89

5.1 Normalized vertical profiles of mean concentration in water channel compared to equation (5-1). 95

5.2 Normalized crosswind mean concentration profiles measured above the ground surface compared to equation (5-2). 97

5.3 Normalized crosswind mean concentration profiles measured at ground surface compared to equation (5-2). 98

5.4 Vertical plume spread in water channel compared to Pasquill category C and D plume spreads. 101

5.5 Comparison of measured crosswind plume spread with equation (5-4). 104

6.1 Crosswind concentration variance profile measured at the ground surface at a downwind distance of x/H=3.97. 109

Figure Page

6.2 Crosswind total fluctuation intensity measured at the ground surface compared to equation (6-3). 113

6.3 Crosswind concentration variance profiles measured above the ground surface compared to equation (6-2). 114

6.4 Crosswind total fluctuation intensity measured above the ground surface compared to equation (6-3). 116

6.5 Crosswind conditional fluctuation intensity measured at the ground surface compared to Wilson's (1982) theory. 118

6.6 Crosswind conditional fluctuation intensity measured above the ground surface compared to Wilson's (1982) theory. 119

6.7 Crosswind intermittency measured at the ground surface compared to equation (6-4). 122

6.8 Crosswind intermittency measured above the ground surface compared to equation (6-4). 123

6.9 Vertical profiles of concentration variance measured at the water channel centerline compared to equation (6-6). 127

6.10 Vertical profiles of concentration variance near the ground surface on water channel centerline compared to equation (6-6). 129

6.11 Vertical profiles of total concentration fluctuation intensity measured at the water channel centerline compared to equation (6-7). 131

6.12 Vertical profile of concentration integral length scale measured at the water channel centerline. 133

Figure Page

6.13 Vertical profiles of conditional fluctuation intensity measured at the water channel centerline compared to equation (6-9). 136

6.14 Vertical profiles of concentration intermittency measured at the water channel centerline compared to equation (4-21) with equations (6-7) and (6-9) used to model I and I_p. 137

Nomenclature

a	exponent in crosswind standard deviation plume spread
a	exponent in vertical mean concentration profile
A	$\ln(2)$
A_{in}	sinusoidal input of amplitude A_{in}
A_{out}	sinusoidal output of amplitude A_{out}
A_1, A_2, A_3	coefficients in conductivity detector static calibration equation
b	exponent in vertical standard deviation plume spread
B	Lagrangian-Eulerian scale ratio
B_1	constant of proportionality
c	mean concentration
c_o	mean concentration at surface or channel centerline
c'	fluctuating concentration component
$\overline{c'^2}$	concentration variance
$\overline{c'^2}_{eff}$	variance measured with conductivity detector
$\overline{c'^2}_p$	conditional concentration variance
$\hat{c}^2$	maximum concentration variance in vertical direction
C	concentration of tracer(NaCl) g/ℓ
C_o	reference concentration(0.1g/ℓ NaCl)
D	molecular diffusion coefficient
E	detector output volts
E_{max}	steady state output in 50g/ℓ NaCl solution
E_o	detector output in C_o, 0.1g/ℓ NaCl solution

$E_c(0)$	value of concentration fluctuation energy spectrum at zero frequency
$E_c(f)$	fluctuating concentration energy spectrum
$E_{c,eff}(f)$	concentration fluctuation energy spectrum measured with conductivity detector
$E_u(0)$	value of longitudinal fluctuating velocity energy spectrum at zero frequency
f	frequency
G(f)	system gain
H	boundary layer thickness, 20cm
i	total concentration fluctuation intensity
i_o	centerline value of total concentration fluctuation intensity
i_p	conditional concentration fluctuation intensity
$i_{p\infty}$	conditional concentration fluctuation intensity with effect of surface removed
i_∞	total concentration fluctuation intensity with effect of surface removed
k	height of "Lego" roughness elements
k_s	sand grain roughness
K_y	crosswind eddy diffusivity of mass
K_z	vertical eddy diffusivity of mass
L_c	magnitude of smallest concentration scale existing due to molecular diffusion
n	exponent in power law mean velocity profile
q	combined strength of variance source pair
$R_c(t')$	autocorrelation of concentration fluctuations
Re_Λ	Reynolds number based on Λ_x and U_δ
s	complex variable
SF	geometric scale factor between atmosphere and water channel

t'	time
t'	time delay
T_c	integral time scale of concentration fluctuations
$T(s)$	system transfer function
T_u	integral time scale of longitudinal velocity fluctuations
u'	longitudinal fluctuating velocity component
$\overline{u'^2}$	longitudinal velocity variance
u_*	friction velocity
U	mean velocity
U	probe flushing velocity
U_c	mean convection velocity
U_δ	mean velocity at top of boundary layer
U_{ref}	reference velocity in power law mean velocity profile
v'	crosswind fluctuating velocity component
$\overline{v'^2}$	crosswind velocity variance
w'	vertical fluctuating velocity component
$\overline{w'^2}$	vertical velocity variance
x	downwind distance from source
y	distance from plume centerline
z	height above surface
z_o	log-law roughness length
z_{ref}	reference height in power law mean velocity profile
α	sink strength for concentration variance

β	location of variance sources
γ	intermittency factor
γ_o	plume centerline value of intermittency
$\Gamma(\ )$	gamma function
δ	boundary layer thickness
δ_y	plume half width in crosswind direction
δ_z	plume half width in vertical direction
η	Kolmogorov microscale
κ	von Karman's constant
Λ_c	integral length scale of concentration fluctuations
$\Lambda_{c,eff}$	integral length scale of concentration fluctuations measured with conductivity detector
Λ_u	integral length scale of longitudinal velocity fluctuations
Λ_v	integral length scale of crosswind velocity fluctuations
Λ_w	integral length scale of vertical velocity fluctuations
Λ_x	integral length scale of longitudinal velocity fluctuations
ℓ	average size of large scale concentration eddies
ℓ_p	probe response distance
ν	kinematic viscosity
π	constant, 3.1415...
σ_y	standard deviation of crosswind plume spread
σ_z	standard deviation of vertical plume spread
τ	conductivity detector time constant
ϕ_p	production of concentration variance

1. INTRODUCTION

1.1 Need to Study Concentration Fluctuations

The acceptable way of disposing of a pollutant in the atmosphere is to release it from an elevated source. This gives the pollutant a chance to disperse and reduce in concentration before it comes into contact with human life and vegetation at ground level. Proper design of an elevated source, taking into account the pollutant emission rate and different atmospheric weather conditions, can ensure that for the majority of the time, ground level concentrations will be kept below maximum acceptable standards. However, this is not the case with an accidental release of a toxic material, such as with a pipeline rupture or gas well blowout, where a high concentration of toxic gas is being emitted uncontrollably at ground level. The concentration levels occurring in the region near the ground can easily surpass maximum safe limits. In fact, fluctuating concentrations observed near the source can have peak values with the same concentration as the source itself. Therefore, determining if the mean concentration will be below some maximum safe level is not sufficient since there can be momentary occurrences when the concentration will be well above the safe limit. With concern for human life and vegetation, the question that immediately arises is what is the risk of momentarily exceeding some harmful level of toxic gas concentration at a given downwind location? Also,

for the case of designing a toxic gas pipeline installation, it is necessary to determine the probability of harmful exposure when deciding how far to locate the pipeline from human inhabitation. To enable one to access this type of risk, it is necessary to quantify the concentration fluctuations that will occur downwind of a ground level release. The scope of this study was to set up a scale model of the atmosphere in a water channel that was capable of simulating these concentration fluctuations.

1.2 Concentration Fluctuations in the Atmosphere

A typical concentration versus time signal that will occur for both ground level and elevated releases in the atmosphere is shown in Figure (1.1). This signal was measured at a receptor downwind of an elevated source emitting SO_2 in a neutrally stable atmospheric wind. The signal is intermittent in nature. The fraction of time that the plume is present at the receptor is termed the intermittency. The value of intermittency can range from 1.0 in the plume core, to very small values in the outer most edges of the plume.

Intermittency is mainly a result of large scale motions, larger than the scale of the plume, forcing the plume to meander back and forth past a fixed receptor. As the plume travels downstream and increases in size, the size of turbulent scales which cause intermittency also increase. On the other hand eddies smaller than the plume are

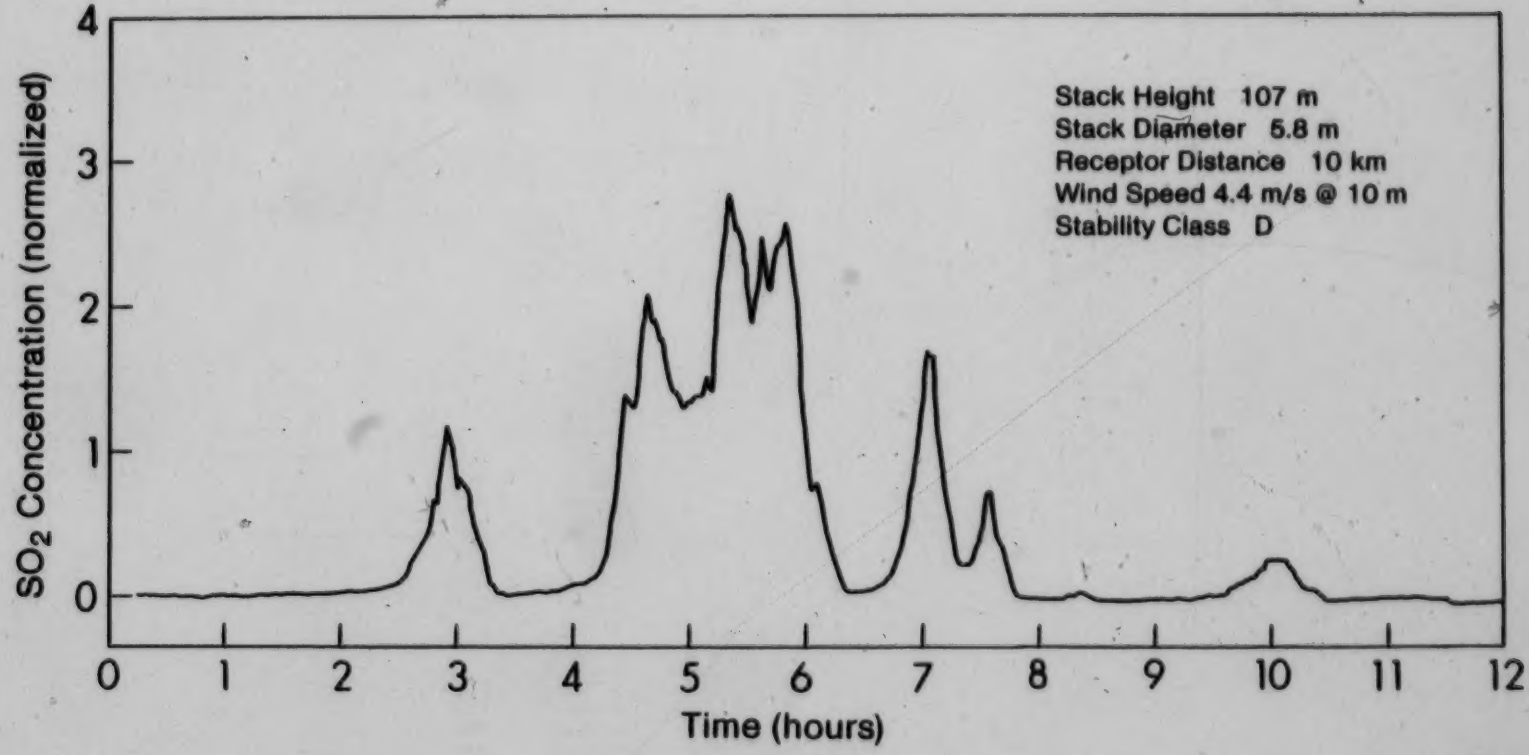

Figure 1.1 Typical concentration signal occuring in atmospheric dispersion from a point source.

responsible for the short duration fluctuations that are observed when the plume is present at the receptor. However short term periods of intermittency can also be observed when the plume is present at the receptor due to the clean ambient air that has been entrained into the plume.

1.3 Purpose of a Water Channel Model

A water channel model enables concentration fluctuation measurements to be made that would either be too expensive or difficult in the atmosphere. Ultimately what is required is experimental data that will be used to assist development and test mathematical models of boundary layer dispersion. Daily variations in atmospheric conditions and the time required for steady statistical values make it nearly impossible to collect enough data of high enough quality to be useful for mathematical model development. However, with events happening at an accelerated rate in the water channel and under the same controlled conditions, a large quantity of reliable data can be generated in short periods of time. This gives the model data the required precision to be useful for applying to boundary layer dispersion models.

The shortcomings of the water channel are that it can not simulate stabiltity effects, wind direction changes with height due to Coriolis forces or wind direction changes with time. It is only suitable for modeling a neutrally stable atmospheric wind which blows in a constant direction. Of course, this is not true of the atmosphere but for short

sampling times, on the order of minutes, the wind can be assumed to be unidirectional. Therefore, releases that last a short time and are not affected by large time scale effects of the atmosphere should be well representated by the water channel model.

Even though this model seems limited to a particular case, it can provide useful physical insight which can be used in the development of more complex mathematical dispersion models. Also, a simple water channel model can be very useful in determining what effect changing parameters, for example surface roughness or wind speed, will have on the dispersion process.

1.4 Study Objectives

The major objective of this study was to set up a water channel system that was capable of modeling concentration fluctuations from a ground level source. No particular full scale situation was to be simulated so, a model of a very fundamental nature was the goal. This being the case a neutrally buoyant passive point release was chosen as the ground level source conditions. The dispersion process was to be simulated in a neutrally stable atmospheric wind since the water channel flow is only capable of simulating neutrally stable conditions. Once the model had been set up to simulate the atmospheric wind, a primary objective was to measure both mean and fluctuating concentration to verify the model.

Because of the large compression of time scales in a small scale laboratory simulation, measuring concentration fluctuations requires a fast response detector which can follow the fluctuations of the tracer injected into the flow. Since an electrolytic solution was to be the tracer material, it was necessary to use a fast response conductivity detector. No such devices are commercially available, so another major objective of this study was to develop a device that had the required time response.

2. SIMULATING THE ATMOSPHERIC WIND

2.1 Introduction

An accurate simulation of the atmospheric wind in the water channel will ensure that a contaminant dispersing in the atmosphere will disperse in a similar manner in the water channel. Care must be taken to produce an accurate simulation to ensure that unusual or unexpected results which may occur are not just being caused by inadequate modeling techniques.

The objective in modeling the atmospheric wind in the water channel was to create a neutrally stable boundary layer flow without any concern for modeling a particular type of terrain. However, since the turbulent structure of a flow is the factor that controls the dispersion process, care was exercised to match the turbulence intensity and simulate the scales of turbulence typical of the neutrally stable atmospheric wind. By using a convenient flow depth and "Lego" base plate as surface roughness, a 3000:1 geometric scale model of a neutrally stable atmospheric wind blowing over a forested terrain was created.

2.2 Water Channel System

The water channel system used for simulating atmospheric dispersion from a ground level source is shown in Figure (2.1) with the components shown schematically in Figure (2.2). The water channel is a recirculating system

Figure 2.1 Water channel system, left to right beside channel are: saline tracer supply tank, pressure regulator and rotameter, 1000 Hz low pass filter, fast response conductivity detector, Digital LSI 11/23 data aqusition system.

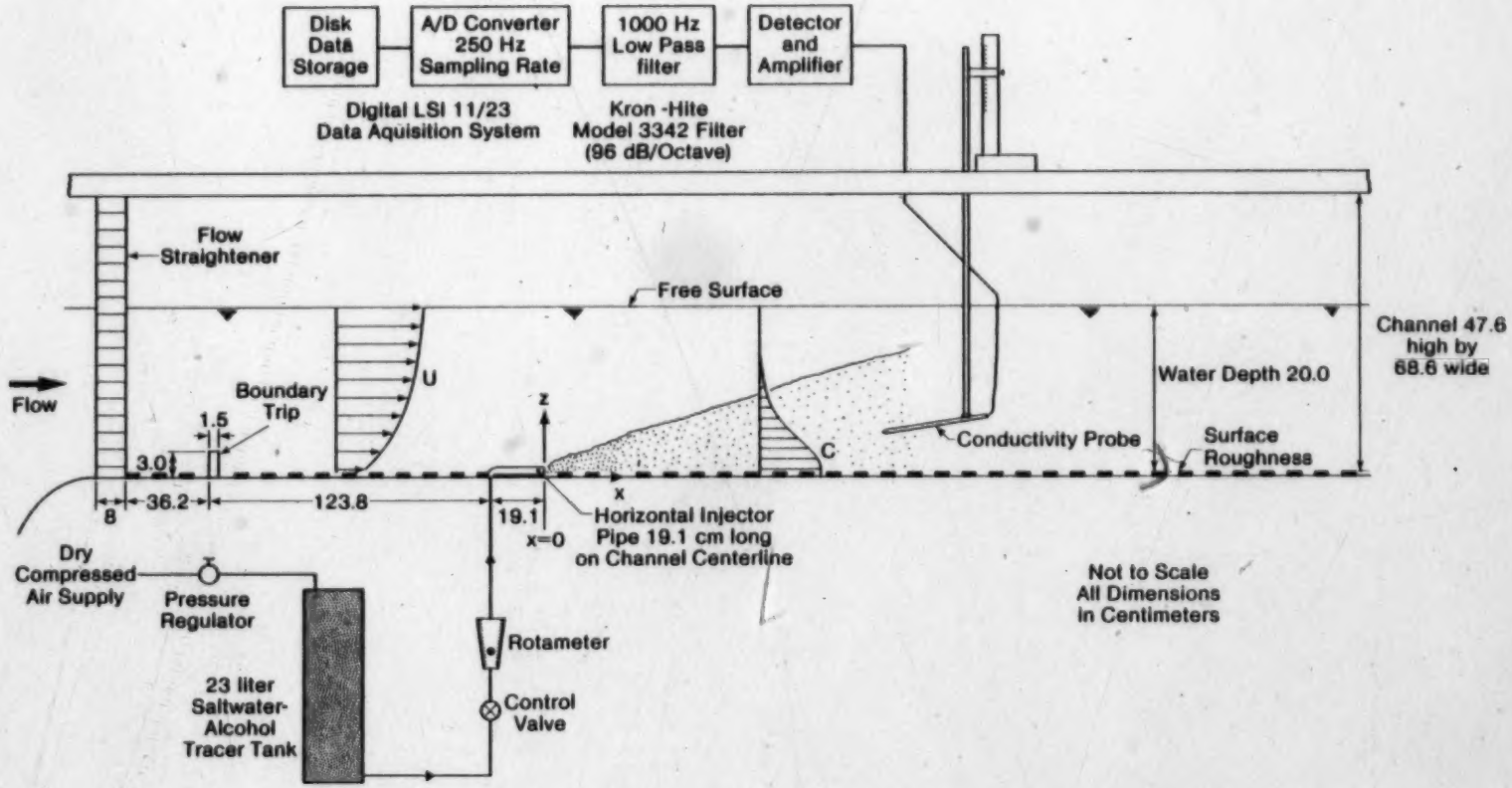

Figure 2.2 Schematic of water channel system used for concentration fluctuation measurements.

consisting of a 5m long channel 68.6cm wide and 47.6cm high connecting two reservoirs. The two centrifugal pumps which pump the water through the channel are capable of a maximum rate of 0.05 m^3/sec. In this study, the water channel pumps were run at maximum and the weir gate set to give a flow depth, H, of 20cm. Based on a typical atmospheric boundary layer thickness of 600m, as suggested by Counihan (1975), this resulted in a 3000:1 scale model.

A neutrally buoyant ground level release was simulated by placing a tube aligned with the flow at the bed of the channel centerline and releasing the tracer, a mixture of salt water and alcohol, passively into the flow. The flow of tracer from a pressurized tank was monitored with a rotameter to ensure a constant volume flow rate. A fast response conductivity detector, described in Chapter 4, was used to detect the tracer in the ambient flow. The concentration time signal from the detector was digitzed and stored on floppy disk. Saving the original concentration time series allowed for any type of analysis to be performed at a later date (details of the data collection methods are given in Chapter 4).

2.3 Velocity Measurements

The key to a successful simulation was to achieve the proper mean velocity profile in the water channel's 20cm depth, H. A laser doppler velocimeter(LDV), operated in backscatter with a 37.2cm focal length, was used to measure

the water channel velocity. Vertical profiles of velocity were measured at 6 different downstream distances from the source, 12.7cm, 100cm, 108cm, 194cm, 200cm and 300cm. Cross stream velocity profiles were measured at one downstream location from the source, 100cm, and at a height of 10cm above the channel surface.

The LDV system used for this study was a one component TSI(Thermo-Systems Inc.) helium-neon system operating in backscatter mode with a 50mW laser. These mean velocity measurements were compared to that of a Prandtl pitot static tube. The close agreement between the two methods is apparent in Figure (2.3) where the deviation was typically 1% or less. The largest deviation in the two methods occurs in the measurements near the bed of the water channel. This is to be expected since the pitot tube was being affected by the presence of a solid boundary and high turbulence levels while the LDV was unaffected.

A photograph of the LDV system is shown in Figure (2.4) and a schematic of the set up is shown in Figure (2.5). The laser was aligned with the plane of the beam crossing perpendicular to the flow and parallel to the bottom of the water channel. This allowed the longitudinal velocity component to be measured. The signal processing was done by a tracker processor which gives an analog output which can only be used for determining mean velocity. However with the use of a Digital LSI-11/23 mini computer, with an analog to digital converter, the tracker processor was made to act as

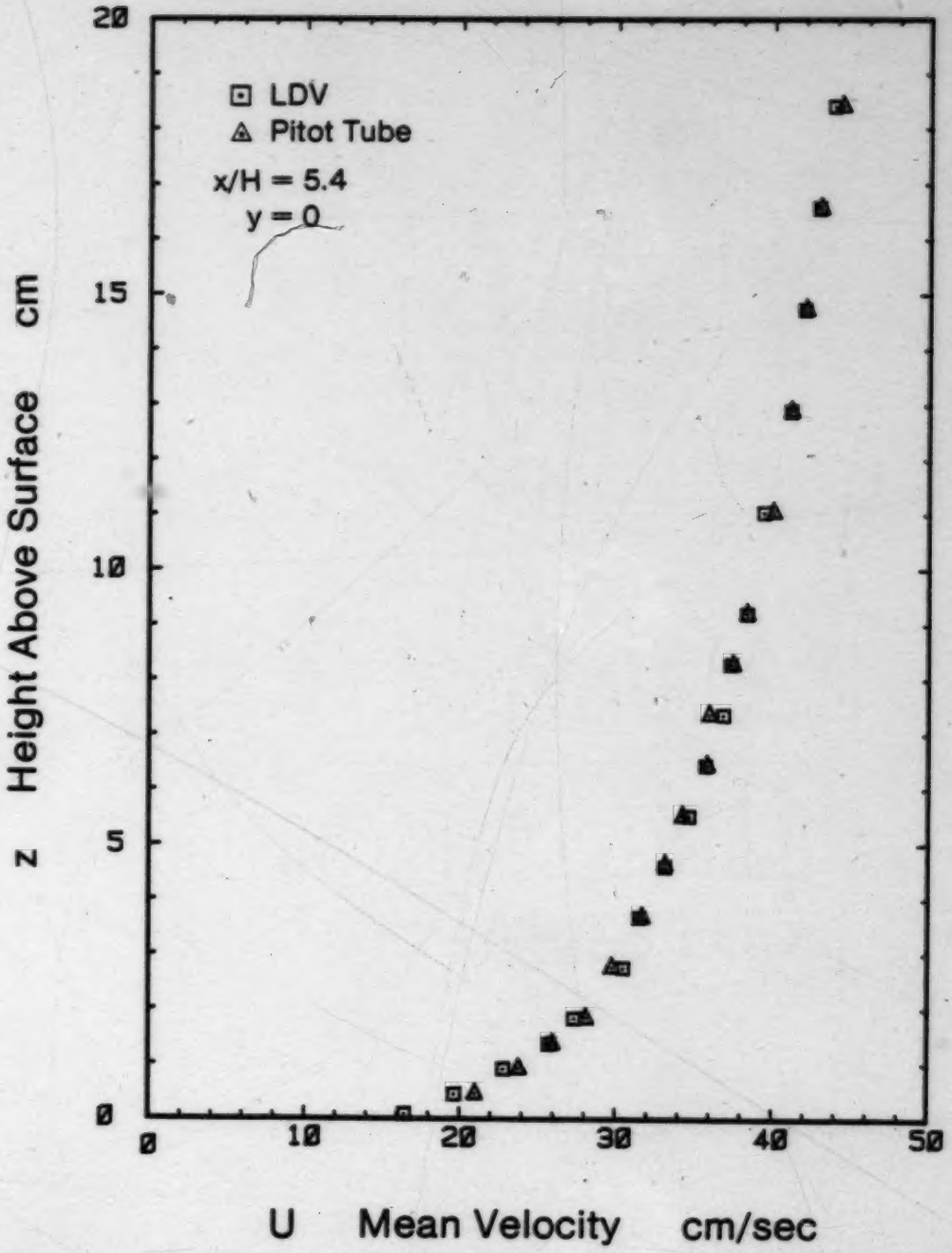

Figure 2.3 Comparison of velocity profiles measured on channel centerline with a pitot tube and laser-doppler velocimeter.

Figure 2.4 LDV system, left to right: 50mW HeNe laser with optics, forward-reverse control for traversing mechanism, T.S.I. tracker processor, direction controller and distance counter for traversing mechanism, Digital LSI 11/23 data aqusition system.

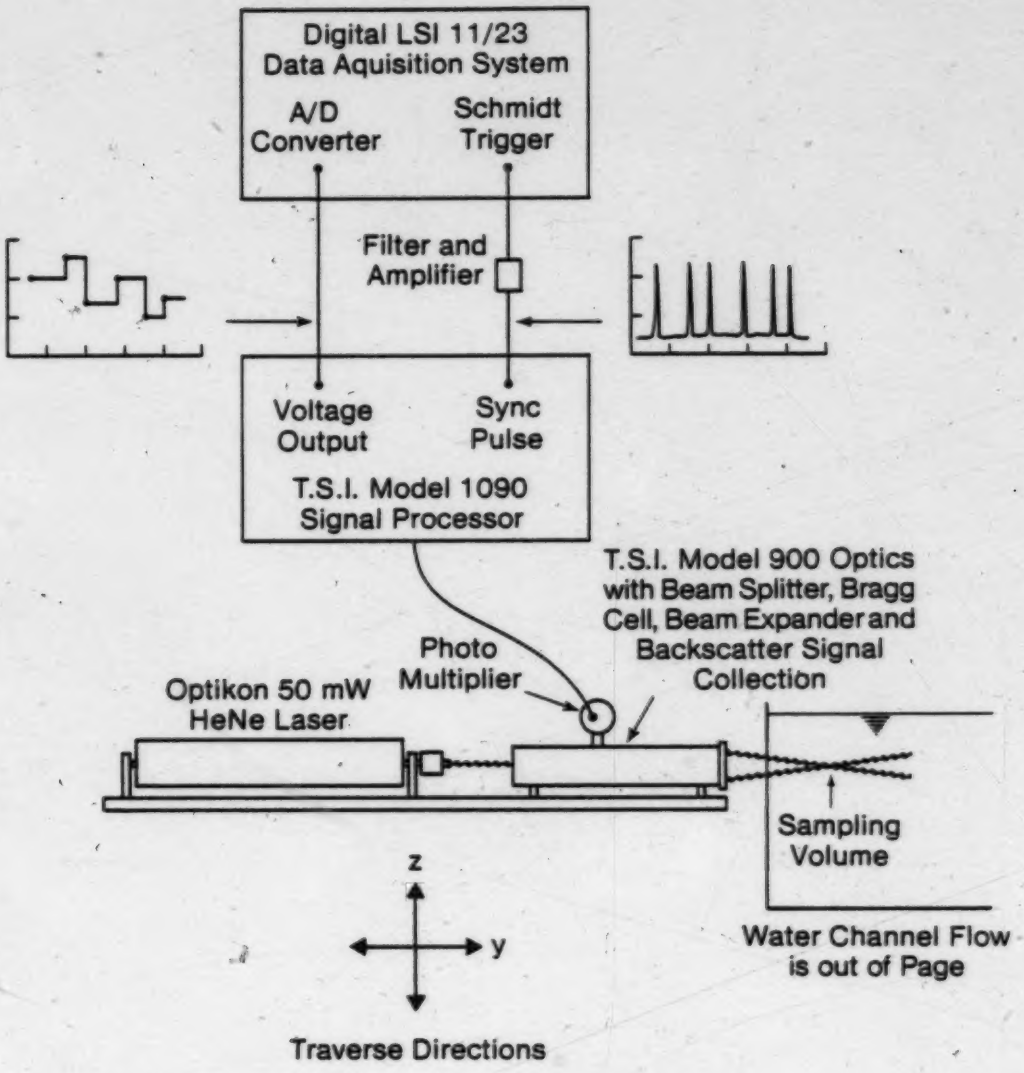

Figure 2.5 Schematic of LDV system used for measuring velocities in water channel (actual x-y beam crossing plane rotated 90° for illustration).

a counter processor (see Appendix A for details of the system and data processing). This allowed turbulence quantities to be measured and compared to the full scale atmosphere as a check on the simulation.

The pitot tube system used to measure mean velocities incorporated a pressure transducer operating in air to measure the dynamic head of the water. The advantages of operating the transducer with air instead of water are that air bubbles in the transducer are eliminated, and the transducer is protected from overpressuring. In order to operate the transducer with air, an isolation cell was used to seperate the pitot tube's water filled lines from the pressure transducer. The system functioned well, with only a 0.5% error in measuring the dynamic head caused by the compressibility of the air in the cell (see Appendix B for details of the system and correction factor to account for the compressibility of the air in the cell).

2.4 Generating Boundary Layer Profiles in the Water Channel

The main objective when setting up the water channel flow was to simulate a mean velocity profile in the vertical direction similar to that of a neutrally stable atmosphere. It was also desired to keep the flow uniform in the downstream and cross stream directions. With neutrally stable conditions in the atmosphere the mean velocity profile in the vertical direction follows a log-law variation

$$\frac{U}{u_*} = \frac{1}{\kappa} \ln \left(\frac{z}{z_0}\right) \qquad (2\text{-}1)$$

where

U = mean velocity

u_* = friction velocity

κ = von Karman's constant

z = height above datum plane

z_0 = roughness length.

As shown from dimensional arguments in Meteorology and Atomic Energy 1968 p. 72, the velocity profile of equation (2-1) is a result of fully developed rough-wall flow. Rough-wall flow, where the roughness elements protrude through the viscous sublayer, was achieved in the water channel by using "Lego" base plate as the surface roughness. Due to the 5m length of the water channel and the flow aspect ratio (68.7cm width and 20cm depth), a developing boundary layer flow was still present at the outlet of the water channel. Therefore a castellated wall boundary trip, with a height of 0.15 times the flow depth, was located 36.2cm downstream from the inlet of the water channel, to artificially thicken the developing boundary layer.

The effect of the boundary trip can be seen in Figure (2.6) which shows a velocity profile, at 287.1cm downstream of the channel inlet, with and without the boundary trip. As

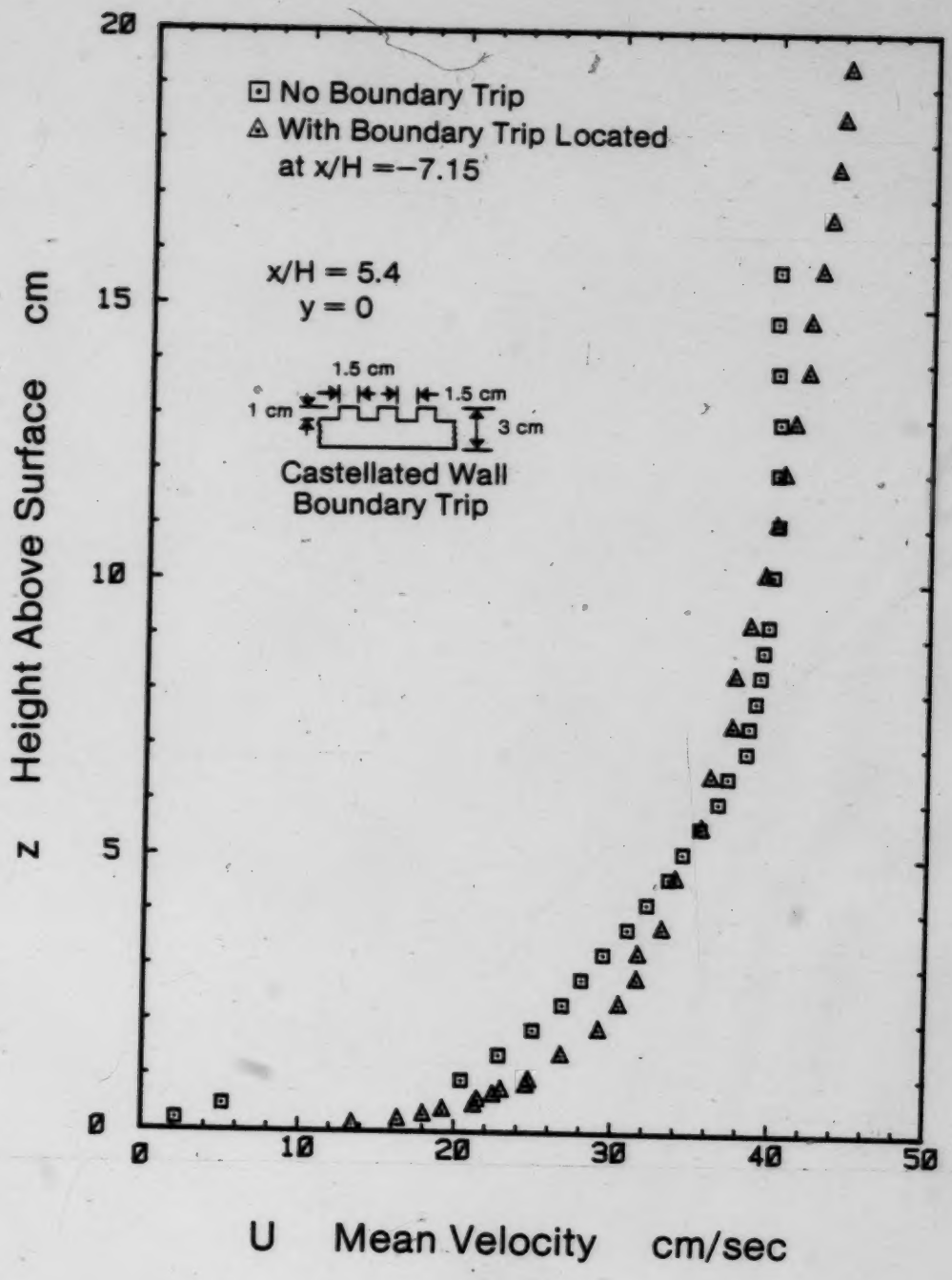

Figure 2.6 Measured velocity profiles, at 287.1cm from inlet of water channel, with and without castellated wall boundary trip.

a result of the boundary trip, fully developed flow was achieved at 190cm downstream of the channel inlet. For convenience a point at 179.1cm from the inlet of the channel was chosen as the start of the test section, x=0, where the tracer material was injected. Figure (2.7) shows the uniformity of the mean velocity profile on the channel centerline at 12.7cm, 100cm, 200cm and 300cm from the start of the test section, x=0. A profile of the mean velocity measured across the channel at 100cm from the start of the test section in Figure (2.8) shows that outside the influence of the sidewall boundary layer the variation in mean velocity is less than 1%. The vertical line on the graph indicates the maximum observed width of dispersion, from which it may be concluded that the sidewalls of the channel did not affect the dispersion process.

Figure (2.9) shows that the logarithmic profile of equation (2-1) is a satisfactory representation of the mean velocity profile measured in the water channel. The slight deviation of the two points at the top of the profile could be caused by the presence of the free surface or the fact that equation (2-1) really has no physical basis for being applicable above the constant shear stress layer. Because tracer material was not detected any higher than eighty percent of the boundary layer height, the deviation in the velocity profile is not a cause for concern.

According to Hinze (1975) p. 635, fully rough flow requires that the roughness Reynolds number, $u_* k_s/\nu$, be

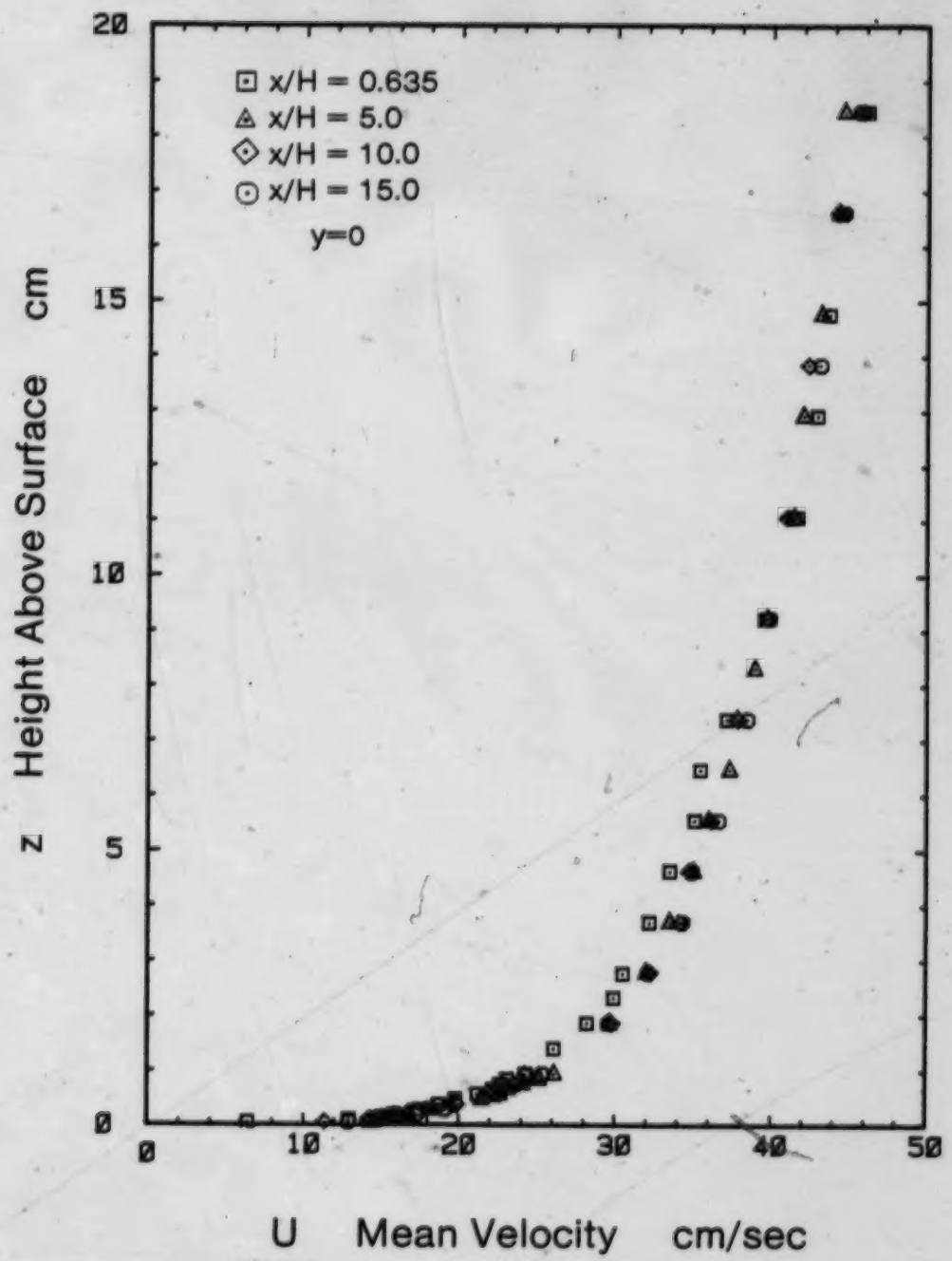

Figure 2.7 Mean velocity profiles at various downstream distances from source location, x=0, showing fully developed flow.

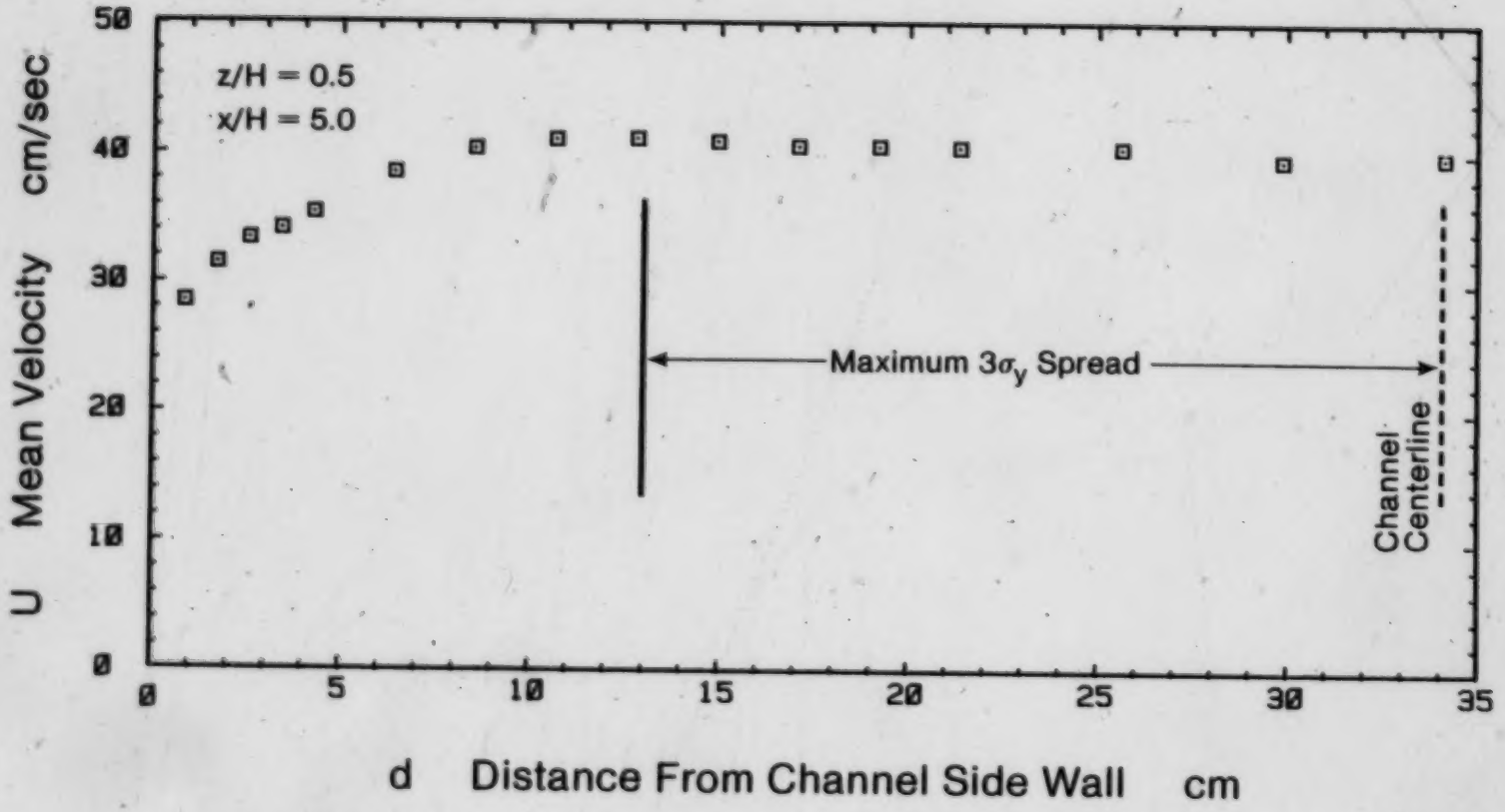

Figure 2.8 Measured mean velocity profile across channel showing flow uniformity outside influence of wall boundary layer.

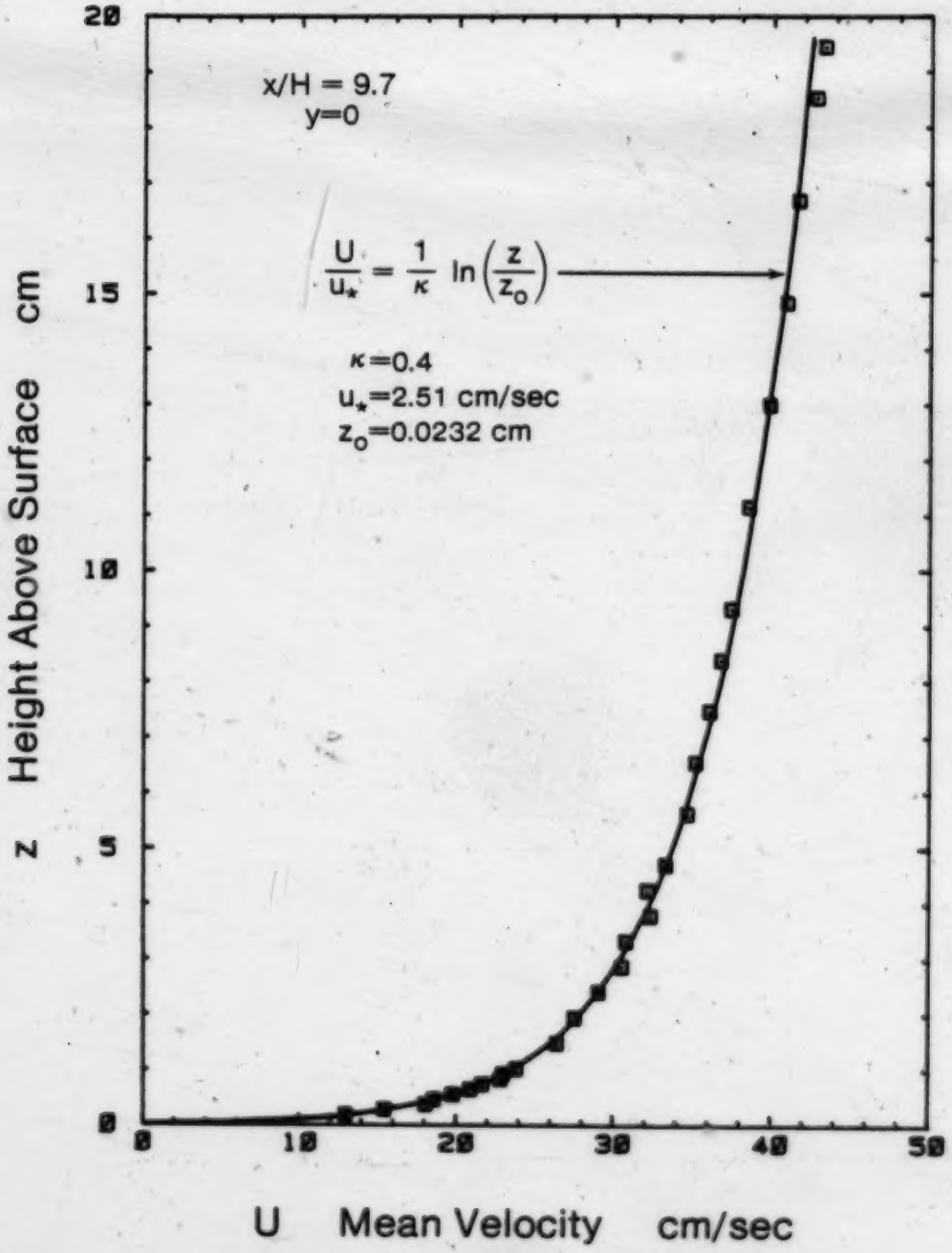

Figure 2.9 Log law boundary layer profile of equation (2-1) compared to mean velocity profile measured at x/H=9.7

greater than 55. The value 55 is based on the uniform sand grain roughness, k_s, and does not necessarily apply to a different type of roughness with height k. The "Lego" base plate roughness elements used in the water channel were cylindrical bumps of height k=0.188cm and diameter 0.48cm with a density of about 30% based on total area. To calculate a roughness Reynolds number for the channel flow that has any meaning the equivalent sand grain roughness of the "Lego" base plate has to be determined. For fully developed flow over densly packed uniform sand grains, Nikuradse found that the following relationship described the velocity profile

$$\frac{U}{u_*} = 5.75 \log \left(\frac{Z}{k_s}\right) + 8.5 \qquad (2\text{-}2)$$

Equating the velocity profile of equation (2-1) to equation (2-2) and using κ=0.4 results in the equivalent sand grain roughness, k_s, being equal to $30z_o$. For the flow in the water channel this results in $u_* k_s/\nu$=180, indicating that the flow is well beyond the lower limit for fully rough flow, where changes in Reynolds number, $U_\delta \delta/\nu$, do not affect turbulence intensity or the ratio between turbulent scales and boundary layer thickness, δ.

A power law profile of the form

$$\frac{U}{U_{ref}} = \left(\frac{z}{z_{ref}}\right)^{n} \qquad (2\text{-}3)$$

where

U = mean velocity

U_{ref} = reference velocity

z = height above surface

z_{ref} = reference height above surface

n = exponent

is commonly used to describe mean vertical velocity profiles in the atmosphere. The best fit to this power law for a velocity profile in the water channel is shown in Figure (2.10). The power law exponent, n, is useful in predicting the shape of mean and fluctuating concentration profiles in the vertical direction, as will be shown in Chapters 5 and 6.

Comparing the power law fit in Figure (2.10) to the logarithmic fit in Figure (2.9) a difference is seen in the way the two curves fit the data near the surface. The logarithmic curve fits the data better near the surface because its form is derived from physical conditions occurring near the surface. Higher above the surface it is seen that the power law profile fits the data better. This is due to choosing the parameters in equation (2-3) to give

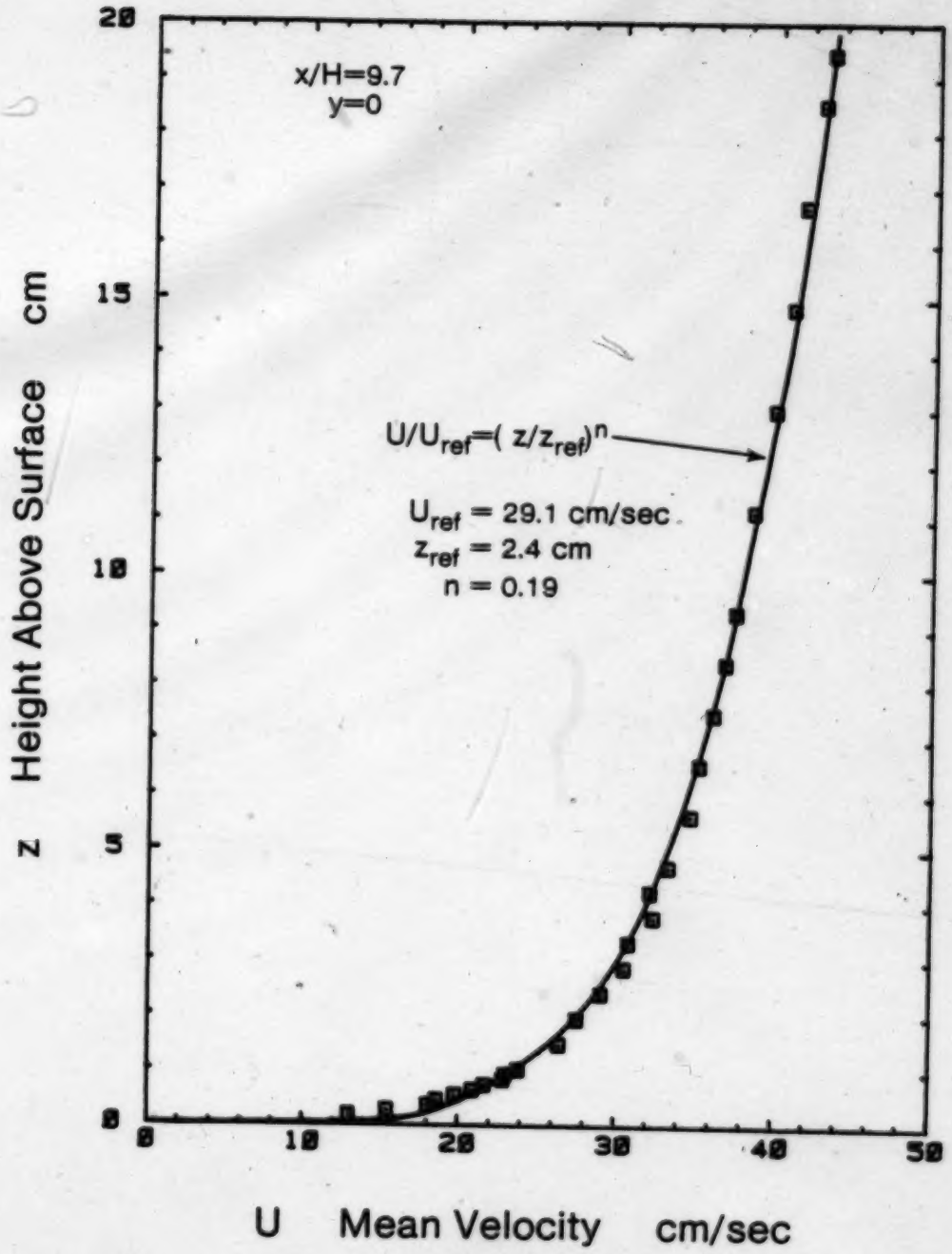

Figure 2.10 Power law variation of equation (2-3) fitted to measured mean velocity profile at x/H=9.7

a best fit. The logarithmic profile does not fit as well in this upper region since the constant shear stress approximation, which was applied at the surface, is no longer valid. This observed behavior of the two different velocity fits is typical for boundary layer flows.

2.5 u_*, Friction Velocity

It was previously seen from Figures (2.7) and (2.8) that the vertical mean flow profile was constant throughout the test section. Since turbulence in the flow determines the dispersion of a contaminant, it would be desirable to know if vertical turbulence profiles are uniform throughout the test section. A means of checking this, without actually measuring the turbulence, is to examine the behavior of the friction velocity, u_*, along the test section since u_* is proportional to the velocity fluctuations. From Figure (2.11) it is seen that u_* is constant along the test section centerline. This constant friction velocity again indicates that fully developed mean flow was achieved. It also suggests that vertical turbulence profiles should be constant in the downstream direction.

The friction velocity, u_*, was calculated by fitting equation (2-1) to the measured mean velocity profiles, using a linear least squares fit of ln(z) vs U and minimizing the error in ln(z). In all cases the calculated line fit the data very well as indicated by a typical profile in Figure (2.12). The friction velocity, u_*, was then calculated by.

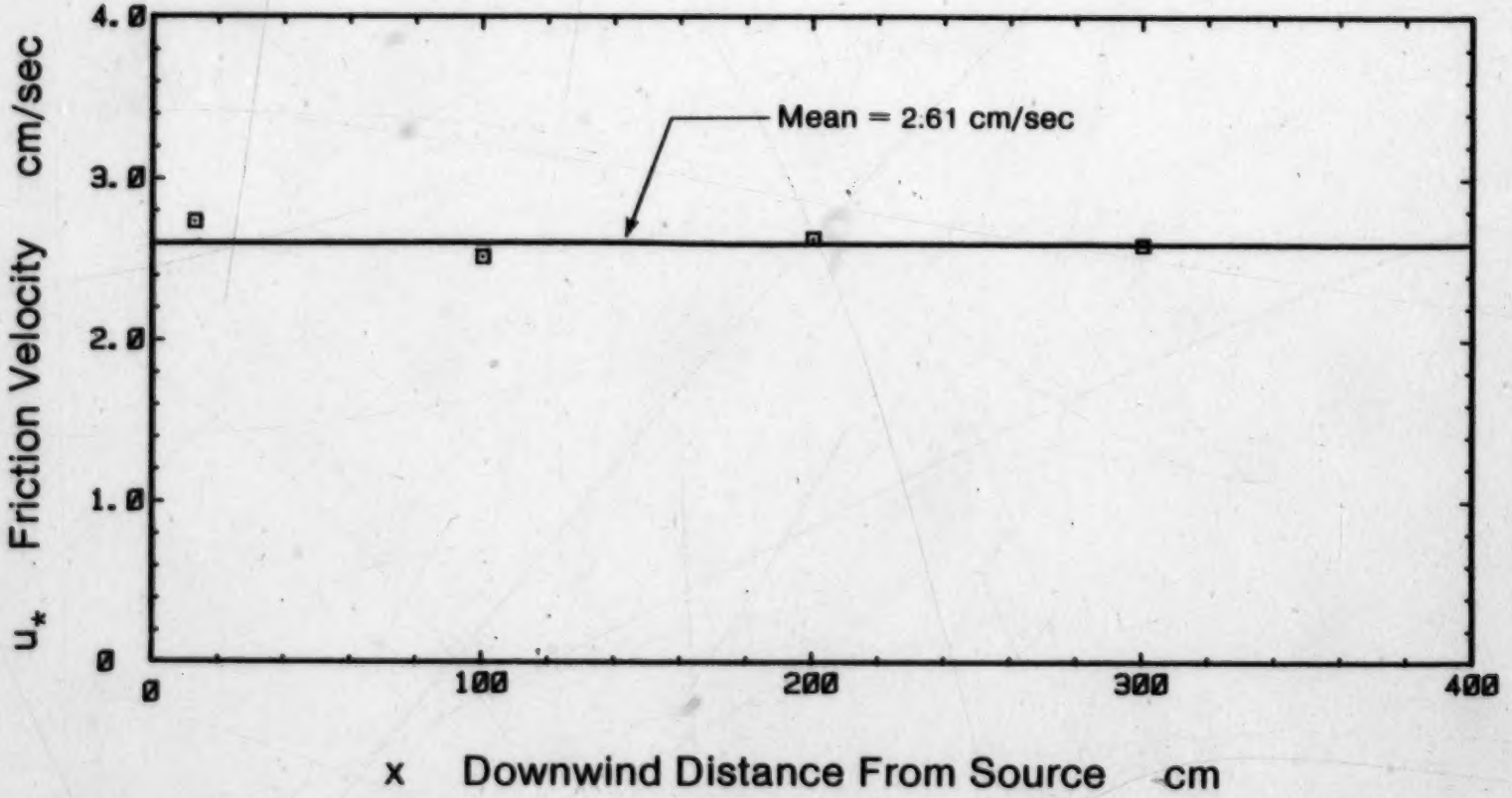

Figure 2.11 Uniformity of friction velocity, u_*, along water channel centerline.

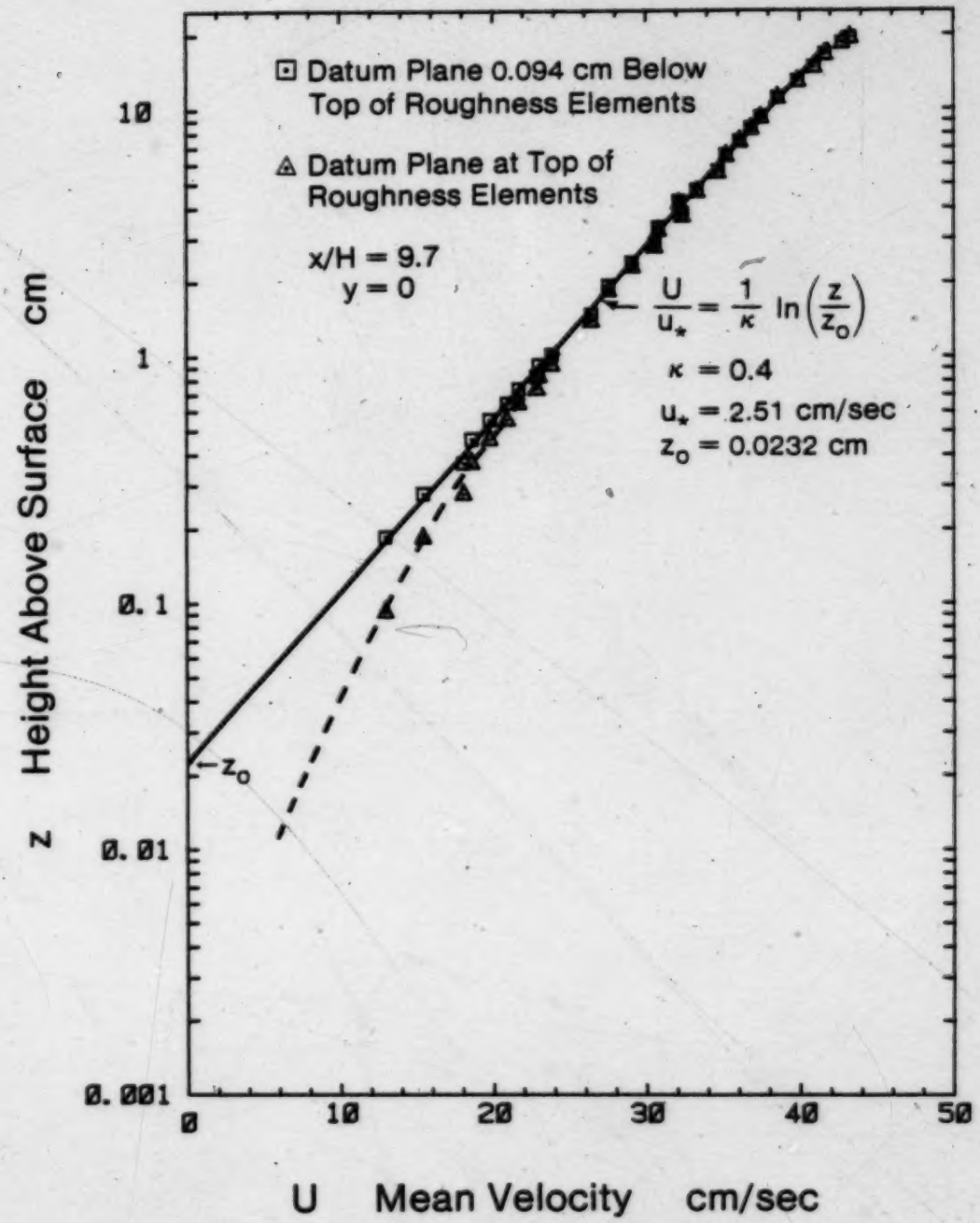

Figure 2.12 Determination of friction velocity, u_*, and surface roughness, z_o.

dividing von Karman's constant, κ, by the slope of the line. The quantity z_o, from equation (2-1), is a measure of the surface roughness which is shown in Figure(2.12) as the y-intercept of the semi-log plot of z vs U. The physical significance of this "log law roughness", z_o, is that when scaled up, it indicates what type of full scale terrain is simulated in the model.

The height above surface, z, is measured above some reference datum plane. Since the surface of the channel is composed of roughness elements protruding above a flat base, it is not clear where to define the level z=0. Is surface level at the flat base or at the top of the roughness elements? The way in which the datum plane was determined was by plotting the velocity profile using different z=0 datum planes. The correct choice of datum plane was taken as the one that forced the velocity data to form a straight line on the semi-log plot of z vs U.

The same set of data plotted with different datum planes is shown in Figure (2.12). A straight line is obtained when the datum plane is set at half the roughness height from the flat base. The curved line is obtained when the datum plane is set at the top of the roughness elements.

In summary it has been shown that the mean velocity profile of equation (2-1), which occurs in a neutrally stable atmosphere, was accurately modeled in the water channel. Downstream and cross stream uniformity was also achieved along the entire length of the test section.

3. MODELING ATMOSPHERIC DISPERSION IN THE WATER CHANNEL

3.1 Introduction

To make a scale model an accurate physical representation of the full scale, it is necessary to understand the physical phenomena which are controlling the processes being simulated. In the case of turbulent dispersion it is the turbulent structure of the flow which determines how a plume will spread. Therefore, the first step in modeling concentration fluctuations in the water channel is to understand how turbulence is involved in dispersion.

3.2 Relation of Turbulence to Plume Spread

Turbulence in a flow is always three dimensional. Even flows with a one dimensional mean field, such as the water channel, are three dimensional in their turbulent structure. Dispersion is the result of a contaminant's interaction with this complex flow field. To physically visualize dispersion it is necessary to develop simple measures of turbulence structure.

The simplest way to view turbulence is to think of it as a collection of different sizes of eddies which are being carried downstream by a mean flow. This range of different eddy sizes influence the spread of a contaminant in different ways. To visualize this, think of a contaminant coming out of a source as a solid tube of material. Eddies

which are larger than the tube will be effective in moving the tube side to side in a flapping motion. This flapping motion will dictate how far the contaminant is spread, and control the overall width of the plume. The flapping motion is also responsible for the property of intermittency. That is, plume material can be observed at a receptor when the large scales bring the plume into contact with the receptor. Periods of zero concentration are then observed when the large scale turbulence moves the plume away from the receptor.

Eddies which are smaller than the tube of material will have little effect on where the tube moves. Instead, they will be effective in moving material around inside the plume itself. Thus, concentration fluctuations are caused by two phenomena. One is plume meandering which is the main cause of intermittency, and the other is the small scale structure which causes fluctuations when the plume is present at a receptor. The effect that a particular size of eddy will have on the dispersion process will depend on the size of the eddy compared to the size of the plume.

Considering the statistical theory of turbulent diffusion in homogeneous turbulence, the plume spreads, σ_y and σ_z, as a function of downwind distance, given by Wilson (1979), are

$$\sigma_y = \frac{\sqrt{\overline{v'^2}}}{U} (2B\Lambda_v)^{1-a} x^a \qquad (3\text{-}1)$$

$$\sigma_z = \frac{\sqrt{\overline{w'^2}}}{U} (2B\Lambda_w)^{1-b} x^b \qquad (3\text{-}2)$$

where

$\frac{\sqrt{\overline{v'^2}}}{U}$ = turbulence intensity in lateral direction

$\frac{\sqrt{\overline{w'^2}}}{U}$ = turbulence intensity in vertical direction

Λ_v = Eulerian integral length scale in lateral direction

Λ_w = Eulerian integral length scale in vertical direction

x = downwind distance

B = Lagrangian-Eulerian scale ratio

The overall plume spread is controlled by the large scale eddies (i. e. integral length scale) and turbulence intensity. The exponents a and b in equations (3-1) and (3-2) respectively, give the rate of plume growth in the downwind direction.

σ_y and σ_z are measures of the overall plume spread. As the plume travels downwind and grows, the size of eddies

effective in causing plume meandering changes. Since the integral length scale is a measure of the large eddy sizes in a flow, we expect its effect to be different on plume spread as the plume grows. That is, the powers a and b should change depending on downwind location.

The statistical theory of particles diffusing in homogeneous turbulence puts bounds on a and b, requiring them to be between 0.5 and 1.0. Very close to the source (i.e. $x<<B\Lambda$) the plume grows linearly. Far away from the source (i.e. $x>>B\Lambda$) the plume grows as a function of downwind distance to the one half power. A value of a and b of unity means the effect of turbulent scale, Λ, is removed. Physically this means that when the plume is very small initially all eddy sizes are effective is increasing its overall size. Far downstream from the source the plume spread will be controlled by the large scales in the flow. This is reflected by a and b becoming smaller and allowing more effect of Λ in equations (3-1) and (3-2).

Equations (3-1) and (3-2) assume homogeneous turbulence. In the case of a boundary layer, both the velocity fluctuations, v' and w', and length scales Λ_v and Λ_w, vary with height above surface, z. This implies the functional form of equations (3-1) and (3-2) is not correct in shear flow. However, the equations are a useful indicator that turbulence intensity and integral length scale are the important parameters controlling plume spread in a boudary layer.

3.3 Scaling Criteria

For a proper simulation of plume spread in the water channel the following is required

$$\frac{\sigma_y}{x}\ \text{model} = \frac{\sigma_y}{x}\ \text{atmosphere} \qquad (3\text{-}3)$$

$$\frac{\sigma_z}{x}\ \text{model} = \frac{\sigma_z}{x}\ \text{atmosphere} \qquad (3\text{-}4)$$

This will ensure that the kinematics are correct. Since the tracer material is neutrally buoyant, no plume buoyancy scaling is required. Substituting equations (3-1) and (3-2) into equations (3-3) and (3-4) respectively, results in the following criteria

$$\frac{\sqrt{\overline{v'^2}}}{U}\ \text{model} = \frac{\sqrt{\overline{v'^2}}}{U}\ \text{atmosphere} \qquad (3\text{-}5)$$

$$\frac{\sqrt{\overline{w'^2}}}{U}\ \text{model} = \frac{\sqrt{\overline{w'^2}}}{U}\ \text{atmosphere} \qquad (3\text{-}6)$$

$$\frac{\Lambda_v\ \text{atmosphere}}{\Lambda_v\ \text{model}} = \text{Geometric Scale Factor} \qquad (3\text{-}7)$$

$$\frac{A_w \text{ atmosphere}}{A_w \text{ model}} = \text{Geometric Scale Factor} \qquad (3\text{-}8)$$

Even though equations (3-5) through (3-8) are based on homogeneous turbulence they are still valid for setting the criteria in a boundary layer shear flow. If the vertical profiles of turbulence intensity and integral length scale meet the requirements of equtations (3-5) to (3-8), then it may be concluded that a correct simulation of plume spread will result.

3.4 Deficiences of Water Channel Model

As described in the previous section if the turbulence integral length scale, Λ, and turbulence intesity are correctly scaled then the overall plume spreads, σ_y and σ_z, will be correct. Even if the turbulence and integral length scale are correctly simulated, this does not guarantee that the same concentration fluctuation statistics will exist at equivalent points in the water channel and atmosphere. Modeling fluctuation statistics requires that <u>all</u> concentration scales in the atmosphere are simulated in the water channel. Mathematically this requires the concentration fluctuation, c', spectra to be the same. The c' spectrum is a direct result of the turbulence spectrum and molecular diffusivity of the tracer into the ambient. Concentration eddies are created by the velocity eddies

while molecular diffusion dictates the smallest concentration scales which can exist. To guarantee the same concentration fluctuation spectrum requires that the turbulence spectra be identical in the model and full scale, and that the molecular diffusion coefficient of the tracer into the ambient be the same for the model and atmosphere.

Due to physical differences between the model and full scale flows, it is not possible to have the same turbulence velocity spectra. The water channel flow lacks both the very low and very high frequency turbulence of the atmosphere. Furthermore in the water channel, a liquid tracer is diffusing into a liquid and in the atmosphere a gas is diffusing into a gas. Due to the large difference in molecular diffusivity, the size of the smallest concentration scale that can exist in the model and full scale will be different. The effect of these differences must be determined.

3.4.1 Absence of Low Frequency Turbulence in Model

Due to the water channel flow being restricted by sidewalls, large atmospheric eddies in the crosswind direction can not be simulated. Also, unsteady wind direction changes with time scales of hours to days can not be modeled. The effect of these large scales in the atmosphere is to cause greater atmospheric plume spreads in the crosswind direction than the model predicts. The large atmospheric scales cause the plume to meander, so the longer

the plume is sampled the larger is the measured spread. In the case of the water channel, constant values for plume spread were obtained for averaging times of 100 seconds. According to Wilson and Simms (1985) the crosswind spread measured in the channel would be representative of a crosswind spread for a sample time of the order of minutes in the atmosphere. Refering back to equation (3-1), what is seen in the atmosphere is an increase of Λ_v as a longer sample period is used. The meandering of the plume due to large atmospheric scales will also cause the plume to have less intermittency as the sampling time is increased. Therefore, when applying the crosswind measurements of the water channel to the atmosphere it must be realized that they represent sampling times of the order of minutes in the atmosphere.

Vertical plume spread is not affected much by large scale meandering motions in the crosswind direction. The vertical spread in the atmosphere would be larger than the model predicted only if there was a large amount of turbulence caused by thermal convection. Since a neutral boundary layer is what is being studied the vertical spread predicted by the model should be representative of a neutrally stable full scale.

3.4.2 Absence of High Frequency Turbulence in Model

Based on boundary layer thickness, δ, as the characteristic length, the water channel flow has a Reynolds

number of about 3500 times less than the full scale atmospheric flow. The effect of this mismatch in Reynolds number is that the model flow will not properly simulate the small scale turbulence of the atmospheric flow. This means that when the model is scaled up it will not contain a certain range of the smallest velocity scales which actually exist in the full scale. This effect can be seen by looking at an estimate of the ratio between the longitudinal integral length scale and Kolmogorov microscale. As given by Hinze (1975) p. 225 the relationship is

$$\frac{\Lambda_x}{\eta} = Re_{\Lambda}^{0.75} \left[\frac{\sqrt{\overline{u'^2}}}{U_\delta}\right]^{0.75} \qquad (3\text{-}9)$$

where

Λ_x = longitudinal integral length scale

η = Kolmogorov microscale

Re_{Λ} = Reynolds number based on Λ_x and U_δ

$\frac{\sqrt{\overline{u'^2}}}{U_\delta}$ = turbulence intensity at top of boundary layer

Using the following typical values in equation (3-9) for the water channel,

Λ_x = 5cm

U_δ = 40 cm/sec

$\sqrt{\overline{u'^2}}$ = 4cm/sec

ν = 0.01cm²/sec

and for the atmosphere,

$$\Lambda_x = 150\text{m}$$

$$U_\delta = 7\text{m/sec}$$

$$\sqrt{\overline{u'^2}} = 0.7\text{m/sec}$$

$$\nu = 15\times10^{-6}\text{m}^2/\text{sec}$$

The following is obtained,

$$\frac{\Lambda_x}{\eta}\ \text{model} = 300 \qquad (3\text{-}10)$$

$$\frac{\Lambda_x}{\eta}\ \text{atmosphere} = 136{,}100 \qquad (3\text{-}11)$$

$$\frac{\dfrac{\Lambda_x}{\eta}\ \text{atmosphere}}{\dfrac{\Lambda_x}{\eta}\ \text{model}} = 450 \qquad (3\text{-}12)$$

From equation (3-12), it is seen that the smallest velocity eddy in the scaled up model is 450 times larger than the smallest scale which actually exists in the atmosphere. The smallest atmospheric eddy which the channel can simulate is 0.5m where as smallest scale which actually exists is approximately 1mm. The effect this has on concentration fluctuations depends on how active the "missing" velocity eddies of 0.5m and smaller, are in dispersion.

3.4.3 Effect of Molecular Diffusion on Concentration Scales

Wilson (private communication) has considered the effect of molecular diffusion using the following arguments. For a point source, there is not a steady supply of tracer material at the surface, so the production of concentration fluctuations does not equal the dissipation. Instead, most of the concentration eddies originate in a region near the source and are then convected downwind. Since the tracer is a passive material, it may be assumed that the original concentration eddies have the same scale range as the velocity eddies. However, as the eddies are convected downwind, molecular diffusion is acting to smear out the smallest concentration scales. This implies that the travel time to a particular downwind location will dictate the smallest eddy size which can exist at that location.

In the water channel a liquid tracer is diffusing into a liquid and in the atmosphere a gas contaminant into a gas. Due to different molecular diffusivities, the smallest concentration scale which can exist relative to the Kolmogorov microscale, η, in each flow will be different. On the other hand, the large concentration eddies in each flow will scale to each other. To compare the concentration scale range between the model and full scale it is necessary to define the scale ratio ℓ/L_c, where ℓ is the size of a typical large scale concentration eddy and L_c is the smallest concentration scale which can exist due to molecular diffusion. L_c depends on travel time, so ℓ/L_c will

be a function of downwind distance.

The magnitude of L_c, can be estimated as being the distance a sharp interface, between the tracer and ambient, would diffuse in a time equal to the travel time. Using the solution in Myers (1971) p. 200 for one dimensional diffusion, the width of the diffused zone, L_c, can be expressed as a function of the molecular diffusion coefficient, D, and time, t, as

$$L_c = 4\sqrt{Dt} \tag{3-13}$$

Assuming that the travel time, t, to a given downwind distance, x, from the source is given by t=x/U results in,

$$L_c = 4\sqrt{\frac{Dx}{U}} \tag{3-14}$$

An earlier assumption was that at the source, concentration eddies have the same scale range of velocity eddies. Therefore, equation (3-14) will be valid only after a travel time where L_c becomes larger than η. Comparing concentration scale ranges in the water channel and atmosphere using equation (3-14) with the subscripts, m and a, denoting the model and atmosphere results in,

$$\frac{\frac{\ell_a}{L_{ca}}}{\frac{\ell_m}{L_{cm}}} = \frac{\ell_a L_{cm}}{\ell_m L_{ca}} = SF\sqrt{\frac{U_a D_m x_m}{U_m D_a x_a}} \qquad (3\text{-}15)$$

where

SF = scale factor between atmosphere and water channel model, 3000:1 scale

U_m = typical mean velocity in water channel, 0.4 m/sec

U_a = typical velocity in atmosphere, 7.0 m/sec

D_m = molecular diffusion coefficient between water and salt water $1.2 \times 10^{-5} cm^2/sec$

D_a = typical molecular diffusion for gas into air, 0.14 cm^2/sec

x_m = downstream distance in water channel

x_a = downwind distance in atmosphere

Equivalent distances in the water channel and atmosphere will be related by the scale factor (i.e. $x_a/x_m = SF$). Inserting the typical values into equation (3-15) results in,

$$\frac{\frac{\ell}{L_c}\text{ atmosphere}}{\frac{\ell}{L_c}\text{ model}} = 2.0 \qquad (3\text{-}16)$$

Equation (3-16) shows that the concentation scale range, at equivalent downwind locations, in the water channel and atmosphere are approximately equal. For example,

at a distance of 1.5km from the source in the atmosphere, the scaled up model suggests that the smallest concentration eddy is 0.5m (from equation (3-14)). The smallest concentration eddy which actually exists in the atmosphere, as given by equation (3-16), is 0.25m. For practical purposes the concentration scale range in the water channel and atmosphere are the same when considering limitations imposed by molecular diffusion.

This is a remarkable result since we are interested in modeling concentration fluctuations. Even though the velocity scale ranges differ by a large amount due to Reynolds number mismatch, as shown by equation (3-12), the combination of the size of the water channel model, its flow velocity and molecular diffusivity of the tracer, results in a good model for concentration flucuations.

3.5 Turbulent Flow Structure in Water Channel

For naturally grown rough-wall boundary layers, the flow structure is similar for all sizes of boundary layers. The problem that arises in the laboratory is that the flow test section is usually too short to grow a fully developed natural boundary layer. Therefore, this requires that the boundary layer be artificially thickened, and by doing this, a turbulence structure may be generated which is not representative of a naturally grown boundary layer.

In wind tunnel shear layers, vortex generators, exaggerated roughness and barrier walls are often used to

artificially create a fully developed boundary layer. By adjusting these elements the model can be fine tuned to produce the desired turbulent structure. However, this procedure usually requires many iterations with many turbulence measurements having to be made. In the water channel, fully developed flow could be obtained simply by tripping the flow with a barrier wall. Once the boundary layer reaches the free surface and has had a chance to stablize, the flow will "forget" that it had been tripped. The turbulence will then be determined entirely by the surface roughness. Hence, the turbulent structure of the water channel will be similar to that of the atmosphere. The only differences which result are the lack of very large and very small velocity scales as discussed previously.

By the time the desired boundary trip was chosen to achieve fully developed open chaennel flow, the method to measure turbulence with the LDV had been developed. This allowed a means of verifying that the turbulence in the water channel did indeed simulate a neutrally stable atmosphere. Examining Table (3.1) it is seen that according to the data of Counihan (1975), the scaled up water channel flow is in good agreement with a neutrally stable atmosphere.

Vertical profiles of longitudinal turbulence intensity at various downstream locations in Figure (3.1) show the uniformity of the turbulence in the downstream direction. The profile closest to the source at x/H=0.635 has a slight

Table 3.1 Comparison of water channel boundary layer with full scale atmospheric data of Counihan (1975).

Parameter		Water Channel 3000:1 Scale	Full Scale Neutral Stability
Roughness Height	z_o	0.7m	0.7m
Power Law Exponent	n	0.19	0.2 ±0.03
Boundary Layer Thickness	δ	600m	600m ±50m
$\frac{\sqrt{\overline{u'^2}}}{U}$ @30m		0.18	0.2 ±0.03
Integral Scale	Λ_u	120m @z=30m 150m @z=150m	130m ±50m @z=30m 200m ±50m @z=150m

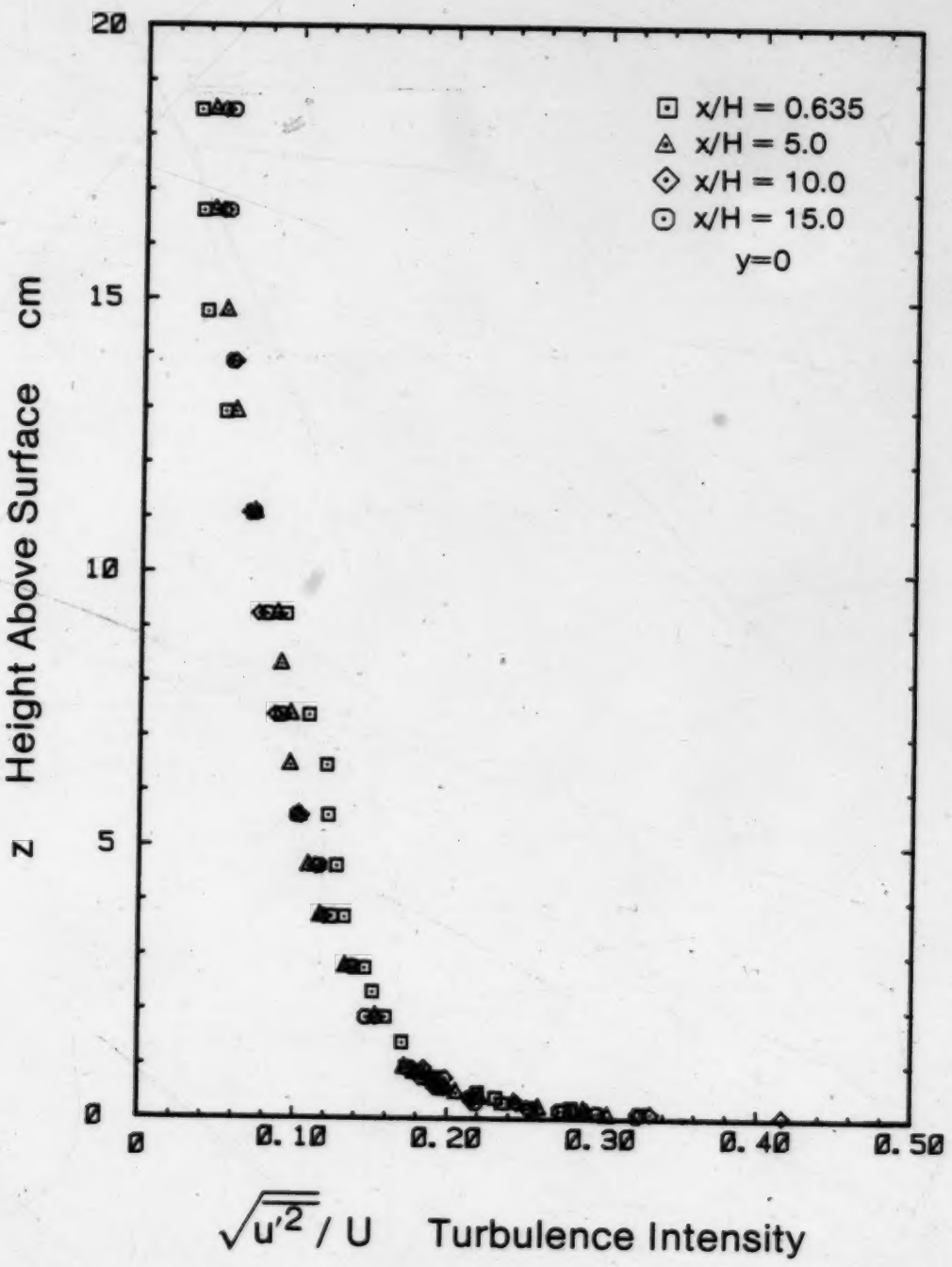

Figure 3.1 Uniformity of vertical proflies of longitudinal turbulence intensity at varying downstream locations.

deviation from the others at a height of 6cm above the surface. This is most likely an effect caused by the boundary trip used to thicken the boundary layer. At x/H=2.38 the vertical half width of the plume was 1.8cm so the effect of a deviation 6cm above the bed at x/H=0.635 is negligible.

Figure (3.2) shows a vertical profile of longitudinal integral length scale measured in the water channel. The smoothed fit was obtained using a curve which appeared to be the average of the two independent measurements. This approach seemed reasonable because, the resulting increase then decrease in scale in the bottom two thirds of the boundary layer was consistent with full scale observations of Counihan (1975). In the atmosphere the longitudinal scale increases with height to about 200-300m and thereafter decreases for further increase of height. The apparent increase of scale with height in the upper third of the channel boundary layer could be due to the free surface or be an effect caused by the smooth fit.

The large repeatability scatter at 4.5cm and 2.0cm above the bed is probably caused by an insufficiently long sampling time. The length scale was calculated from the following relationship as given by Hinze (1975) p. 65

$$\Lambda_u = T_u U = \frac{E_u(0)\, U}{4\, \overline{u'^2}} \qquad (3\text{-}17)$$

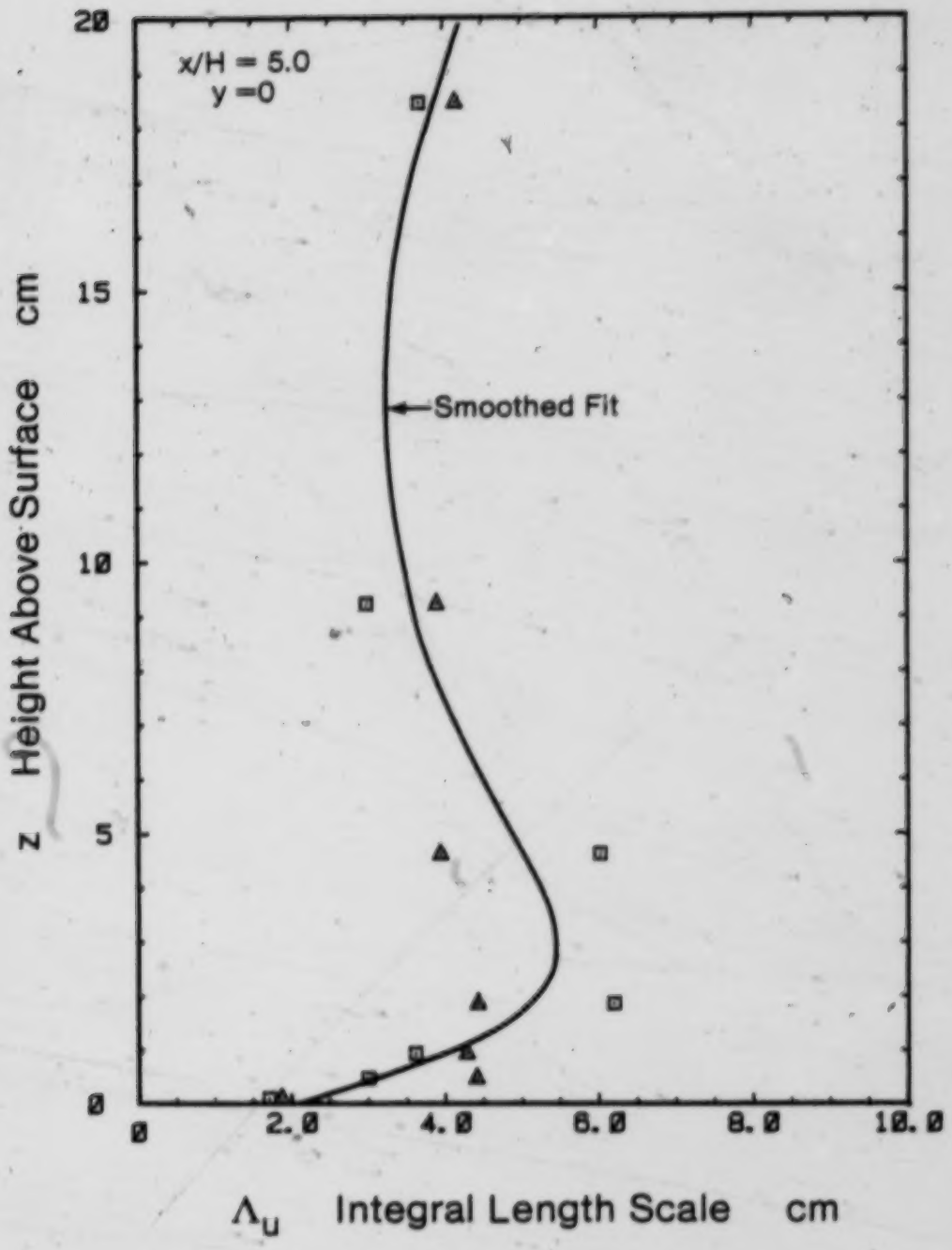

Figure 3.2 Vertical profile of longitudinal integral length scale showing scatter in two sets of independent measurements.

where

Λ_u = Eulerian integral length scale

T_u = Eulerian integral time scale

U = mean flow velocity

$E_u(0)$ = value of the power spectral density function for u' at zero frequency.

$\overline{u'^2}$ = variance of the longitudinal velocity fluctuations.

The scatter occurring in the length scale, Λ_u, was a result of variability that occured in the estimates of the zero frequency intercept, $E_u(0)$, in equation (3-17). The value of $E_u(0)$ is determined by the large scale turbulence in the flow. Stable values of $E_u(0)$ require sufficiently long sampling times to adequately sample the large scales. Typically 10^4 integral scales of turbulence need be sampled to produce stable estimates of the power spectral density function, $E_u(f)$, at the low frequencies. Sampling intervals in the water channel, when determining the power spectrum, were about 140 seconds. This allowed only 700 turbulent integral scales to be sampled which is an order of magnitude smaller that what is required for repeatable values of $E_u(0)$.

The cross stream profile of longitudinal turbulence intensity in Figure (3.3) indicates good uniformity (±2% of channel centerline value) in the region where the plume disperses. Turbulence intensity increases near the sidewall as expected, due to the wall boundary layers. The

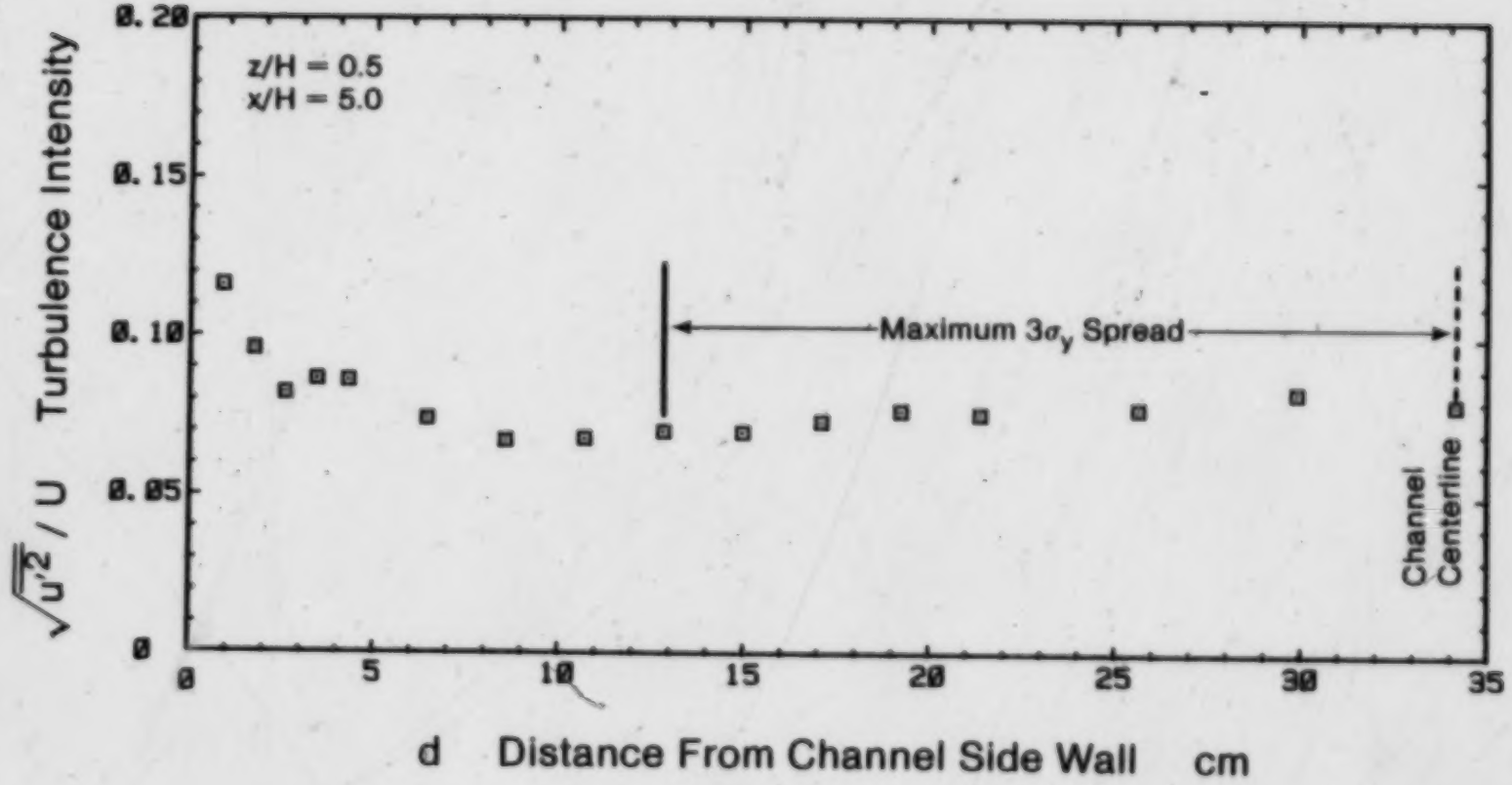

Figure 3.3 Longitudinal turbulence intensity measured across the water channel at z/H=0.5, showing negligible effect of channel sidewalls.

longitudinal integral length scale across the channel where the plume was observed is also constant, as shown by Figure (3.4). The scatter in the data can again be attributed to the method used to calculate the length scale. From Figures (3.3) and (3.4) it can be concluded that the channel sidewalls did not affect the spread of the tracer in the channel.

All turbulence measurements made in the channel were in the longitudinal direction. The vertical and lateral turbulence, which determine the spread of a plume, were not measured in the channel. Counihan (1975) points out that the vertical and lateral turbulence will be directly proportional to the longitudinal turbulence in a neutrally stable boundary layer.

3.6 Effect of Tracer Injection on Flow

The injection of a passive tracer at the surface of the water channel was designed to minimize flow disturbances. The injector was a tube 0.635cm in diameter and 19.1cm long placed on the surface of the channel at the centerline (see Figure (2.2)). Relative to the depth of the boundary layer, H, which is 20cm thick, this is a large obstruction. The effect this had is shown in Figure (3.5) which shows the mean velocity with and without the injector installed. The only noticeable difference is a 50% change in mean velocity very near the surface.

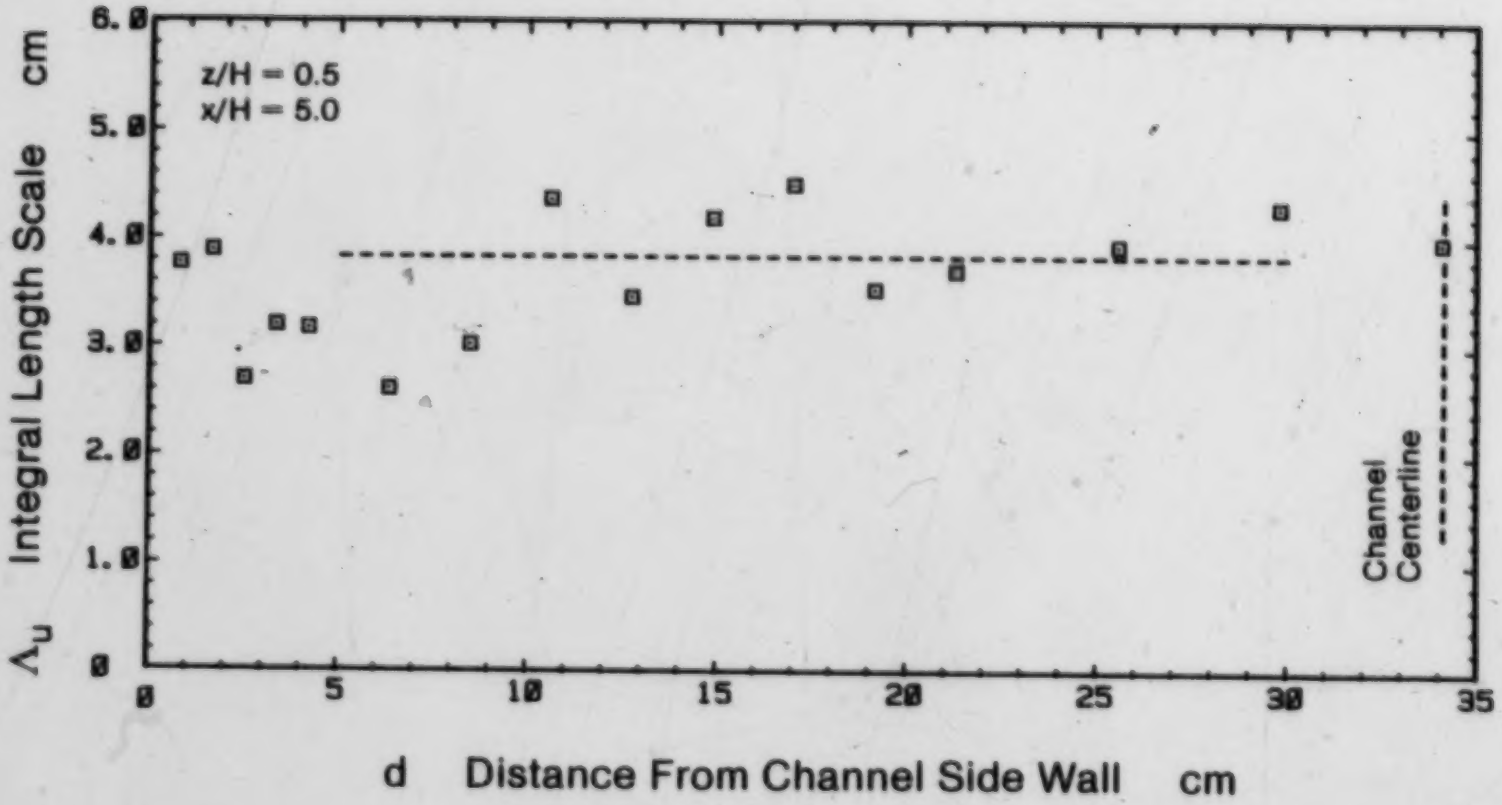

Figure 3.4 Longitudinal integral lenghth scale of turbulence measured across water channel at z/H=0.5, showing negligible sidewall influence.

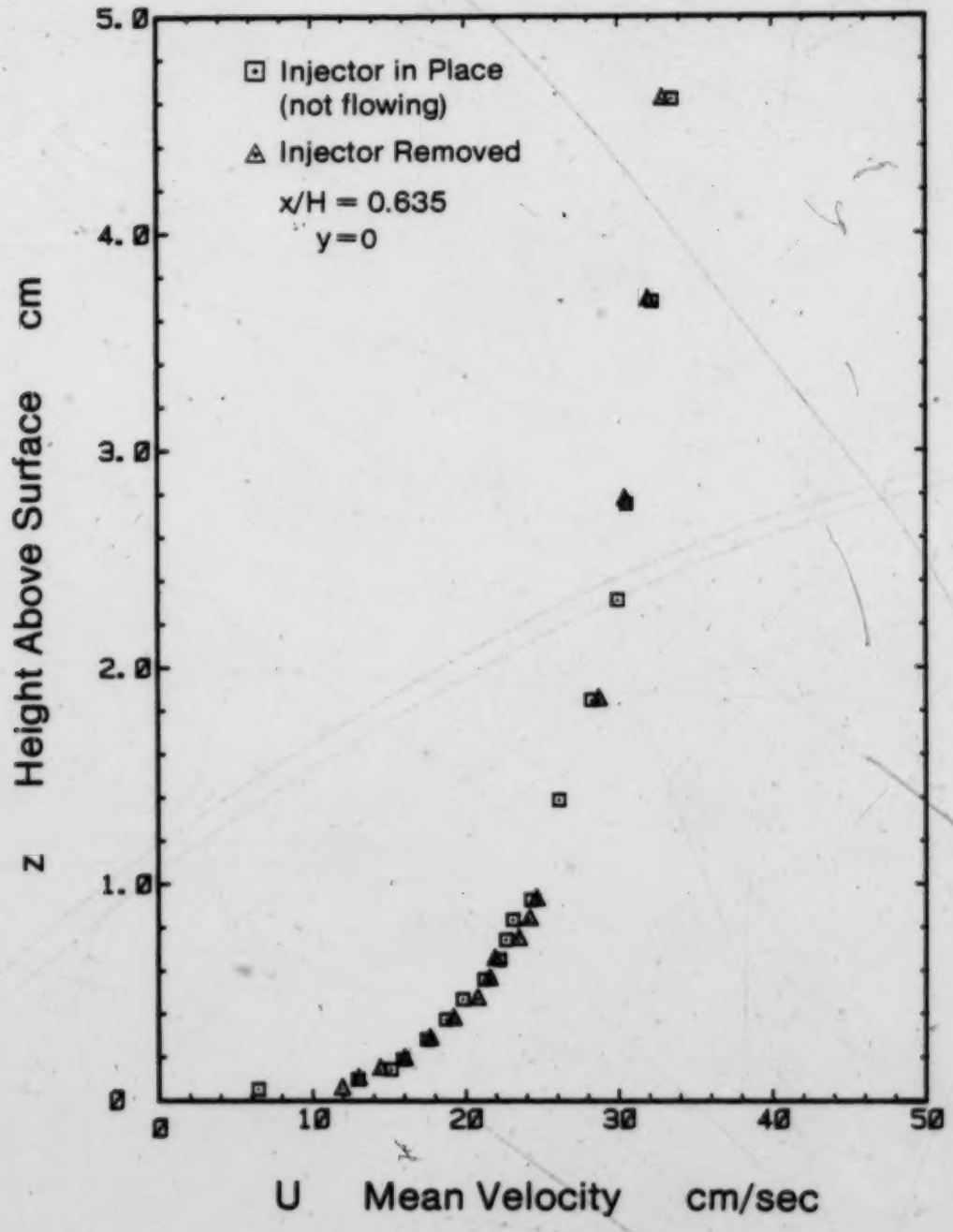

Figure 3.5 Mean velocity profile measured at the injector location, with and without the injector, showing influence of injector on flow.

The velocity at which the tracer leaves the injector is important since the tracer is to behave in a completely passive manner. To assure isokinetic conditions the mean exit velocity of the tracer should be equal to the local mean flow. Under isokinetic conditions as shown in Figure (3.6) the turbulence of the flow was unaffected. In an attempt to obtain higher detector output signals the injector flow rate was doubled. The profiles in Figure (3.6) show that the turbulence intensity was reduced for a substantial distance above the surface. The jet issuing from the injector obviously had an undesirable effect, so the slower isokinetic flow rate was used for all tests.

3.7 Effect of Source Size on Concentration Fluctuations

As pointed out in the previous section the size of the source was large relative to the boundary layer thickness. Scaled up, it corresponds to a 16m diameter source in the atmosphere. In the atmosphere, the source could be any size. The question then is, how general is the data of this study, or does it apply only to a single case?

Fackrell and Robins (1981) carried out a series of measurements in a boundary layer with equivalent full scale ground level source sizes ranging from 1.5m to 7.5m. They concluded that the size of a ground level source is unimportant in determining the fluctuating concentration field downwind of the source. The opposite is true for fluctuations from an elevated source where there is a strong

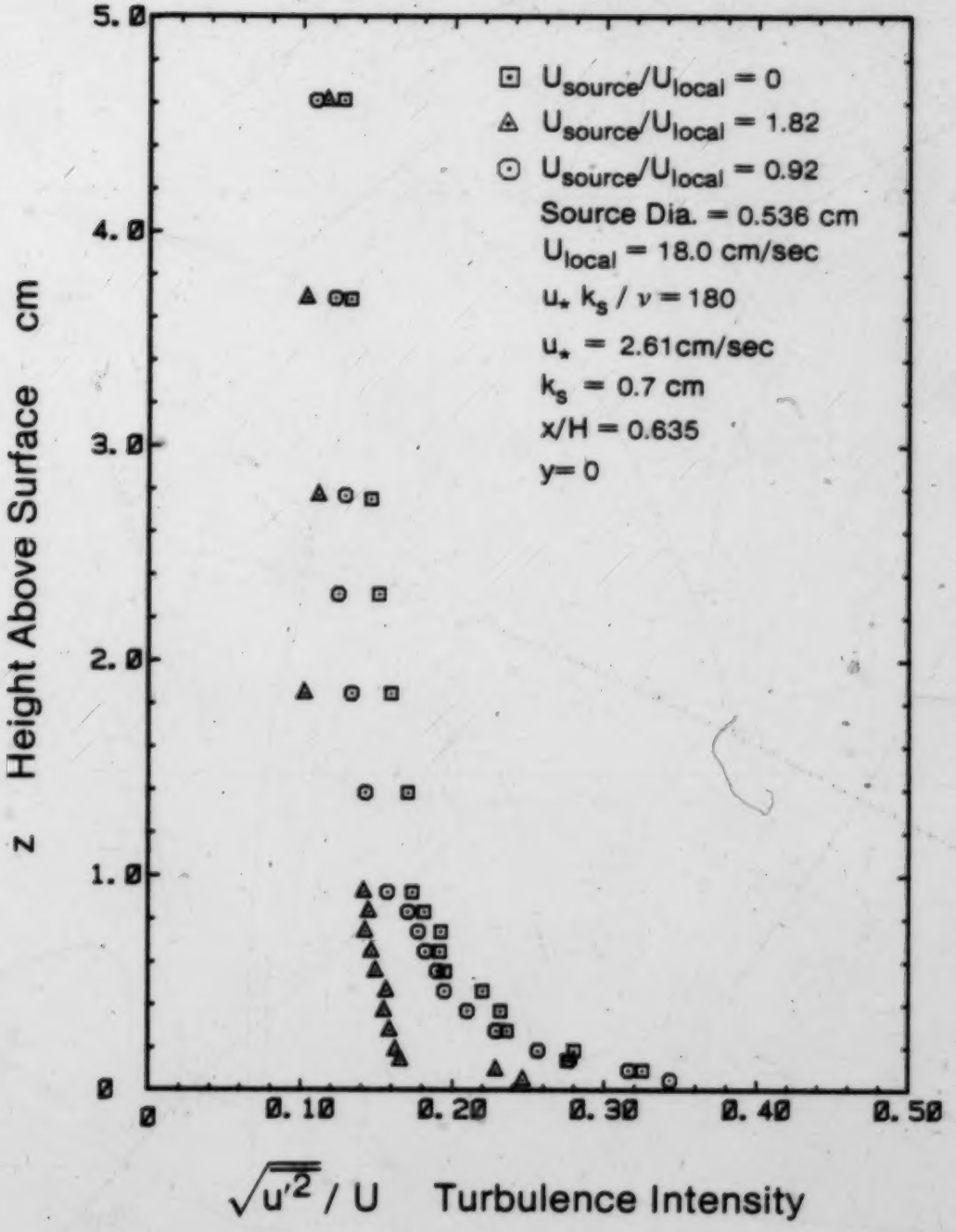

Figure 3.6 Effect of injector flow rate on turbulence intensity at 12.7cm, (20 injector diameters), downstream of injector.

sensitivity to source size. For an elevated source the turbulent length scale, Λ, is much larger than the source size, hence the amount of meandering that a plume experiences as it leaves the source is very dependent on the physical size of the plume. On the other hand, near the ground surface the turbulent scale, Λ, increases linearly with height so for a source located at the surface the turbulent scale, Λ, will be approximatly the same scale as the source size. The reduced meandering plus the fact that there is a strong decorrelation effect due to wind shear, dU/dz, results in the fluctuations becoming insensitive to source size.

4. MEASUREMENT OF CONCENTRATION FLUCTUATIONS

4.1 Introduction

The smallest concentration fluctuations in the atmosphere that are of interest would typically have spatial variations of about 3m. With a typical wind speed of 3 m/sec this would correspond to a fluctuation with a time scale of 1 sec. To model a 3m spatial variation at 3000:1 scale requires a spatial resolution of 1mm in the water channel. Also, with a channel velocity that is about 10 times slower than the atmosphere, there is still a 300:1 compression of the time scale in the channel. An obvious problem, when measuring concentration fluctuations in the water channel, is sophisticated instrumentation is required to achieve spatial resolutions on the order of 1mm and time responses on the order of 3ms.

4.2 Design of the Conductivity Probe

The main objective when designing the probe was to have a small spatial resolution as well as a suitable hydrodynamic shape to obtain adequate frequency response. Another important consideration was to have a probe that would be rugged enough to survive normal laboratory use.

Figure (4.1) shows the type of probe used in this study. It is a two electrode probe with a teflon tip and stainless steel body. The tip is cone shaped with a beveled end to give it a hydrodynamic shape. Figure (4.2) shows the

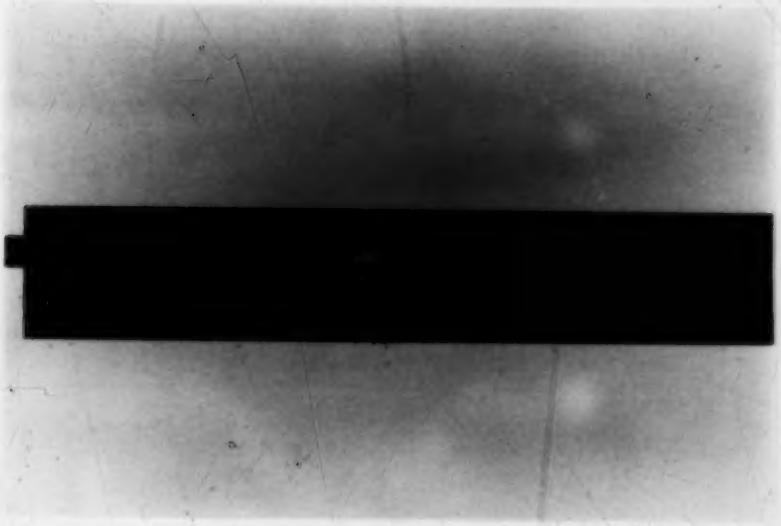

Figure 4.1 Wedge shaped double electrode probe.

Figure 4.2 Probe immersed in channel for measurement.

probe immersed in the water channel for a typical measurement. The entire length of the probe is approximately 20cm to ensure the tip is far enough away from the support. Measurements with the LDV indicated that the mean velocity 3mm in front of the probe tip was changed less than 1% due to the presence of the probe.

The principal reasons for choosing a double electrode over a single electrode configuration were ruggedness and good spatial resolution. A single wire probe, which uses a remote ground, requires a very small electrode diameter for good spatial resolution. A rough estimate of the spatial resolution for a single wire probe, given by Gibson and Schwarz (1963), is a sphere with a radius 10 times the electrode radius. As a rough estimate for the double wire probe used in this study, the spatial resolution would be approximately a sphere of diameter equal to the distance between electrode centerlines. With electrode diameters of 0.33mm spaced at 0.7mm on center this corresponds to a sphere 0.7mm in diameter. For the same spatial resolution a single wire probe would require an electrode diameter of 0.14mm. A glass tip would be required with that small a wire, hence more delicate construction would be necessary. To avoid delicate and fragile probes, the double wire design was selected. Also, since measurements close to the water channel surface were required the contained electrical field of the two electrode probe seemed more appealing. The electrical field of a single electrode probe is more likely

to be affected when an electrically grounded surface is in very close proximity. The double electrode probe used in the study showed only a 2% change in output when brought to within 2mm of the channel surface. A single electrode probe with the same electrode diameter could be expected to experience a 10% to 20% change in output.

The black color of the electrodes in Figure (4.1) is due to the porous platinum plating used to stabilize the detector output and reduce electrical noise. The platinum blacking procedure consists of immersing the electrodes in a 0.1M solution of chloroplatinic acid and passing a constant current to the electrodes to electroplate the platinum onto the platinum electrodes. The amount of current used was slightly less than the current required to produce gas bubbles off the electrodes (typically 60-100μA). In this plating procedure the electrodes were first soaked in nitric acid for 10 minutes to remove impurities. This acid cleaning step required the use of a teflon tip since other machinable plastics tested dissolved in the nitric acid.

4.3 Creating a Neutrally Buoyant Tracer

Because a neutrally buoyant release was to be studied, an electrolytic tracer with the same density as the tap water in the channel was required. Due to availability and low cost, sodium chloride was selected as the salt which would provide the ions in the tracer solution. Ethanol was mixed with the saltwater to achieve a tracer solution with

the same density as tap water. Ethanol, being lighter than tap water, compensates for the density increase that the salt causes in solution.

To produce the largest possible signals from the conductivity detector far downstream from the source it is desirable to release a high concentration of ions. This means that the tracer solution should contain the largest amount of salt possible. Therefore, the highest concentration saltwater solution that could be easily made, 250g/ℓ NaCl, was diluted with ethanol until the mixture had a density equal to that of tap water. From Figure (4.3) it can be seen that this mixture, Test Mixture #1, originally the same density as tap water, increased in density as it was diluted with tap water. This was very undesirable because even a slightly denser than ambient tracer causes turbulence near the surface to be damped, resulting in significant changes in the turbulent dispersion process.

The second mixture, Test Mixture #2, having a larger amount of ethanol in it, had a density 1.7% less than that of tap water. However, when this solution was diluted with tap water, as seen from Figure (4.3), the maximum density reached was just slightly higher than tap water. To avoid density effects, it was decided to use the second mixture diluted by a factor of two as the plume tracer material. As seen in Figure (4.3), after the factor of two dilution, the mixture shows no significant density changes with further dilution.

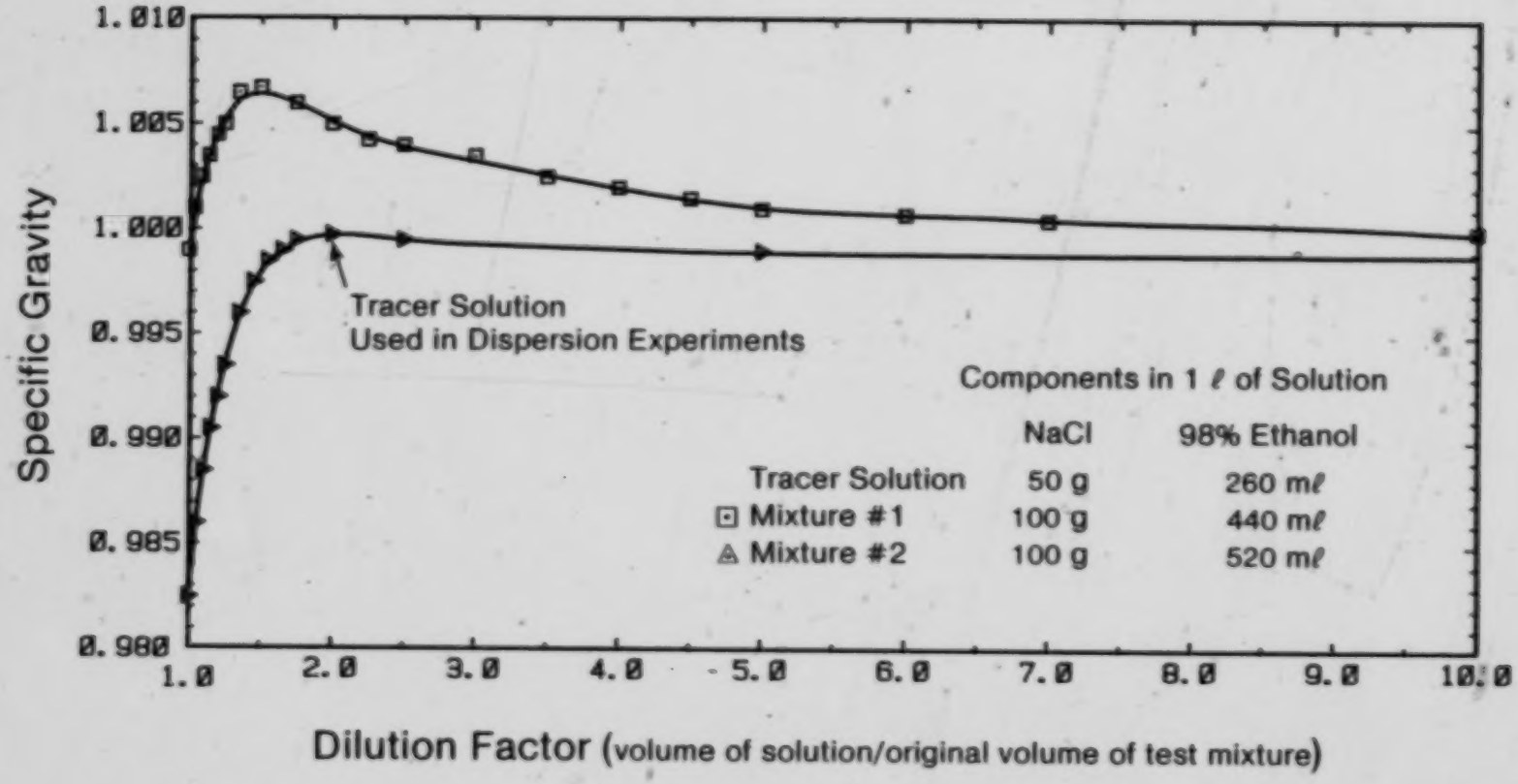

Figure 4.3 Optimizing composition of tracer injection solution to produce a neutrally buoyant mixture.

4.4 Static Calibration of Detector

A static calibration of the conductivity detector was carried out to determine the linear range of the probe circuit. Because all concentration profiles were nondimensionalized in the final analysis and measurements were limited to the linear range, it was not necessary to know absolute concentrations. The calibration procedure involved measuring detector output voltage while the probe was immersed in several solutions of varying concentrations, covering the range of 0.1g/ℓ to 50g/ℓ. This range was selected since the concentration of the tracer injector solution was 50g/ℓ and the "effective" background concentration of the tap water in the channel was 0.15g/ℓ. Figure (4.4) shows the relationship between detector output voltage and concentration of NaCl for the above range of concentrations. One calibration equation that fit the data well is

$$C = \frac{A_1(E - E_o)}{1 + A_2(E - E_o) + A_3(E - E_o)^8} - C_o \qquad (4-1)$$

where

C = concentration of NaCl, g/ℓ

E = detector output, volts

E_o = detector output in 0.1g/ℓ NaCl solution, volts

C_o = 0.1g/ℓ NaCl

A_1, A_2, A_3 = adjustable coefficients

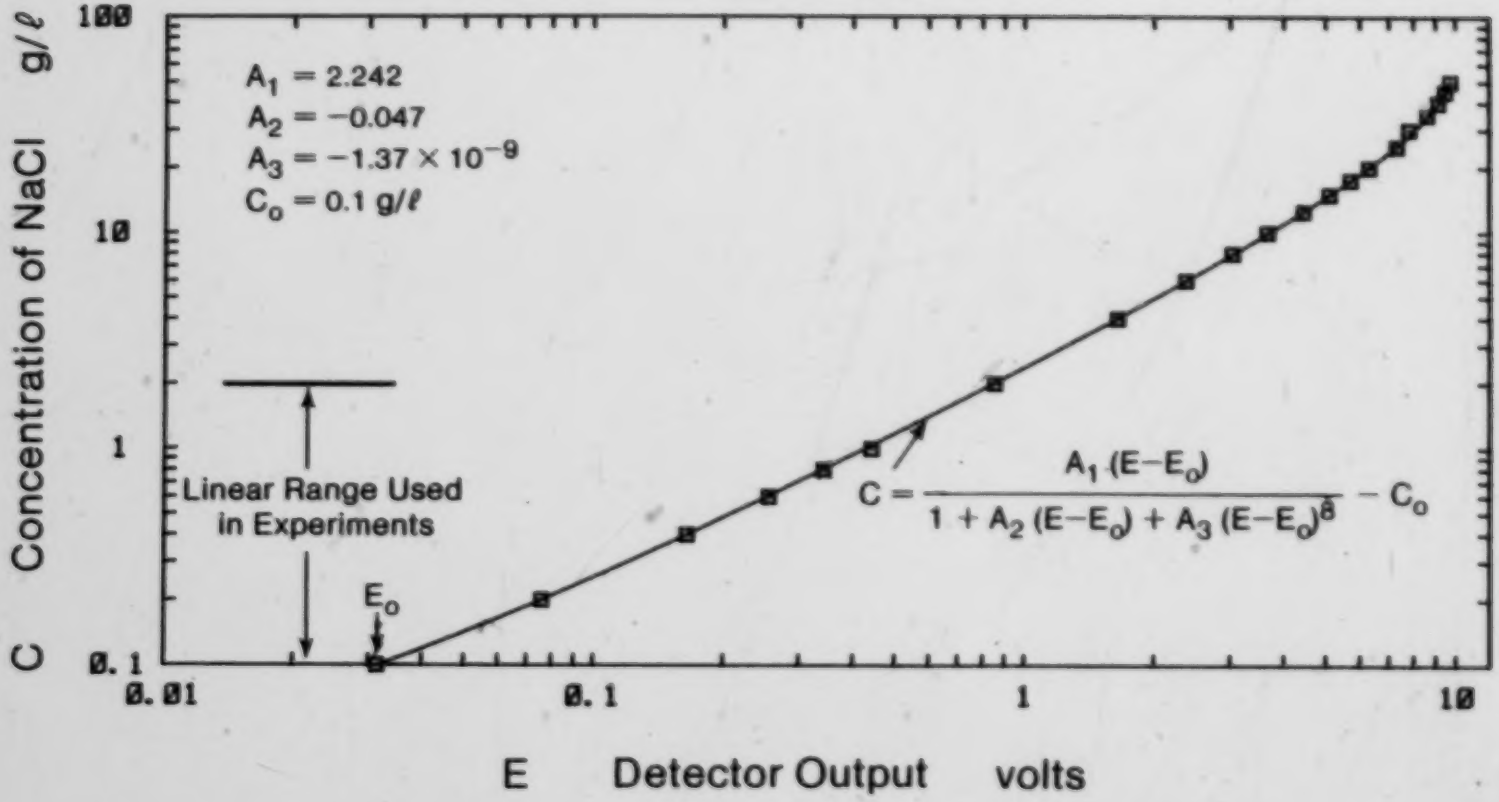

Figure 4.4 Steady state calibration curve for conductivity detector showing linear range.

The coefficients A_1, A_2 and A_3, which gave the best fit to the data in Figure (4.4), were calculated by using the measured voltage values at 6g/ℓ, 17.5g/ℓ and 40g/ℓ.

For concentrations between 0.1g/ℓ and 1.0g/ℓ the relationship between detector output voltage and concentration is linear. Extrapolating this to 2.0g/ℓ the deviation from linearity is approximately 3%. All concentration measurements made in the water channel were in the range of 0.1g/ℓ to 2g/ℓ. The lowest concentration measured was that of the tap water in the channel which had an equivalent concentration of 0.15g/ℓ NaCl. The mean concentration at the channel surface for the closest measurement station was less than 1.0g/ℓ. Also, from the measured concentration flucuations no peak concentration over 2.0g/ℓ was observed. Therefore, all voltage measurements resulted from concentrations that were within the linear range.

4.5 Dynamic Calibration of Detector

Dynamic calibration was necessary to determine how the detector would respond to rapidly changing concentrations. The electronic circuitry could respond up to 3000Hz, so the frequency response of the detector was limited by how fast the probe could respond to a change in concentration. The response time of the probe is determined by its spatial resolution and tip flushing time. To visualize this, consider the probe passing through a step change in

concentration. The probe will pass into the new concentration level but the proper output voltage will not be reached until the sample volume is completely flushed out and replaced with the new concentration fluid. The time this takes is dependent on the size of the sample volume, the speed at which the spatial variation in concentration is convected past the probe and the stagnation flow field created by the shape of the probe tip.

Frequency response is the attenuation of sinusoidal inputs, at different frequencies, due to the sensor response time. The obvious way to determine frequency response is to input a known amplitude sinusoidal variation at a given frequency and measure the amount that the instrument attenuates the input amplitude. By repeating this for different frequencies, the relationship between attentuation and frequency can be determined. For the conductivity detector the inputs would be to subject the probe to a sinusoidal spatial variation in concentration convected past the probe at different frequencies. Unfortunately, such a test is virtually impossible to carry out, so the concept of a transfer function has to be used to determine frequency response.

A transfer function of a given system is the ratio of the Laplace transforms of the output function to the input function. Once the transfer function is known, a simple substitution of a quantity into the function results in the attentuation-frequency relationship. To determine the

transfer function of the detector, the probe has to be subjected to a known input and then the output has to be measured.

The input function to the conductivity detector is to subject the probe to a known spatial variation in concentration. The simplest and most practical spatial variation is a step change in concentration. Due to molecular diffusion a stationary razor-sharp interface is nearly impossible to achieve. The key in achieving a sharp and stable interface is to have the saltwater in motion relative to the freshwater. A sharp interface was created by flowing a 50g/ℓ NaCl saltwater solution up a tube which was immersed in fresh water. When the saltwater reached the top of the tube it simply flowed over the edge. The relative motion of the saltwater past the freshwater resulted in a stable interface. Also, because there was a constant supply of new saltwater at the top of the tube, molecular diffusion could not smear the interface. To determine the output function, the probe was simply lowered through the interface and the detector output was recorded.

Figure (4.5) shows a schematic of the system used to subject the probe to the sharp interface and measure the detector output. The probe was lowered through the interface at a constant velocity by attaching it to a line that was spooling off a constant speed rotating drum. The speed of the motor was varied, allowing the output response to be measured over a range of probe velocities. The probe

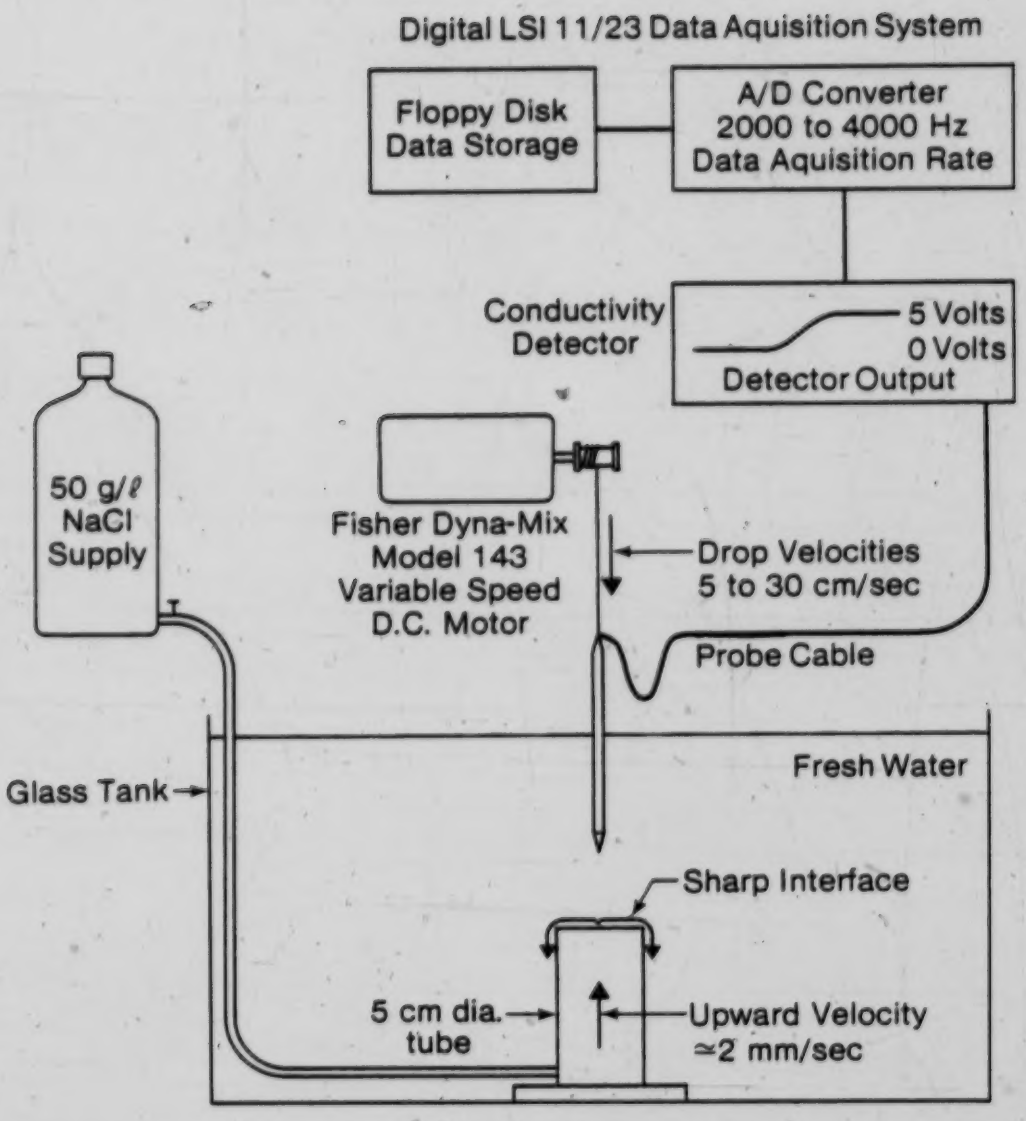

Figure 4.5 Test apparatus to measure dynamic response of conductivity probe.

velocities chosen were 5 to 30 cm/sec, which were the mean velocities that the probe would be subjected to in the water channel. The output voltage of the conductivity circuit was digitized at 2000 to 4000Hz (depending on probe velocity) as the probe passed through the interface. The digitized data was then recorded on floppy disk to facilitate future analysis.

A typical response output of the detector is shown in Figure (4.6). The dotted line is the measured detector response for a probe velocity of 18.0 cm/sec. From the solid line it is seen that the detector response can be modeled quite accurately as a simple first order system with time constant, τ,

$$\frac{E}{E_{max}} = 1 - \exp\left(\frac{-t}{\tau}\right) \qquad (4\text{-}2)$$

where

E = detector output voltage

E_{max} = steady state voltage in 50g/ℓ NaCl solution

τ = detector time constant (dependent on probe velocity)

t = time

The value of the time constant, τ, was determined by trying different values of τ in equation (4-2) then choosing the one that appeared to produce the best fit. Using this method

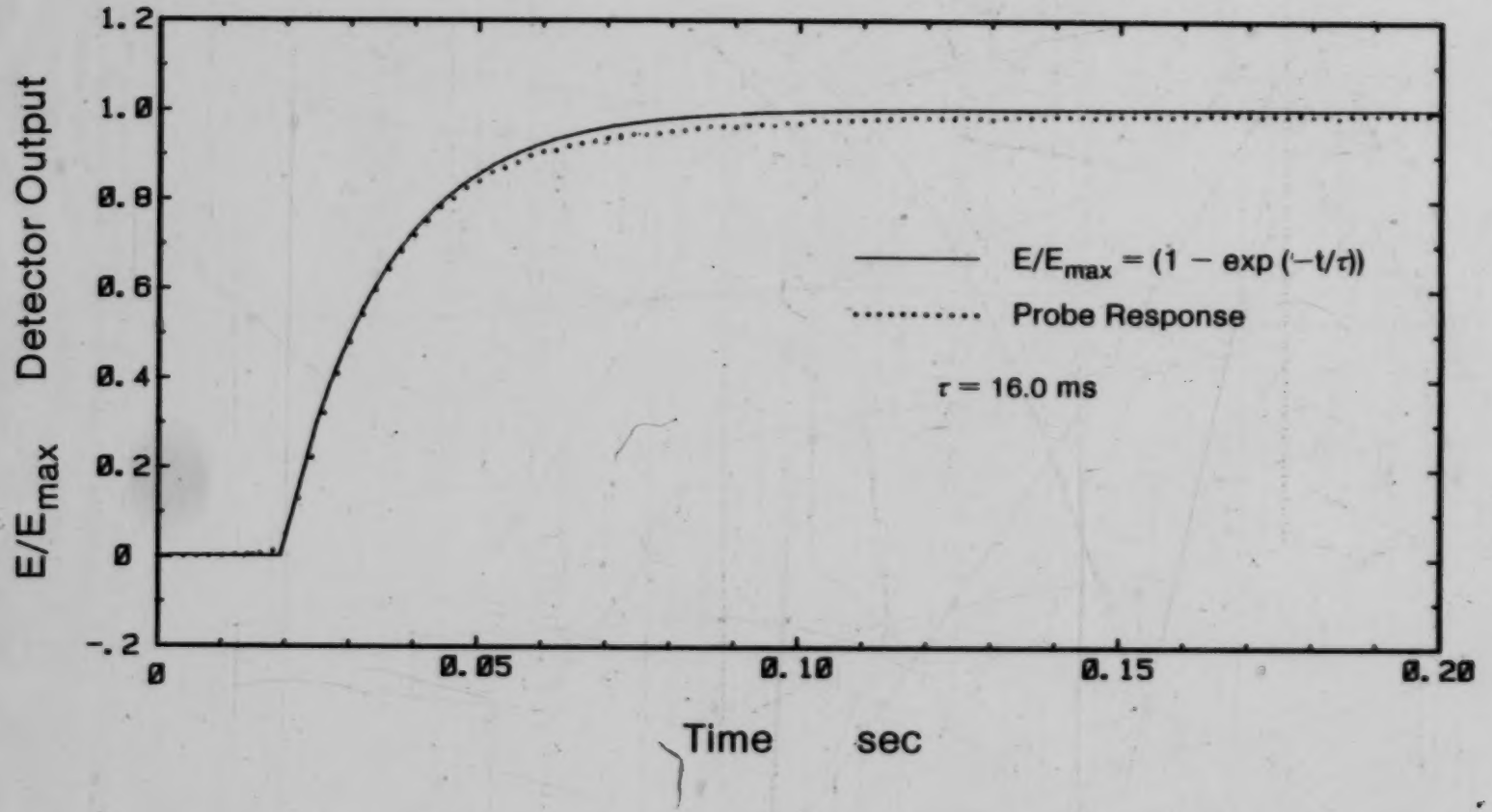

Figure 4.6 Measured response of conductivity probe to a step change in concentration for a probe velocity of 18.0 cm/sec.

a "best fit" τ was determined for each of the tested probe velocities.

The step change in concentration is equivalent to the following voltage input function,

$$E = 0 \text{ for } t < 0$$
$$E = E_{max} \text{ for } t \geq 0 \qquad (4\text{-}3)$$

Taking the Laplace transform of equation (4-2) and dividing it by the Laplace transform of equation (4-3) results in the system's transfer function

$$T(s) = \frac{1}{1 + s\tau} \qquad (4\text{-}4)$$

Where s is a complex quantity.

The frequency response is the magnitude of equation (4-4) when $s=j\omega$ ($\omega=2\pi f$, $j=\sqrt{-1}$). This results in the frequency response gain function

$$G(f) = \frac{A_{in}}{A_{out}} = \frac{1}{\sqrt{1 + (2\pi f \tau)^2}} \qquad (4\text{-}5)$$

where

G = system gain

f = frequency

τ = detector time constant

A_{in} = sinusoidal input with amplitude A_{in}

A_{out} = sinusoidal output with amplitude A_{out}

The frequency response in equation (4-5) is dependent on the detector time constant, τ, which is determined by the velocity of the fluid moving past the probe tip. Since the water channel has a vertical mean velocity profile the frequency response of the detector becomes slower in the slower moving fluid near the surface.

Making use of the fact that a velocity multiplied by time has the dimensions of length it is possible to define a probe response distance,

$$\ell_p = U \tau \qquad (4\text{-}6)$$

where

ℓ_p = probe response distance

U = probe velocity through interface

τ = detector time constant (dependent on probe velocity)

ℓ_p can be interpreted as the length of fluid travel necessary to flush the tip of the probe. To see if ℓ_p was truly a constant it was plotted against the probe velocity. From Figure (4.7) it can be seen that for all practical purposes ℓ_p is a constant for all probe velocities in the

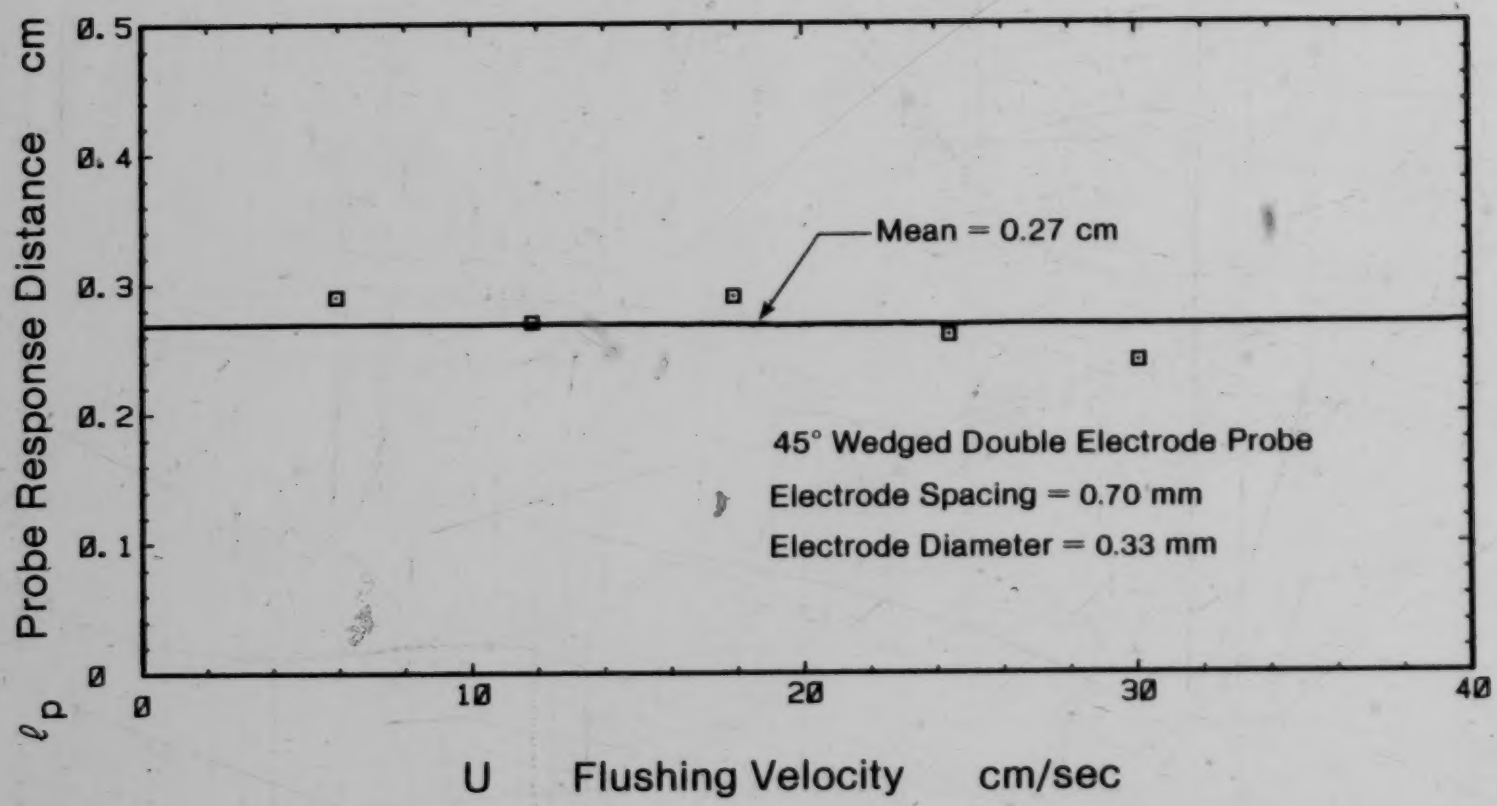

Figure 4.7 Probe response distance, ℓ_p, for varying probe flushing velocities.

tested range. Independent of velocity, the same length of fluid travel is necessary to flush the probe before it fully responds. An increased time response, at faster probe flushing velocities, only means that the same length of fluid necessary for probe flushing passes in a shorter time.

4.6 Corrections for Probe Induced Signal Attenuation

The effect that frequency dependent gain has on the concentration fluctuation, c', about the mean, can be seen by looking at the energy spectrum, $E_c(f)$, of the fluctuations. The energy spectrum is a measure of the square of the fluctuation amplitude, c', for all fluctuation frequencies present in the flow. The square of the fluctuation amplitudes will be attenuated by the square of the gain, so the "effective" energy spectrum which is measured by the detector can be expressed as,

$$E_{c,eff}(f) = G^2(f)\, E_c(f) \qquad (4\text{-}7)$$

where

$E_{c,eff}(f)$ = spectrum measured by detector

$G^2(f)$ = square of detector gain, see (4-5)

$E_c(f)$ = true energy spectrum

Since the gain of the detector is inversely proportional to

frequency, $E_c(f)$ is attenuated more at higher frequencies. The variance, $\overline{c'^2}$, of the concentration fluctuations is related to the energy spectrum, $E_c(f)$, by

$$\overline{c'^2} = \int_0^\infty E_c(f)\, df \qquad (4\text{-}8)$$

It can be inferred from equation (4-8) that due to $E_c(f)$ being attenuated the "effective" variance, $\overline{c'^2}_{eff}$, that is measured will deviate from the true variance, $\overline{c'^2}$. A way of estimating the amount of error in the measured value of variance, $\overline{c'^2}_{eff}$, is to assume that the auto time correlation of c' is exponential

$$R_c(t') = \exp\left(\frac{-t'}{T_c}\right) \qquad (4\text{-}9)$$

where

$$R_c(t') = \frac{\overline{c'(t)c'(t+t')}}{\overline{c'^2}}$$

$$T_c = \int_0^\infty R_c(t')\, dt'$$

$R_c(t')$ = auto time correlation

T_c = integral time scale of the concentration fluctuations

t = time

t' = time delay

An exponential autocorrelation of c' means that the system is inertialess, that is, knowing that c' is increasing at one instant does not indicate if c' will continue to increase or decrease the next instant. A process such as this is termed a first order or Markov process. Even though equation (4-9) is physically unrealistic, Hinze (1975) p. 66 points out that it is often a satisfactory approximation of the shape of the true autocorrelation curve.

The energy spectrum, $E_c(f)$, is defined as the Fourier cosine transform of $R_c(t')$, Hinze (1975) p. 64

$$E_c(f) = \overline{c'^2} \int_0^\infty R_c(t') \cos(2\pi f t') \, dt' \qquad (4\text{-}10)$$

Substituting equation (4-9) into equation (4-10) and integrating results in the Markov spectrum for a first order process,

$$E_c(f) = \frac{4 \overline{c'^2} T_c}{1 + (2\pi f T_c)^2} \qquad (4\text{-}11)$$

Hinze (1975) p. 66 points out that the Markov spectrum appears to approximate measured spectrum curves quite satisfactory, particularly at low frequencies. The

unrealistic part of equation (4-11) is that it predicts that $E_c(f) \propto f^{-1}$ at very high frequencies. This is of course untrue since the concentration eddies cease to exist at some finite upper frequency, and $E_c(f)$ dies away more rapidly than f^{-1} at high frequencies.

An estimate of the spectrum measured by the conductivity detector is obtained by substituting equations (4-5) and (4-11) into equation (4-7). This results in,

$$E_{c,eff} = \left[\frac{1}{1 + (2\pi f\tau)^2}\right]\left[\frac{4\,\overline{c'^2}\,T_c}{1 + (2\pi f T_c)^2}\right] \qquad (4\text{-}12)$$

An estimate of the "effective" variance, $\overline{c'^2}_{eff}$, that the detector measures is simply

$$\overline{c'^2}_{eff} = \int_0^\infty E_{c,eff}(f)\,df \qquad (4\text{-}13)$$

By substituting equation (4-12) into equation (4-13) and noting that the true variance, $\overline{c'^2}$, appears in equation (4-12) results in the following relation between the measured and true variance,

$$\frac{\overline{c'^2_{eff}}}{\overline{c'^2}} = \int_0^\infty \left[\frac{1}{1 + (2\pi f\tau)^2}\right]\left[\frac{4T_c}{1 + (2\pi f T_c)^2}\right] df \qquad (4\text{-}14)$$

As shown in Appendix D, equation (4-14) can be integrated to obtain a remarkably simple correction to the measured variance of a Markov process.

$$\overline{c'^2} = \left[1 + \frac{\tau}{T_c}\right] \overline{c'^2_{eff}} \qquad (4\text{-}15)$$

It is seen from equation (4-15) that the error in the measured variance depends on the detector time constant compared to the time constant of the concentration fluctuation autocorrelation.

Equation (4-15) can be expressed in another form by making use of Taylor's frozen turbulence assumption which assumes,

$$\Lambda_c = U\, T_c \qquad (4\text{-}16)$$

where

Λ_c = integral length scale of concentration fluctuations

U = mean convection velocity

T_c = integral time scale of concentration fluctuations

Using equations (4-6) and (4-16) in equation (4-15),

$$\overline{c'^2} = \left[1 + \frac{\ell_p}{\Lambda_c} \right] \overline{c'^2}_{eff} \qquad (4\text{-}17)$$

Equation (4-17) is a more useful form because Λ_c is the only variable. Λ_c increases as the surface is approached so the error in the measured variance becomes less the closer the probe is to the surface. The actual frequency response of the probe is slower as the surface is approached, but because $\ell_p \approx$ constant and Λ_c increases the percent error due to probe response is less near the surface. The improved performance of the detector near the surface makes it useful for measuring the fluctuation statistics where they are of the most concern.

In order to determine a correction for the measured variance, equation (4-17) requires that the true integral length scale, Λ_c, be known. The true concentration integral length scale can be calculated from the relationship given by Hinze (1975) p. 65,

$$\Lambda_c = \frac{E_c(0)\, U}{4\, \overline{c'^2}} \qquad (4\text{-}18)$$

where

Λ_c = integral length scale of concentration fluctuations

$E_c(0)$ = zero intercept of concentration energy spectrum

U = mean convection velocity

$\overline{c'^2}$ = true concentration variance

Since the detector can only measure "effective" values the actual length scale which is measured is

$$\Lambda_{c,eff} = \frac{E_{c,eff}(0)\, U}{4\, \overline{c'^2}_{eff}} \qquad (4\text{-}19)$$

The gain at zero frequency from equation (4-5) is 1.0 so from equation (4-7) $E_{c,eff}(0) = E_c(0)$. Substituting equation (4-17) into equation (4-19) results in,

$$\Lambda_c = \Lambda_{c,eff} - \ell_p \qquad (4\text{-}20)$$

The true length scale is simply the measured length scale minus the response distance of the probe. The probe response distance, ℓ_p, is a very useful quantity since it allows actual correction factors in equation (4-17) to be evaluated. Typical errors in variance measurements near the surface, as calculated by equation (4-17), were 1% to 2%.

It should be remembered that all corrections are based on the concentration fluctuation, c', having an exponential auto time correlation. These corrections are not exact, but do give a very good estimate of the measuring error of the

detector. More important than the magnitude of the error is the physical insight gained of how the probe's time response affects measured concentration fluctuations.

4.7 Data Aquisition and Analysis Methods

The data aquisition method for concentration fluctuations used in this study was to digitize and store the original record of concentration versus time. Because the voltage signal was linear with concentration, the raw voltage signal from the detector was saved. A schematic of the data aquisition set up is shown in Figure (2.2). The output of the detector after its final stage of amplification was fed into a 1000Hz low pass filter. This was required to eliminate the high frequency electronic noise of the detector before the signal was digitized. A Digital LSI 11/23 minicomputer, with a differential input analog to digital converter, sampled the concentration signal at 250Hz and recorded the data on floppy disk. For each measurement position in the water channel a 122.88 second time record of the voltage signal was saved. This allowed for analysis of the time series at a later date.

Before the prerecorded digitized data could be analyzed, it was corrected for background concentration. Since the tap water in the channel contains small amounts of ions, a background voltage is observed at what is to be zero input concentration. Also, the channel is a recirculating system, so the background concentration continues to rise as

salt ions are continuously injected into the flow. Due to the small volume of tracer being injected at a constant rate during each measurement, the increase of background concentration is linear with time. To correct for background concentration a voltage reading was taken before and after each measurement. Using a linear relationship of increasing background voltage between the start and end of a measurement, the appropriate background voltage was subtracted from the recorded detector voltage. As mentioned previously, concentration was linear with voltage at the levels being measured, therefore it was possible to correct for background by simply subtracting voltages. All programs written to analyze the data read the original data from disk, corrected it for background effects and then calculated the desired statistics.

4.7.1 Calculating Intermittency

In the fringes of the plume the concentration signal spent a significant fraction of time at a level corresponding to the background concentration. The fraction of time that the plume is present at a receptor is called the intermittency, γ. For a ground level source, the intermittency varies from a value of unity in the plume core to zero in the uncontaminated fluid, outside the plume. The top illustration of Figure (4.8) shows a typical intermittent signal where detectable levels of tracer, above the background concentration, were present only about one

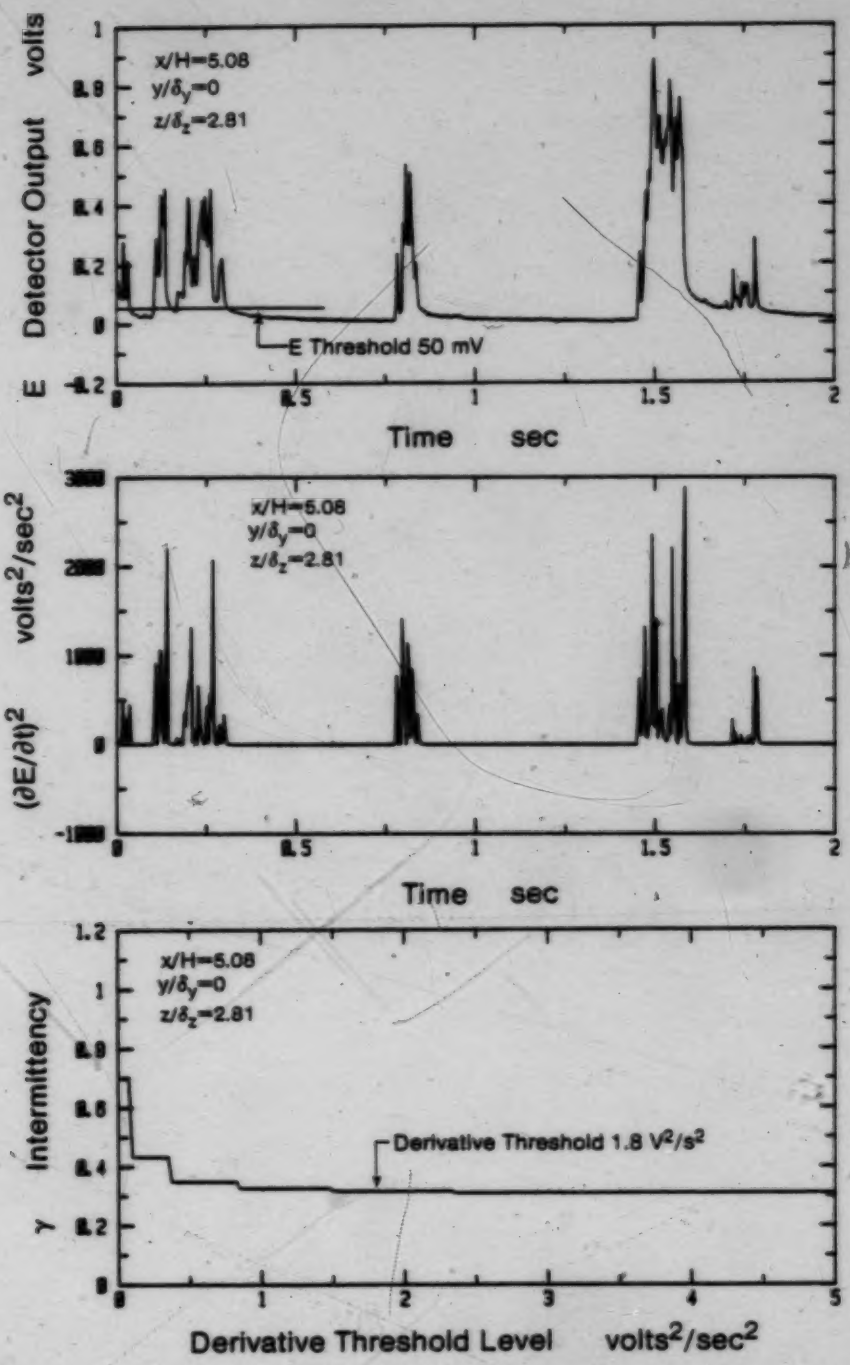

Figure 4.8 Intermittent concentration signal measured in water channel illustrating method used to determine intermittency factor γ.

third of the time. The signal has the background voltage subtracted.

Unlike calculating the mean and variance, and energy spectra, there exists no standard algorithm for calculating intermittency. To calculate intermittency it is necessary to determine the fraction of time that the concentration is zero. However, determining if the signal is at zero concentration is not a trivial task. Because of electronic noise, probe response time and background voltage corrections, the signal did not register zero volts when no plume material was present. To get around this problem a common method used is simply to set a threshold level. If the value of the signal is below this level then that value is counted as zero concentration. However, in Figure (4.8) it is seen that due to probe response, the signal slowly approaches zero after each burst of detected plume material. Therefore, when only a voltage threshold was used, the value of intermittency calculated was dependent on the threshold level chosen.

This problem was overcome by choosing two threshold levels. One threshold level was set on the voltage signal and the other was set on the square of the derivative of the voltage signal. If a digitized data point was below the voltage threshold, and the square of the derivative at the same point in time was below the derivative threshold, then the data point was taken as being at zero concentration. The second illustration in Figure (4.8) shows the square of the

time derivative of the detector output voltage signal plotted against time. The first derivative was calculated using Newton's 3 point second order central difference formula and then squared. This procedure provides an extremely sharp contrast between the areas where there is plume material and areas where the slope of the signal is very low, (i.e. where no plume is present). In effect, this compensates for the voltage decay that the probe causes after the plume boundary has moved past the probe. However, examining Figure (4.9) it is seen that for a signal in the core of the plume, where the intermittency is unity, the square of the first derivative also has flat spots. Therefore, simply counting the fraction of time the square of the derivative is below some threshold is not sufficient to determine the fraction of time no plume is present. To avoid counting flat spots in the square of the derivative, which actually resulted when the plume was present, a voltage threshold level was used.

The threshold level set on the detector output signal, after it had been corrected for the background concentration, was 50mV. This value was chosen to be slightly above the voltage decays without being above a low fluctuation peak. The threshold value set on the square of the derivative was 1.8 volts^2/sec^2. This value was based on the noise contained in the background signal as shown in Figure (4.10). The value of intermittency should be zero for this signal (since it is below the 50mV threshold), so, as

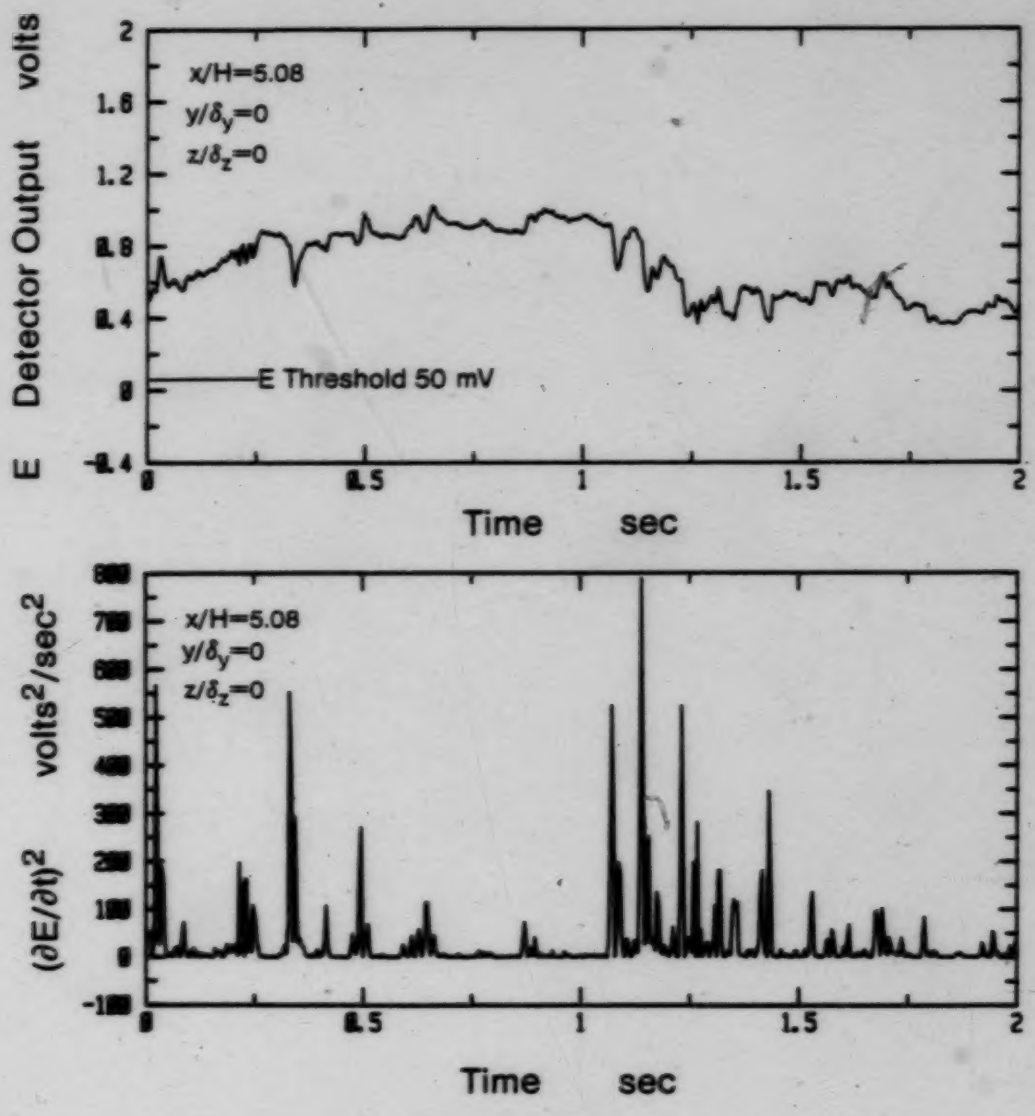

Figure 4.9 Signal with no intermittency illustrating continued existence of zeros of derivative.

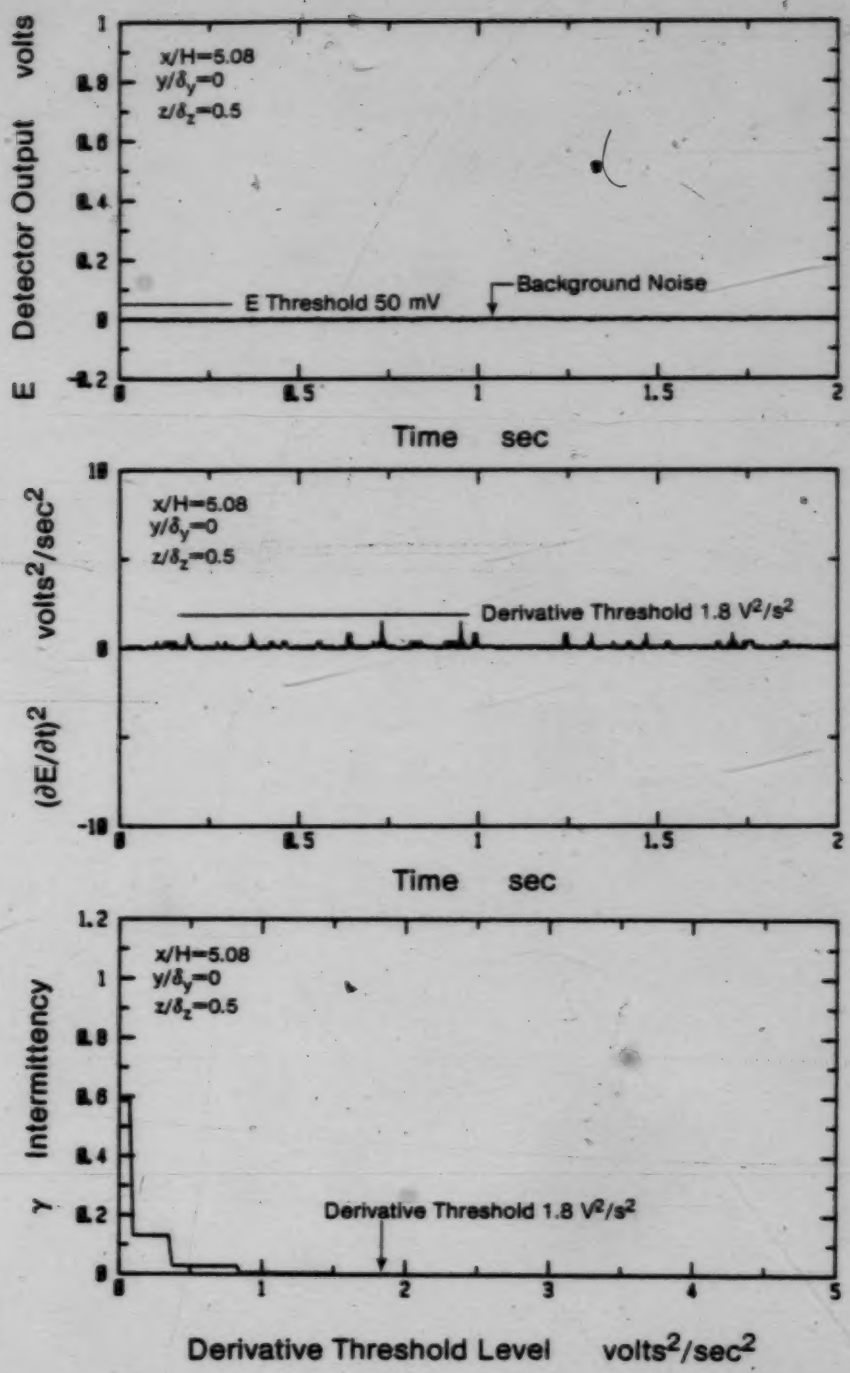

Figure 4.10 Setting threshold values to eliminate effect of background noise.

the derivative threshold level is increased, as shown in the bottom illustration, a value is reached where the correct value of intermittency is obtained.

Referring to the bottom illustration of Figure (4.8), it is apparent that using a 50mV threshold on the original signal and then increasing the derivative threshold, a constant value of around 0.3 for intermittency is obtained for values of the derivative threshold above 1.8 volts^2/sec^2. Since increasing the derivative threshold above 1.8 volts^2/sec^2 still gives the same value for intermittency, it indicates that noise is responsible for the high values of intermittency factor when the threshold level is below 1.8 volts^2/sec^2. Of course, if the threshold level is too large then the value of intermittency will start to drop off. Therefore, the constant plateau that results for a range of threshold levels means that the correct value of intermittency is obtained in that range. In the bottom illustration of Figure (4.8) it is seen that up to the end of the plot at 5 volts^2/sec^2 the intermittency is still in the constant plateau region.

The intermittency, γ, is exactly related to the total and conditional fluctuation intensities by

$$\gamma = \frac{i_p^2 + 1}{i^2 + 1} \qquad (4\text{-}21)$$

where

γ = intermittency factor

i_p = conditional fluctuation intensity

i = total fluctuation intensity

$$i_p = \frac{\sqrt{\overline{c_p'^2}}}{c_p}$$

$$i = \frac{\sqrt{\overline{c'^2}}}{c}$$

$\overline{c_p'^2}$ = conditional variance

c_p = conditional mean

$\overline{c'^2}$ = total variance

c = overall mean

The conditional statistics are calculated by excluding the periods where the concentration is at zero, (i.e. conditional statistics are only calculated when the plume is present at the receptor). When calculating i_p it is necessary to determine when the plume is present at the receptor. This was done by using the two threshold level method described previously. Using equation (4-21) and comparing it to the values of γ measured by the two threshold level method, it is seen in Figure (4.11) that the two threshold method is internally consistent.

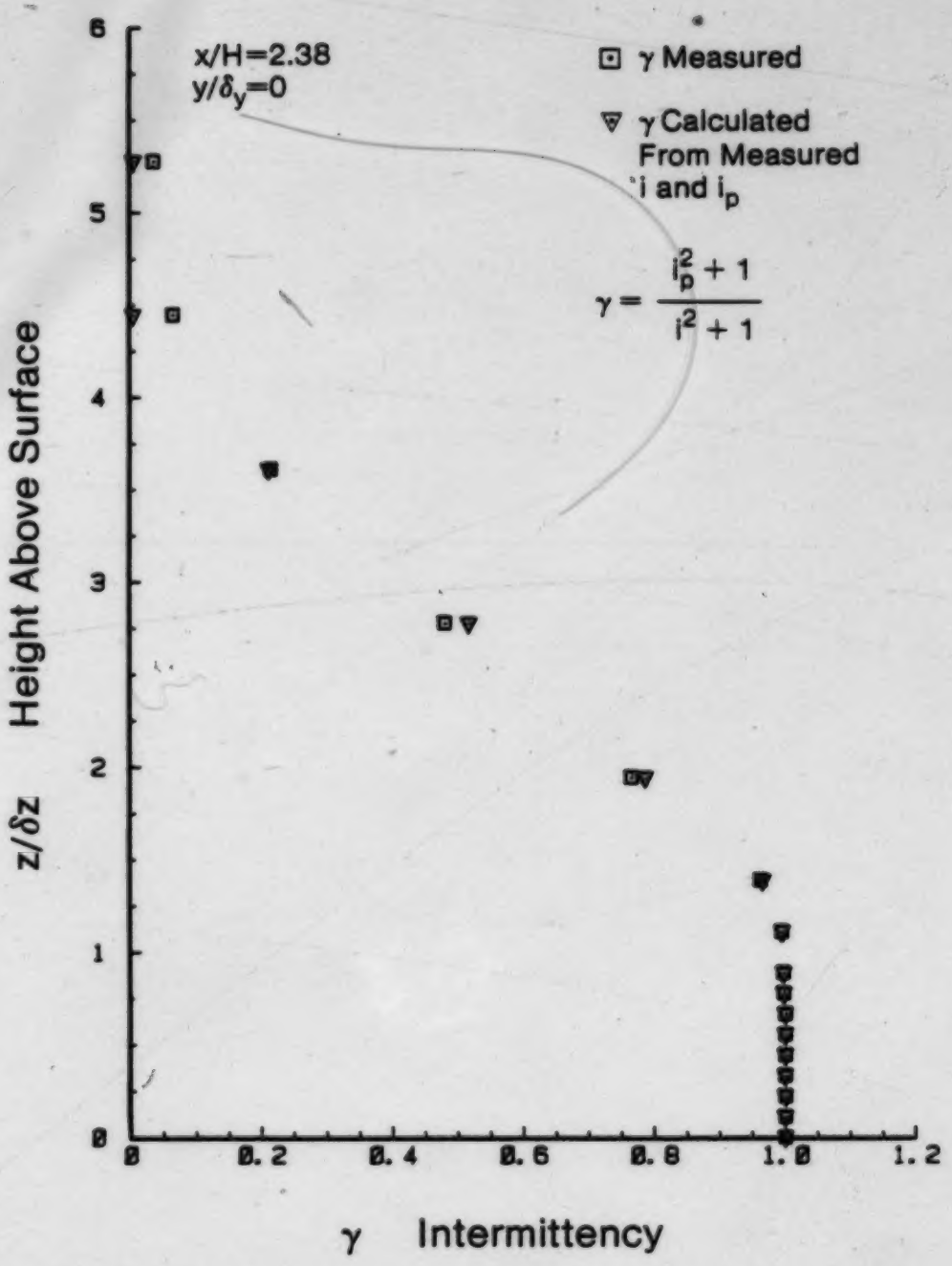

Figure 4.11 Test of closure for threshold method for determining intermittency.

5. MEAN CONCENTRATION FIELD

5.1 Introduction

The major objective of this study was to set up a model which would be able to simulate concentration fluctuations in the atmosphere. The first step in verifying if the water channel is valid for simulating concentration fluctuations is to see how it models the mean concentration field. Discrepancies in the mean field will indicate that something is fundamentally wrong with the simulation. Once confidence has been established in the mean field then the fluctuation statistics measured in the channel have some credibility. Very little full scale data exists for concentration fluctuations, therefore it is important to have this credibility if results are to be used for predictions in the atmosphere.

5.2 Analytical Theory for Mean Concentration Field

Comparing water channel measurements to dispersion thoery is a useful way of checking on the physics in the model. Good agreement between experiment and theory will build confidence in the model as well as add credibility to the theory. If the theory describes the model accurately then it should also describe the full scale situation that is governed by the same equations. However due to the variability of atmospheric conditions that control the dispersion process, care must be taken as to when the theory

will be applicable.

Robins (1978) used gradient diffusion theory to predict vertical and horizontal mean concentration profiles and rates of plume growth. His analysis was for a ground level source in a undirectional, neuturally stable boundary layer flow with a power law mean velocity profile with power n. The vertical and horizontal eddy diffusivities follow power law profiles in the vertical direction with the powers of m and k respectively. Using the conjugate power law where m=1-n and assuming that k=n Robins found an exact solution to the governing three dimensional plume dispersion equation. The mean concentration profiles for the vertical and horizontal directions yield similarity solutions of the form

$$\frac{c}{c_o} = \exp\left[-A\left(\frac{z}{\delta_z}\right)^a\right] \qquad (5\text{-}1)$$

$$\frac{c}{c_o} = \exp\left[-A\left(\frac{y}{\delta_y}\right)^2\right] \qquad (5\text{-}2)$$

where

c = mean concentration

c_o = concentration at the surface in equation (5-1)

c_o = concentration on plume centerline in equation (5-2)

z = height above surface

y = distance from plume centerline

δ_y, δ_z = plume half widths

$A = \ln(2)$

$a = 1+2n$

The theory also predicts the rates of plume growth as

$$\delta_z \propto x^t \qquad (5\text{-}3)$$

$$\delta_y \propto x^s \qquad (5\text{-}4)$$

where

x = downwind distance
$t = 1/a$
$s = (2+k-m)t/2$

In the the following sections this theory will be compared to the water channel measurements.

5.3 Mean Concentration Profiles in Water Channel and Atmosphere

Concentration measurements in the water channel were made at 5 different downstream locations from the source. At each downstream location one vertical and two cross stream profiles were measured. The vertical profile was measured at

the channel centerline and the horizontal profiles were measured at the ground surface (i.e. ground surface was at the top of the roughness elements) and at some distance above the surface. Table (5.1) summarizes the concentration mesurement locations in the water channel.

In Chapter 2 a power law profile of the form of equation (2-3) was fitted to the measured mean velocity profile in the water channel. The exponent n that was found to fit the data the best was 0.19. Using this power and applying it to equation (5-1) an exponent of a=1.38 should apply to the vertical mean concentration profile. In Figure (5.1) equation (5-1) is compared to the measured vertical mean concentration profiles from the water channel using a=1.4. Each experimental profile was normilized with a value which resulted in a "best fit" of the theoritical curve. This is the reason for some of the experimental data points at the surface not being equal to 1.0. The profiles are self similiar, and the overall agreement between equation (5-1) and the experimental data is very good. The only noticeable difference is that between the heights of z/δ_z=1.0 and z/δ_z=3.0, the experimental data has slightly larger values than equation (5-1) predicts. This type of behavior was also observed in the data of Wilson Robins and Fackrell (1982). The conjugate power law which was used in the derivation of the theory is no longer valid at heights above the constant stress region. This, plus the assumption of eddy diffusivities following power law profiles is probably the

Table 5.1 Measurement locations of concentration profiles in water channel.

Horizontal Concentration Profiles

Downstream Distance from Source	Height Above Surface	Plume Half Width δ_y
47.6cm	0cm, 0.6cm	3.41cm, 3.53cm
79.4cm	0cm, 2.0cm	4.95cm, 5.18cm
101.6cm	0cm, 2.0cm	5.53cm, 6.00cm
117.5cm	0cm, 2.0cm	6.36cm, 6.36cm
158.8cm	0cm, 3.5cm	7.06cm, 7.30cm

Vertical Concentration Profiles

Downstream Distance from Source	Distance from Channel Centerline	Plume Half Width δ_z
47.6cm	0cm	1.8cm
79.4cm	0cm	2.6cm
101.6cm	0cm	3.2cm
117.5cm	0cm	3.7cm
158.8cm	0cm	4.7cm

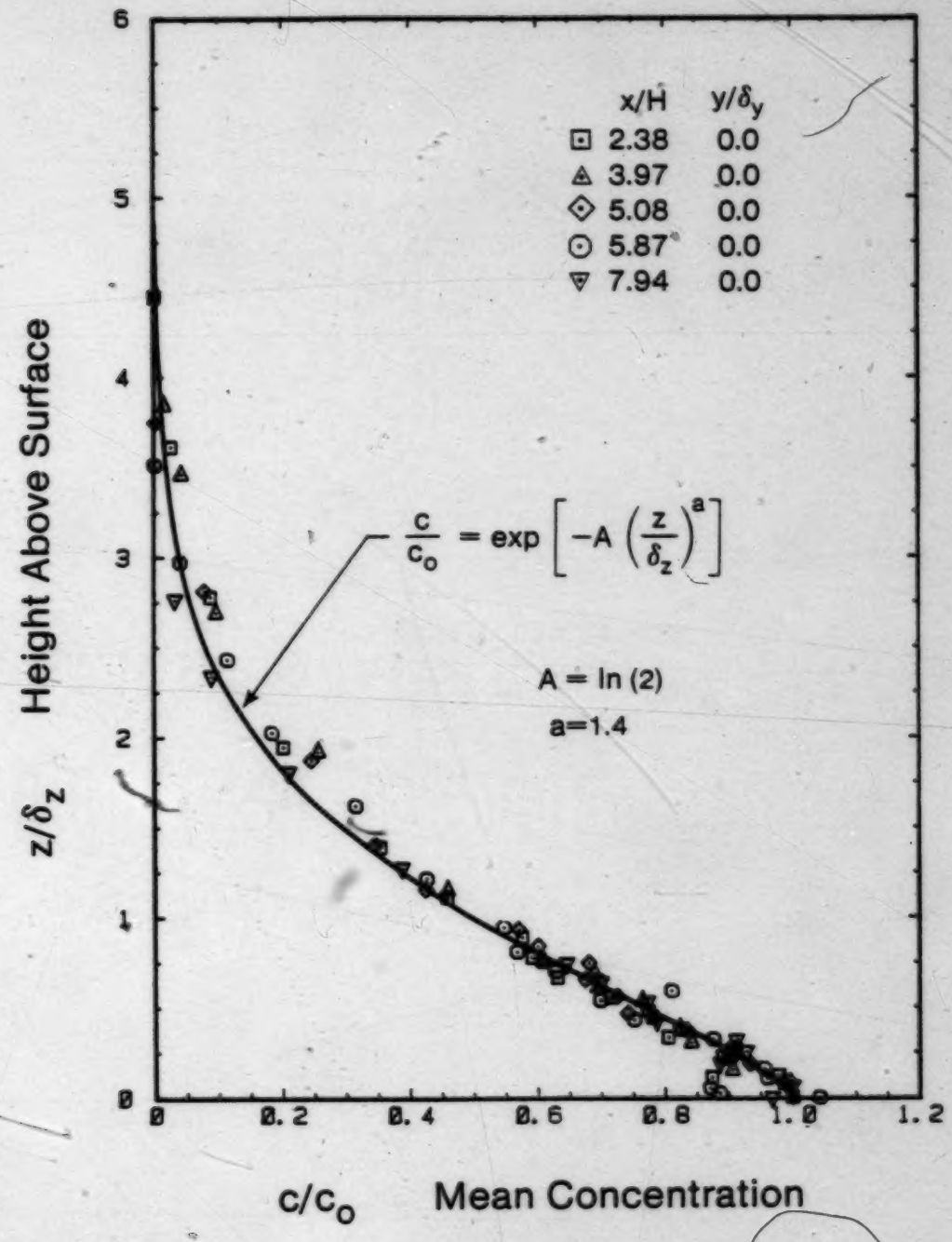

Figure 5.1 Normalized vertical profiles of mean concentration in water channel compared to equation (5-1).

cause of the slight deviation of equation (5-1) from the experimental data. However, for all practical purposes, equation (5-1) is an excellent model of the vertical mean concentration profiles in the water channel.

Pasquill and Smith (1983) p. 205 states that from the latest analysis of numerous full scale measurements the exponent, a, in equation (5-1) tends to be 1.35 for neutral flow. Also, there is a reduction in the exponent, a, during unstable conditions and a close approximation to Gaussian, with a=2.0, only in the most stable conditions. Calder (1949), (see Pasquill and Smith (1983) p. 209) uses a power law wind variation with n=0.187, determined from full scale measurements of a neutral wind over the Porton terrain, to estimate a=1.37 (i.e. by using a=1+2n). From the full scale measurements it is obvious that the water channel is a very good model for the vertical mean concentration profile in a neutrally stable atmospheric flow. Also the model verifies the full scale measurements that the vertical profile is indeed not Gaussian for a ground level source.

Figures (5.2) and (5.3) indicate excellent agreement between equation (5-2) and the measured crosswind mean concentration profiles in the water channel. Each experimental profile was normalized with a value which resulted in a "best fit" of the theoritical curve. This accounts for some of the normalized experimental data being greater than 1.0. This method was chosen over using experimental centerline values for normalizing since error

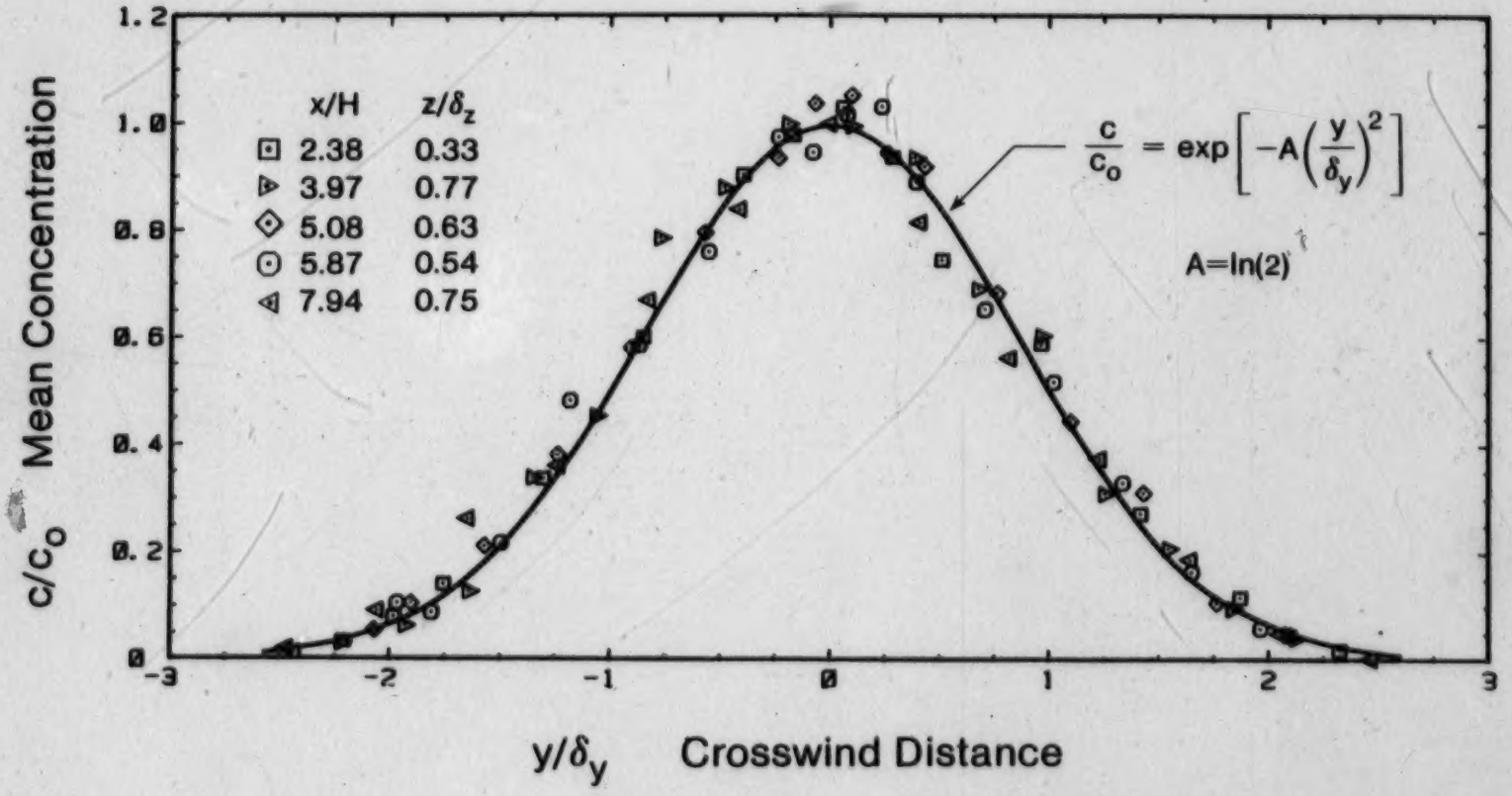

Figure 5.2 Normalized crosswind mean concentration profiles measured above ground surface compared to equation (5-2).

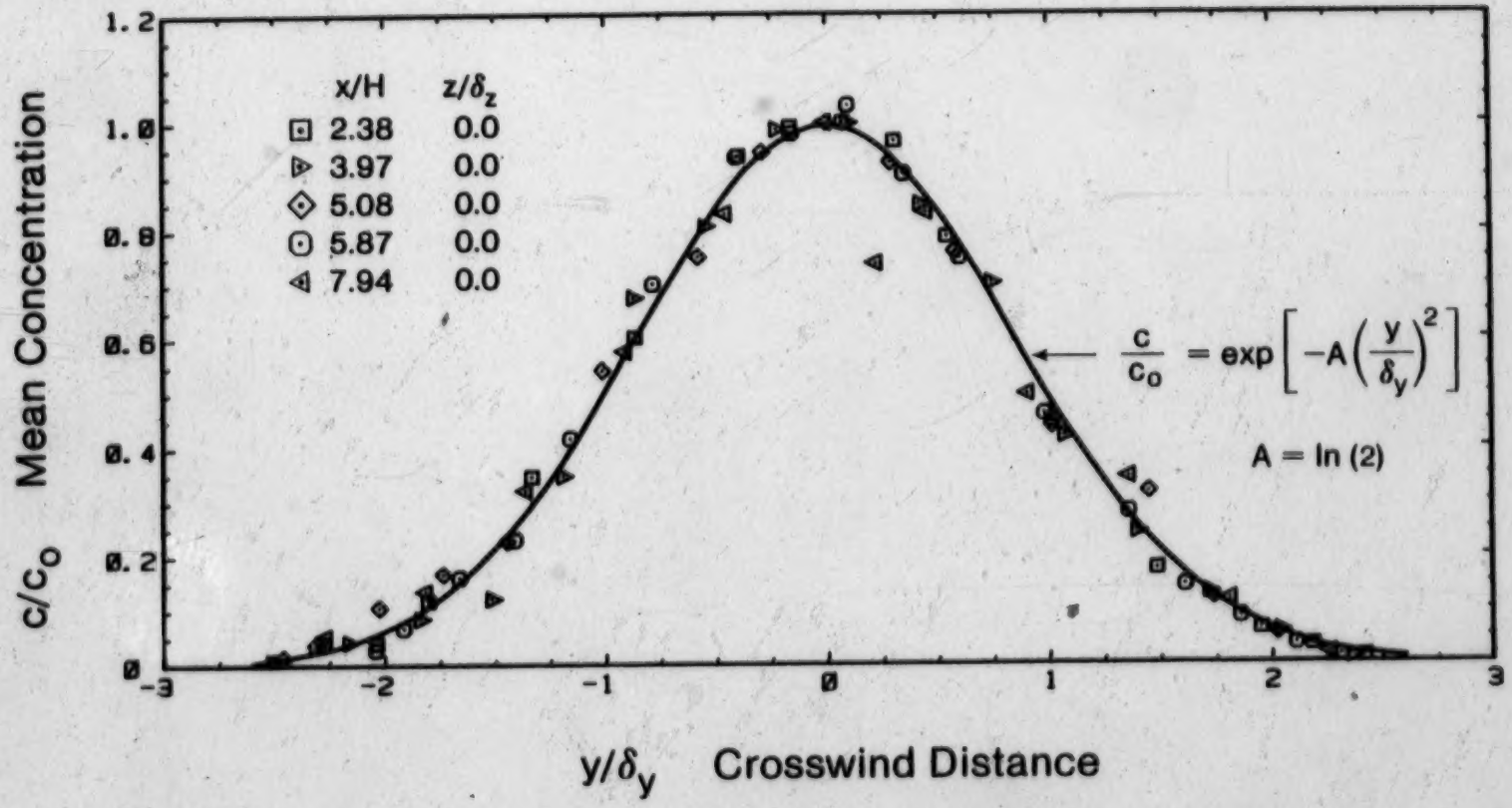

Figure 5.3 Normalized crosswind mean concentration profiles measured at ground surface compared to equation (5-2).

in a centerline value will affect the entire normalized profile.

The crosswind profiles in the water channel are also self similar. Robins (1978) also found from wind tunnel measurements that the horizontal mean concentration profiles followed a Gaussian, and Pasquill and Smith (1983) p. 189 suggests that for a ground level source in level open country a Gaussian profile is a good description of atmospheric measurements.

5.4 Rates of Plume Growth in Water Channel

In the last section the theoretical variation for the mean concentration profiles and the experimental data in the water channel and full scale atmosphere were all in very good agreement. Even though the profile shapes are in good agreement, this does not imply similarity of the geometry between the plume widths σ_y and σ_z in the model and full scale. From Chapter 3, equations (3-1) and (3-2), put in a general form, give the plume spreads as $\sigma=B_1x^d$. For homogeneous turbulence the exponent, d, changes both in the crosswind and vertical directions as the size of the plume increases compared to the size of eddies causing dispersion. In a shear layer the turbulent velocity scale increases with height above the surface, so for a ground level source the effective scale causing dispersion increases with x as σ_z spreads upward. In this special case it could then be possible for the vertical spread exponent, d, to actually

remain constant with x. However, for describing atmospheric plume spreads, it is common practice to neglect any variation of d with x and use an x dependent form with a constant value for the exponent, d.

For the vertical spread given by equation (5-3) a value of t=0.725 is found using the power n=0.19 for the velocity profile from the water channel. Using the functional form $\delta_z=B_1x^{0.725}$ the constant, B_1, was adjusted to produce a visual best fit to the water channel data. No correction was made for a virtual origin due to the size of the source or for the laminar jet from the source. Introducing a shift due to a virtual origin will cause the exponent, d, to change, so the experiments are not an absolute verification of the theory. The solid line in Figure (5.4) indicates that the theoretical value of t=0.725 agrees well with experiment. Fackrell and Robins (1982) point out that simple gradient-transfer theory is adequate to describe the vertical dispersion from a ground level source. Because the vertical scale of the plume always exceeds that of the turbulence, dispersion progresses in a "far-field" manner. This is not the case for elevated sources or for crosswind dispersion from sources at any height. The theory gives an accurate description for vertical dispersion in the water channel but does not indicate how the channel relates to the atmosphere.

Pasquill and Smith (1983) p. 338 provides general x dependent power law extimates of vertical spread, σ_z, based

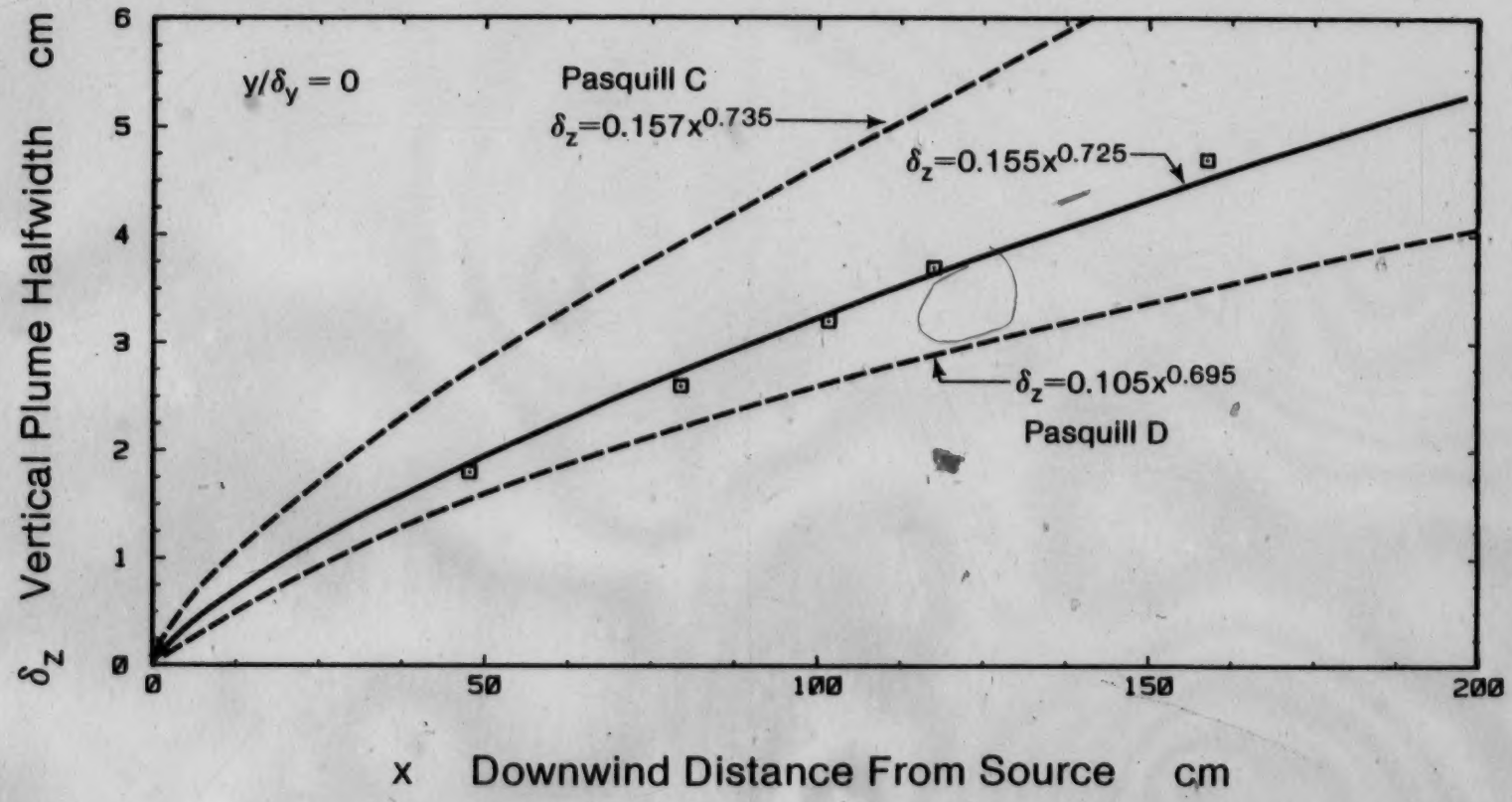

Figure 5.4 Vertical plume spread in water channel compared to Pasquill category C and D plume spreads.

on 3 minute averaging times for a full scale ground level source, depending on the stability of the atmospheric flow and the surface roughness z_o. Using 0.7m as the scaled up value of z_o from the water channel in 3000:1 and $\delta_z=0.884\sigma_z$, which applies when the power, a, in equation (5-1) is 1.4, the half-width plume spreads for Pasquill stability classes C and D were calculated. These full scale curves were then scaled to the water channel coordinates and are shown in Figure (5.4). From this it is seen that the vertical spread in the water channel corresponds to slightly unstable atmospheric conditions. This same slightly unstable behavior was observed in the laboratory flow of Robins (1978) and also in the elevated source experiments carried out in a wind tunnel by Netterville (1979). The water channel is consistent with other laboratory flows indicating that it is a good model for vertical spread in a nearly neutral flow.

The full scale plume spreads were scaled to the water channel based on a full scale boundary layer thichness of 600m. The actual height of a neutrally stable atmospheric boundary layer can vary ±50-100m from the 600m value suggested by Counihan (1975). However, the resulting change in scale factor due to a varying atmospheric boundary layer height has negligible effect on the scaled plume spreads. An extreme change in scale from 3000:1 to 6000:1 or 1500:1 will only result in a ±20% change in the δ_z value of the 3000:1 transformation. Therfore the measurements of vertical plume spread in the channel are applicable over a wide range of

atmospheric boundary layer heights.

From an evaluation of the exponent, s, in equation (5-4) the lateral plume spread is proportional to $x^{0.5}$. A good fit was obtained to the lateral water channel data using this theoretical square root variation. The $x^{0.5}$ curve fits the data quite well except for the points closest to the source, as shown in Figure (5.5). This deviation of the theoretical curve from the data may be attributed to a virtual origin shift or to the fact that at this close distance the spread occurs with a power greater than 0.5. At the larger downwind distances the square root variation which occurs for the spread is the lower limit predicted by the statistical theory of dispersion. This 0.5 power implies that the plume is large as compared to the integral scale, Λ_v, of crosswind turbulence. Near the surface where the measurements were taken the velocity scales are small so the 0.5 power for the spread is not unrealistic.

It is difficult to compare the water channel crosswind spread to the full scale atmosphere. The atmospheric wind is not contained between side walls like the channel flow, so more plume meandering occurs in the atmosphere. As a result, crosswind spreads, σ_y, in a near neutral atmosphere are typically proportional to $x^{0.8}$ (see Pasquill and Smith (1983) p. 194). A proper comparison would require a measurement of the steady state plume spread for a unidirectional wind. Due to the time variability of the atmospheric wind it is impossible to achieve a long enough

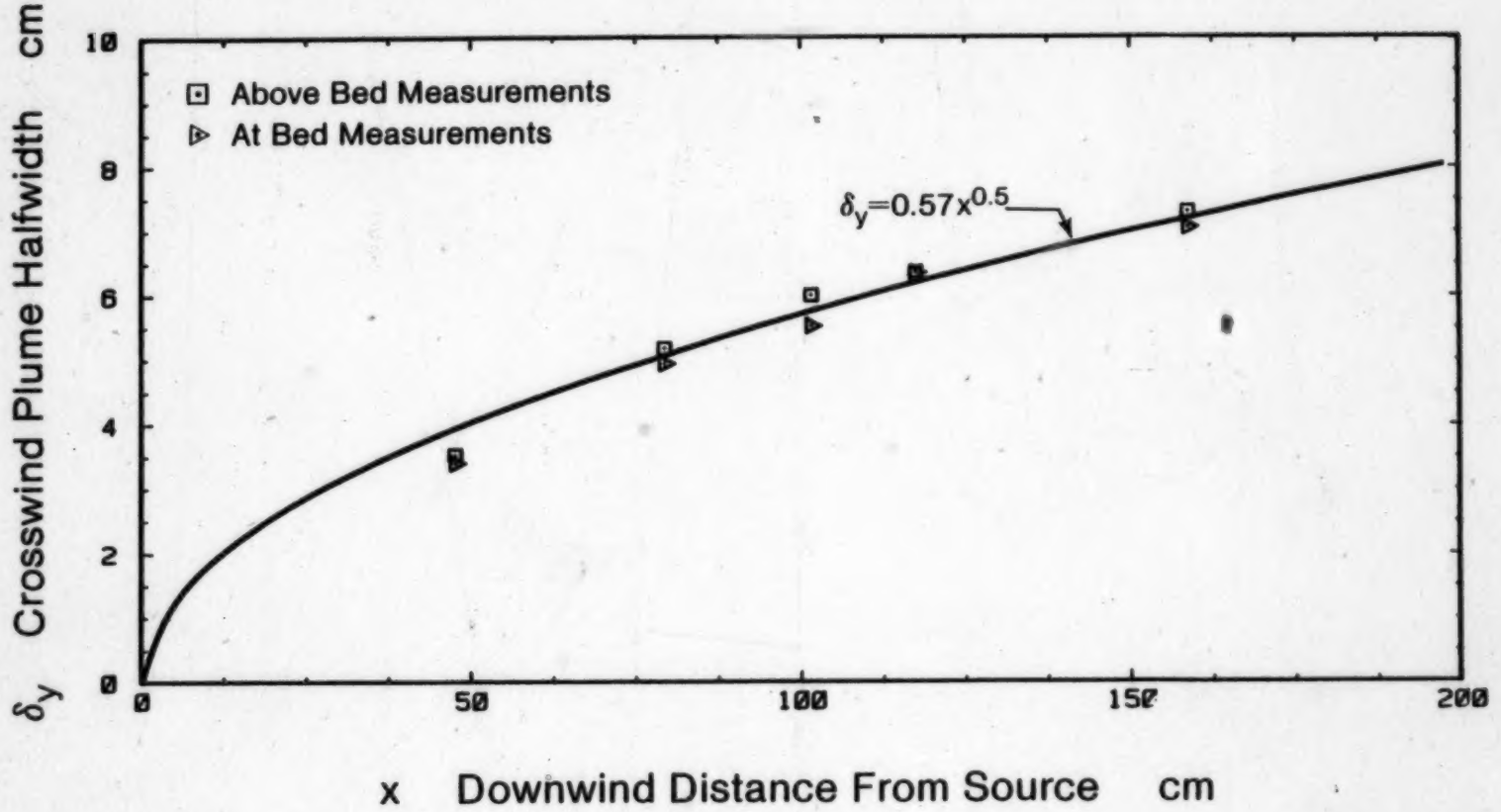

Figure 5.5 Comparison of measured crosswind plume spread with theory, equation (5-4).

sample time under these conditions.

It is common to associate the water channel spreads with short sample times in the atmosphere where the wind direction remains relatively constant. However, care must be taken when doing this because the water channel spreads are a steady state measurement as compared to a short sample time of a unidirectional wind which is not a steady state measurement.

5.5 Summary

The way in which the dispersion theory of Robins (1978) fits the water channel data indicates that the experimental system is a good simulation of unidirectional, fully developed turbulent flow over a rough surface. The vertical plume spread in the channel is a good model of the vertical spread in a near neutral atmosphere, which leads us to expect that the fluctuation statistics should also be representative of the full scale. Crosswind plume spread in the channel is difficult to compare to the full scale, so caution must be taken if applying the horizontal fluctuation statistics to the atmosphere. However, the model is physically sound and should be a valuable insight into the physics of the fluctuating concentration field in the atmosphere.

6. FLUCTUATING CONCENTRATION FIELD

6.1 Introduction

A knowledge of the concentration fluctuations that occur at a downwind receptor, is necessary when dealing with pollutants that can have damaging effects on life forms over a short time of exposure. As seen from the intermittent signal in Figure (1.1), it is the intermittent peaks of concentration that are the concern.

The key to understanding these peak concentrations lies in the concept of intermittency. Intermittency, γ, as given in equation (4-21), is defined as the fraction of time that source material is present at the receptor. Turbulent velocity scales larger than the size of the plume cause the plume to meander back and forth past a receptor resulting in periods of zero concentration. Lateral velocity scales are much larger than vertical scales, so intermittency is mainly caused by horizontal meandering and to a lesser extent by vertical meandering.

For practical purposes of predicting the probablity of exposure to some harmful concentration level it is necessary to quantify statistical values of the concentration fluctuations. The overall probablity that some concentration level is exceeded is a combination of the fraction of time that a plume is present at a receptor and the probability of exceeding that concentration level when the plume is actually present. Therefore, the statistics that are

important are the intermittency and the probability distribution of the concentration fluctuations when the plume is in contact with the receptor.

Models for the probability distribution, such as the exponential and log-normal distributions used by Wilson (1982), require mean and variance of the "conditional" or "plume" statistics to define them. The conditional or plume statistics are determined by excluding the zero concentration portions of the signal. The problem that arises is that most dispersion models only predict the total statistics of the fluctuations which include the zero concentration portions. However, Wilson (1982) showed that the desired conditional statistics could be derived from the total statistics with intermittency, γ, as the only additional information required. Therefore, it is necessary to be able to model the intermittency or the conditional statistics in equation (4-21) from which γ can be determined. Other statistics may be required depending on the complexity of the probability distribution function used but for most practical applications, the additional ability to predict γ would be sufficient.

The values of intermittency measured in the water channel will differ from those in the atmosphere because of the inability of the water channel to simulate large scale meandering in the crosswind direction. Unlike the water channel, where the flow is in the direction of the receptor at all times, slow wind direction changes in the atmosphere

result in a receptor seeing the plume for a shorter time period. Because of this, water channel measurements of γ can not be directly applied to the full scale atmosphere when wind direction changes are a factor. However, the water channel measurements can be used to gain physical insights which are useful for developing models that apply to the atmosphere. The purpose of this chapter is to examine the fluctuation measurements made in the channel and to fit a theoretical model to the measurements in an attempt to gain some insight into modeling the full scale situation.

6.2 Crosswind Profiles of Concentration Variance and Total Fluctuation Intensity

A strongly bimodal distribution for concentration variance was measured at the surface in Figure (6.1). The variance has been normalized by the maximum value measured in the profile. From Csanady (1973) p. 236, the production of concentration variance, $\overline{c'^2}$, as given by his concentration variance balance equation for a slender plume is,

$$\phi_p = 2K_y\left(\frac{\partial c}{\partial y}\right)^2 + 2K_z\left(\frac{\partial c}{\partial z}\right)^2 \qquad (6\text{-}1)$$

where

ϕ_p = production of concentration variance

K_y = lateral eddy diffusivity of mass

K_z = vertical eddy diffusivity of mass

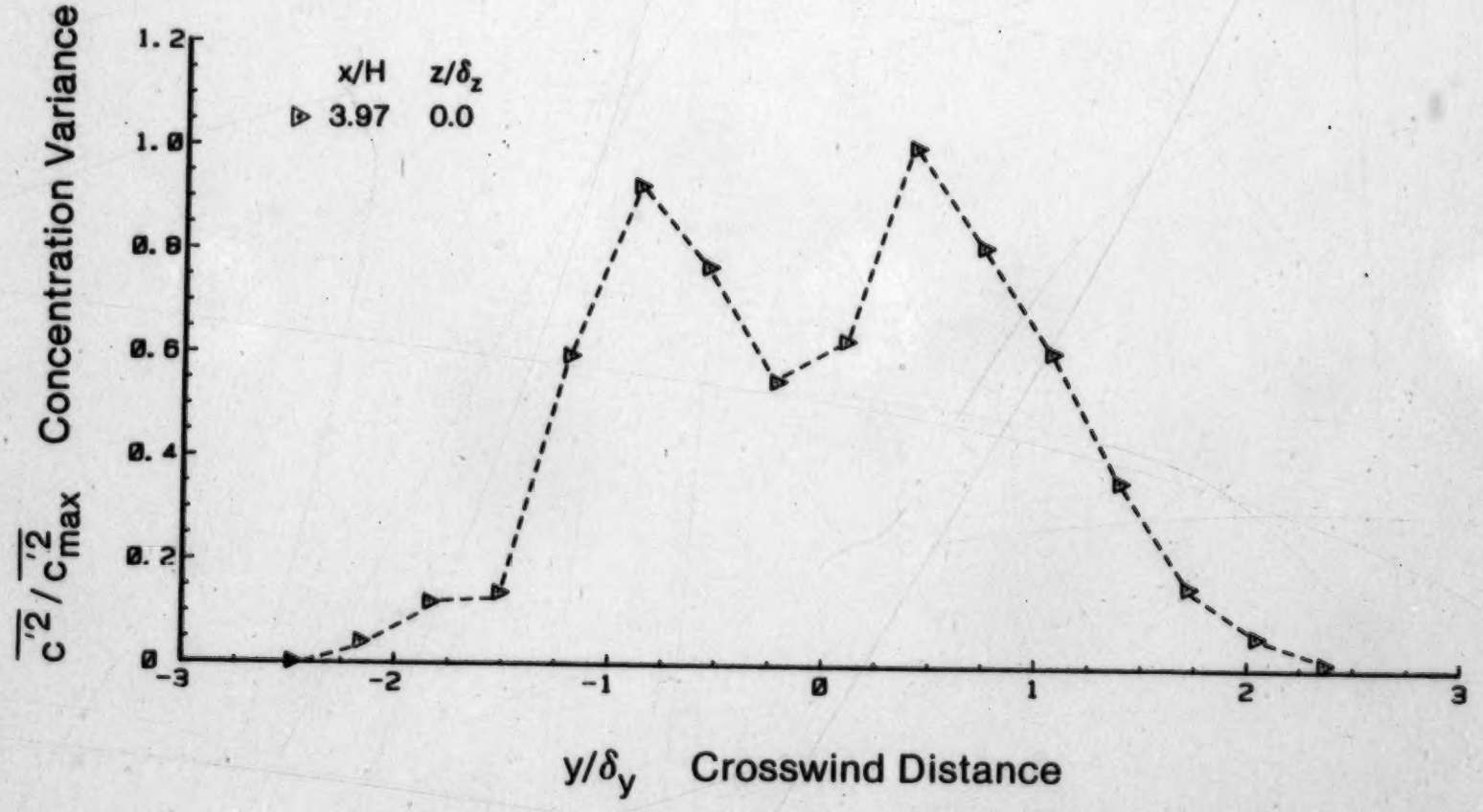

Figure 6.1 Crosswind concentration variance profile measured at the ground surface at a downwind distance of x/H=3.97.

c = mean concentration

For a Gaussian mean profile in the crosswind direction, equation (6-1) gives a maximum production at $y/\delta_y=0.85$, explaining the off-axis maximum seen in Figure (6.1). Variance measurements at the surface for the other downstream locations are shown in Appendix E. The bimodal distribution is also evident at these locations but there seems to be a tendency for it to become less pronounced as the distance from the source is increased. Wilson, Robins and Fackrell (1982) point out that most of the concentration variance is produced close to the source then redistributed in the crosswind direction and dissipated as it moves downwind. This behavior would tend to smooth out the spatial variation in the variance profile as the downwind distanced increased thus resulting in the observed behavior.

The total fluctuation intensity, I, is defined as the square root of the variance, $\sqrt{\overline{c'^2}}$, divided by the mean concentration, c. Since a model for c exists from equation (5-2) a model for I can be developed by determining a functional form to model the variance. Netterville (1979), using Csanady's (1973) variance balance equation, obtains Gaussian profiles for concentration variance, $\overline{c'^2}$, by assuming zero in plume variance production and a decay time scale for the fluctuations as exactly equal to the travel time of the fluctuations from their effective origin.

Applying this functional form to the crosswind direction results in,

$$\frac{\overline{c'^2}}{\overline{c'^2}_{smooth}} = \exp\left[-A\left(\frac{y}{\delta_y}\right)^2\right] \qquad (6\text{-}2)$$

where

$\overline{c'^2}$ = concentration variance

$\overline{c'^2}_{smooth}$ = value used for normalizing

y = distance from plume centerline

δ_y = plume half width

$A = \ln(2)$

The functional form of equation (6-2) is a totally unrealistic model of the variance profile in Figure (6.1) since it does not reproduce the bimodal behavior. Dividing the square root of equation (6-2) by equation (5-2) results in the following function for the total fluctuation intensity, i,

$$i = \sqrt{i_o^2 \exp\left[A\left(\frac{y}{\delta_y}\right)^2\right]} \qquad (6\text{-}3)$$

where

i = total fluctuation intensity

i_o = centerline value of total fluctuation intensity

y = distance from plume centerline

$\delta_{\frac{1}{2}}$ = plume half width

$A = \ln(2)$

Using a representative centerline value of i_o for all downwind profiles, equation (6-3) is compared to the measured values of i in Figure (6.2). Equation (6-3) models the measurements of i reasonably well even though the variance model of equation (6-2) was unrealistic. This indicates that i is not very sensitive to the correct modeling of the variance profile.

Variance measurements were also made above the surface and are compared to equation (6-2) in Figure (6.3). The values used to normalize each profile were obtained from a "best fit " of equation (6-2) to each profile. This was done to give a smoothed effect, since all of the profiles are presented on one curve. The measured values of variance have a broader profile than predicted by equation (6-2). This broader profile is mainly due to production of variance located off axis of the centerline, which the Gaussian profile does not include.

These measurements above the surface indicate a slight bimodal distribution, but less pronounced than the measurements at the bed. This phenomena can be explained by looking at equation (6-1). At the surface the gradient of the mean concentration on the plume centerline with respect to both y and z is zero, indicating no production of

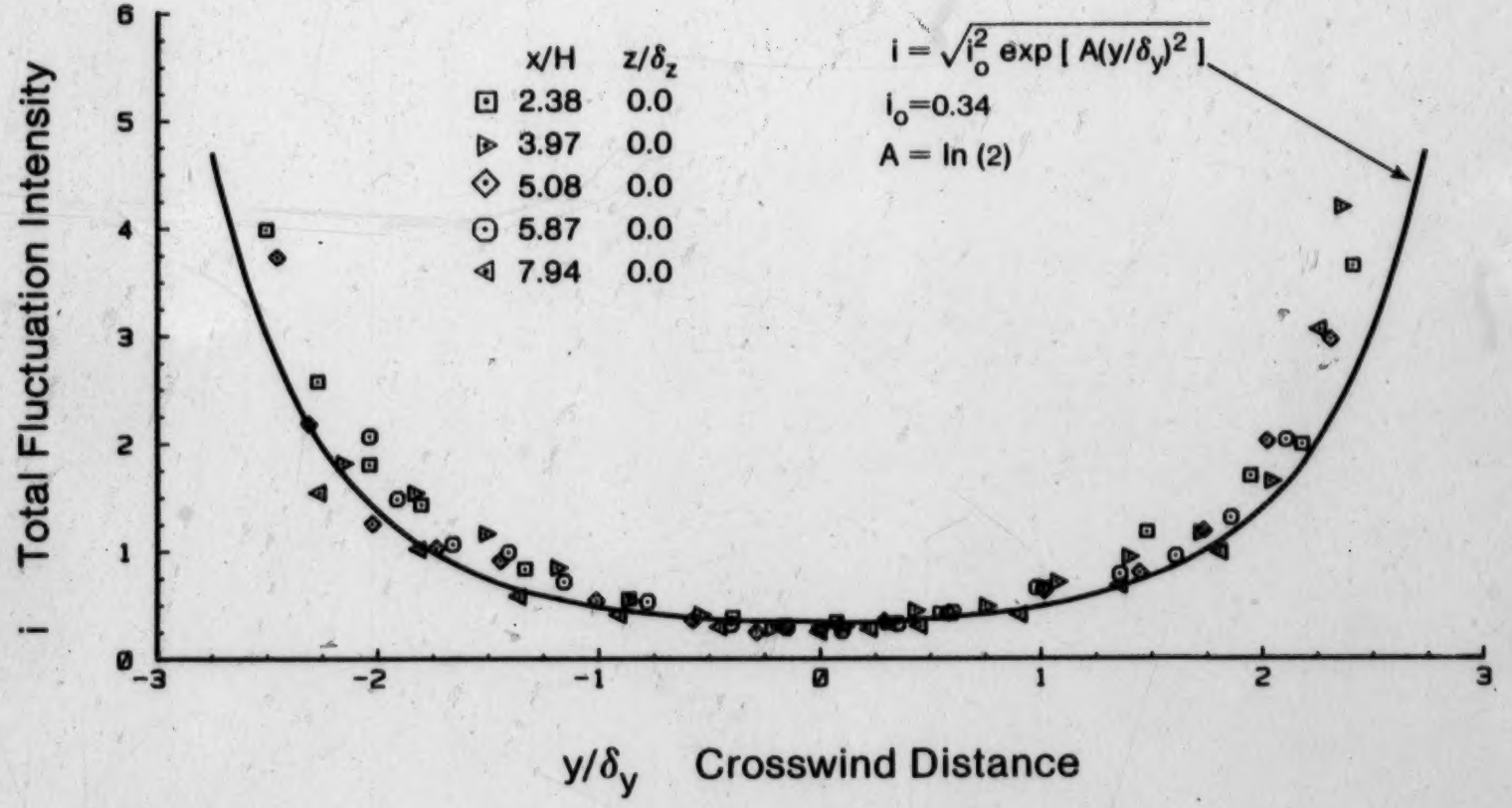

Figure 6.2 Crosswind total fluctuation intensity measured at the ground surface compared to equation (6-3).

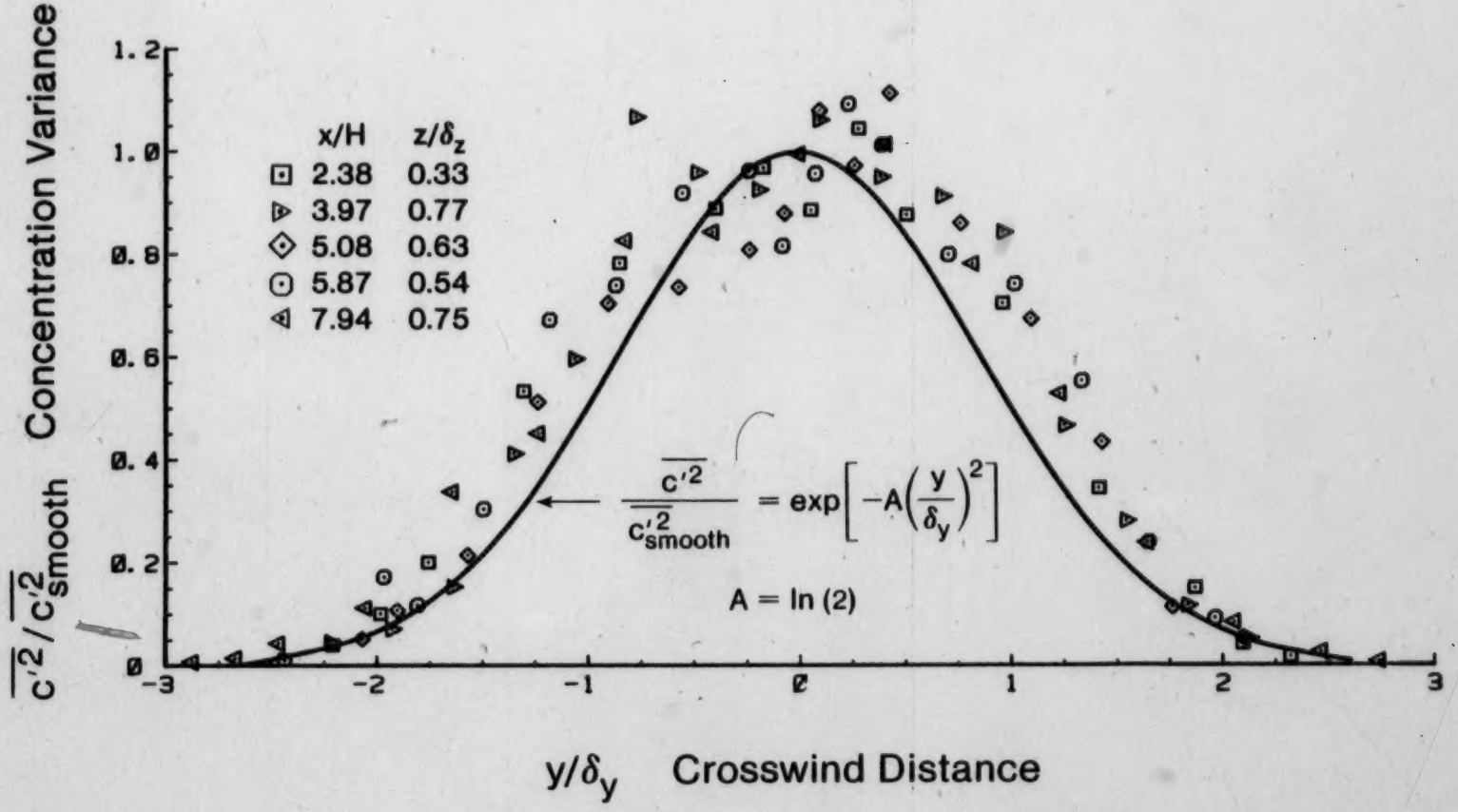

Figure 6.3 Crosswind concentration variance profiles measured above the ground surface compared to equation (6-2).

variance. Above the surface the gradient on the centerline with respect to y is still zero but the gradient of the mean concentration in the vertical direction is non-zero. This production of variance on the centerline when above the surface explains the less pronounced bimodal distribution.

It is difficult to tell how self similar the variance profiles are in Figure (6.3) due to the amount of scatter in the data. The variance profiles in Figure (6.1) and (E-1a,b,c,d) are also subject to scatter, due to not using a long enough sample duration to obtain a stable variance value. Netterville (1979) points out that stable values of concentration variance with a maximum of 1% to 2% variability require that 10^4 integral length scales of turbulence must be sampled. With a representative water channel velocity of 25 cm/sec and a turbulent velocity scale of 5cm means a sample duration of 2000 seconds is required. The actual sample duration used was 122.88 seconds which is only one twentieth of the required duration. The mean concentration values in the water channel would probably be stable but, due to the short sampling time concentration variance measurements could be subject to a ±15% to 20% error.

Equation (6-3) is compared to the measured profiles of total intensity i in Figure (6.4) using the average value of i_o measured in the channel to define the function. As in Figure (6.2), the model is again in good agreement with the measurements. Larger values of total fluctuation intensity,

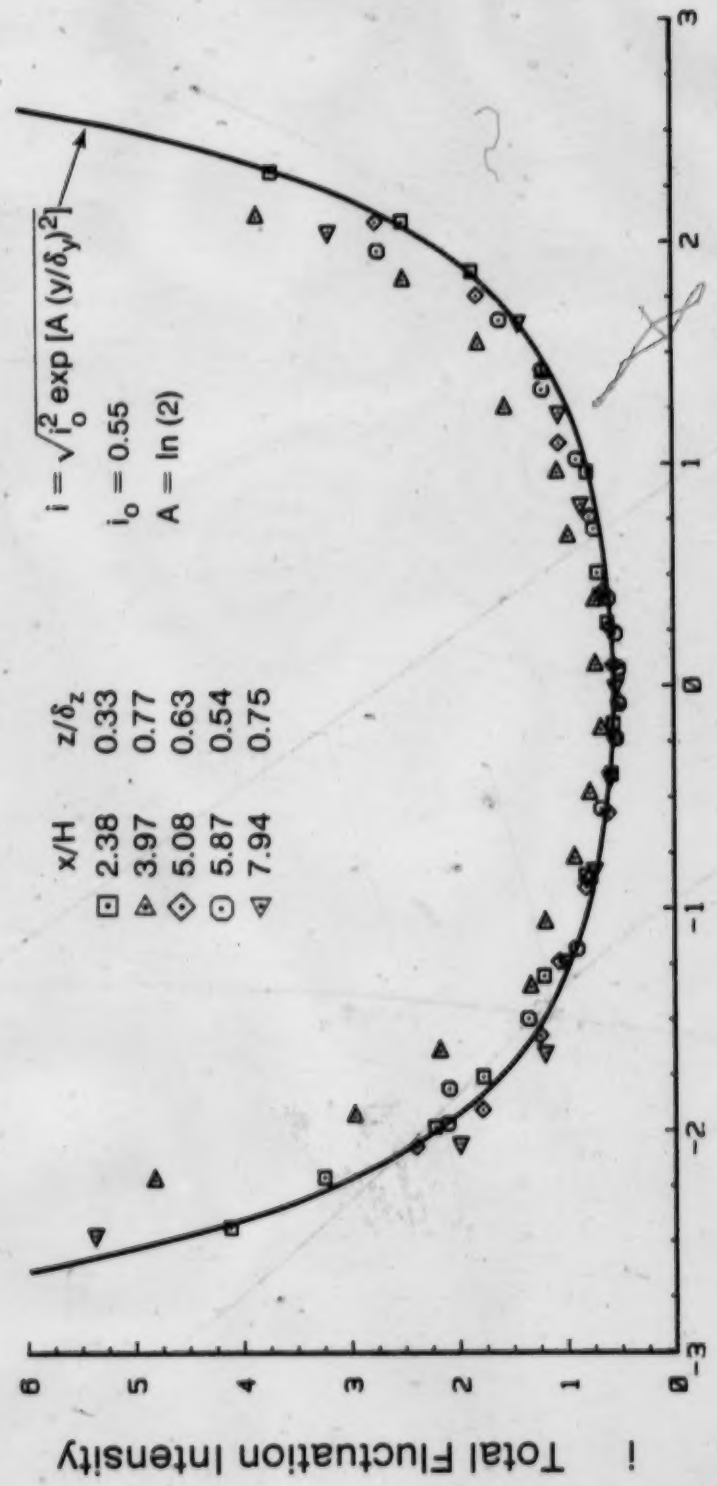

Figure 6.4 Crosswind total fluctuation intensity measured above the ground surface compared to equation (6-3).

i, were measured with increasing distance above the surface, as expected, since the concentration fluctuations are not being suppressed by the presence of a solid boundary. Another interesting point is that for a fixed distance z above the surface the plume centerline value of fluctuation intensity, i_o, remained fairly constant with downwind distance.

6.3 Crosswind Profiles of Conditional Fluctuation Intensity and Intermittency

As was mentioned previously it is essential to know the intermittency if a probability of exceeding some concentration is to be calculated. A model for intermittency, γ, can be developed directly or γ can be determined from equation (4-21) by modeling both i and i_p. Wilson (1982) models i_p in the crosswind direction by assuming that it is constant. This approach is appealing from a modeling point of view because determing γ is now a simple task using equation (4-21). However the actual variation of i_p in the horizontal direction is not a constant as seen in Figures (6.5) and (6.6). Both the ground level and above surface measurements indicate that i_p is constant only over a small central core, and increases in some instances up to 4 times its centerline value in the fringes of the plume. In fact, the only profile which is relatively constant across the entire plume is the measurement at x/H=7.94 in Figure (6.5).

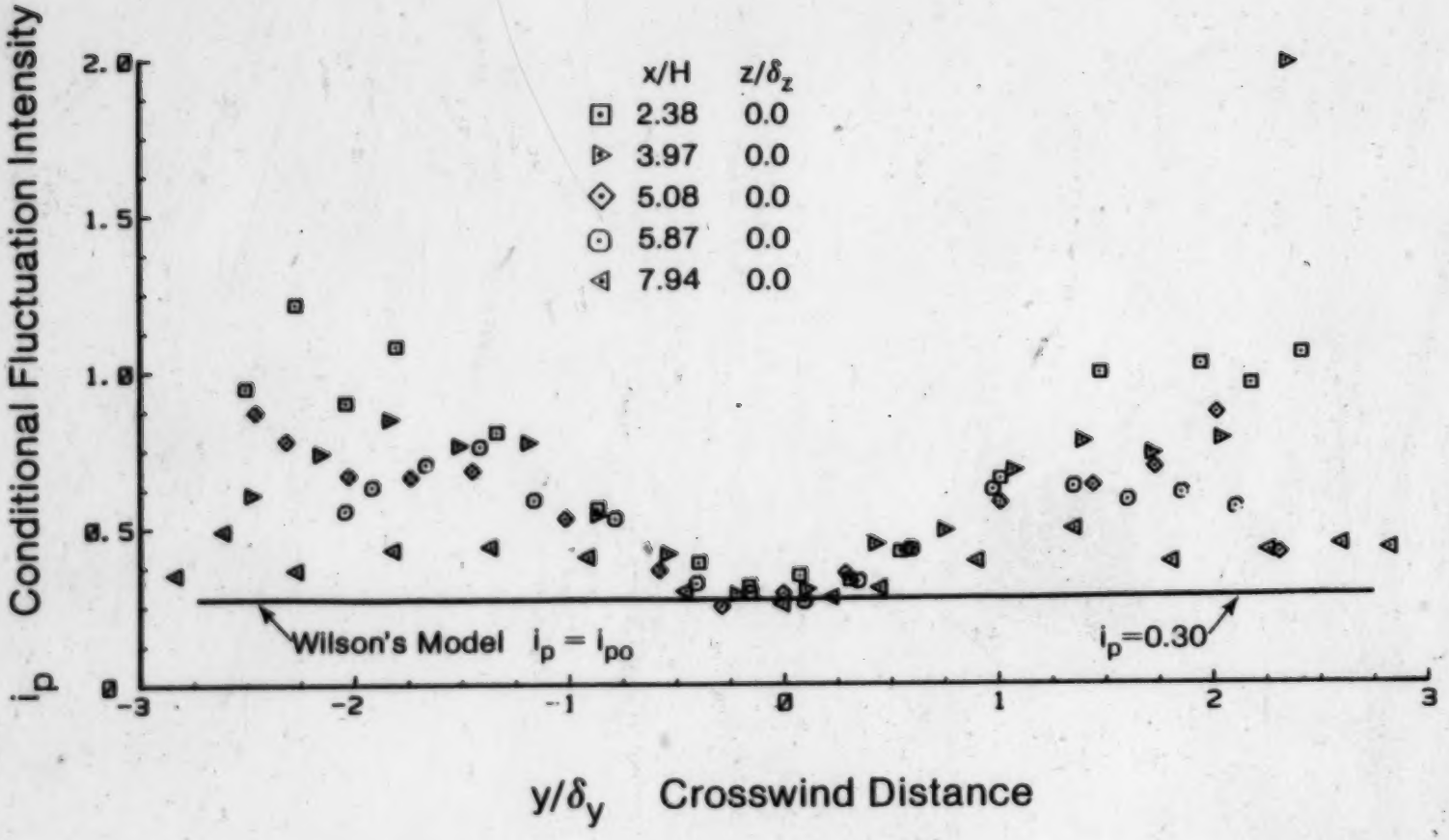

Figure 6.5 Crosswind conditional fluctuation intensity measured at the ground surface compared to Wilson's (1982) theory.

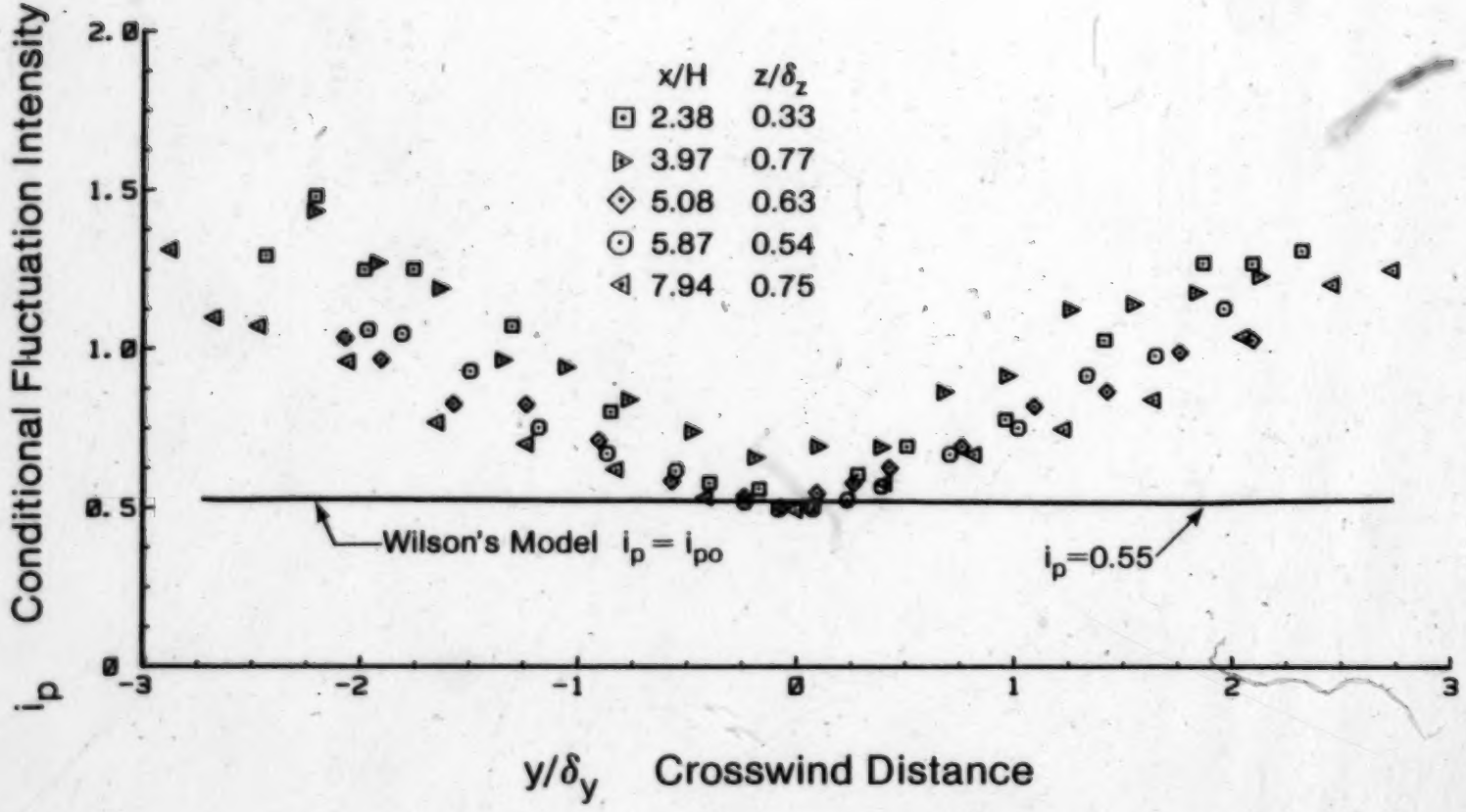

Figure 6.6 Crosswind conditional fluctuation intensity measured above the ground surface compared to Wilson's (1982) theory.

Full scale atmospheric measurements by Eidsvik (1980) also exhibited this increase of i_p in the fringes of the plume. Eidsvik's data was taken from experiments where a constant continuous source of fluorescent particles were released at 2m above the sea surface. He made measurements at approximately 0.5km downwind of the source at a height of 1.5m and found the conditional fluctuation intensity, i_p, to vary from a value of 1.35 on the plume centerline to 2.9 in the near fringes of the plume.

The model of constant i_p across the plume is not representative of the water channel data. However, as seen in Wilson (1982) the constant i_p assumption is representative of full scale elevated source data. The difference may be explained by the considerable more plume meandering in the atmosphere causing any variation of i_p across the plume to be flattened out. In fact, if the measured profiles of i_p in Figures (6.5) and (6.6) were allowed to be flapped back and forth a flatter profile would result. Judging from the case of the water channel, where there is virtually no plume meandering, to the case of the atmosphere, where there is considerable meandering, it appears that the amount of meandering determines the flatness of the i_p profile.

Using equation (4-21) the centerline value of intermittency can be written as

$$\gamma_o = \frac{1 + i_p^2}{1 + i_o^2}$$

Normally the above expression requires i_p to be the centerline value, but since i_p is assumed constant it can be directly substituted into equation (4-21) along with equation (6-3) to produce

$$\gamma = \frac{\gamma_0(1 + i_0^2)}{1 + i_0^2 \exp\left[A\left(\frac{y}{\delta_y}\right)^2\right]} \qquad (6\text{-}4)$$

where

γ = intermittency factor

γ_0 = centerline value of intermittency

i_0 = fluctuation intensity on centerline

δ_y = plume half width

$A = \ln(2)$

Using the values of i_0 above surface and at ground level, equation (6-4) is seen to model the channel's measurements reasonably well in Figures (6.7) and (6.8). The surface measurements in Figure (6.7) have a larger value of intermittency than the corresponding value at the same horizontal location above the surface in Figure (6.8). This is expected because the larger turbulence length scales above the surface are causing more plume meandering than the smaller scales at the surface.

The shape of intermittency profiles measured in the channel exhibit a dependence on downwind distance which equation (6-4) does not model. Also, we see in Figure (6.7),

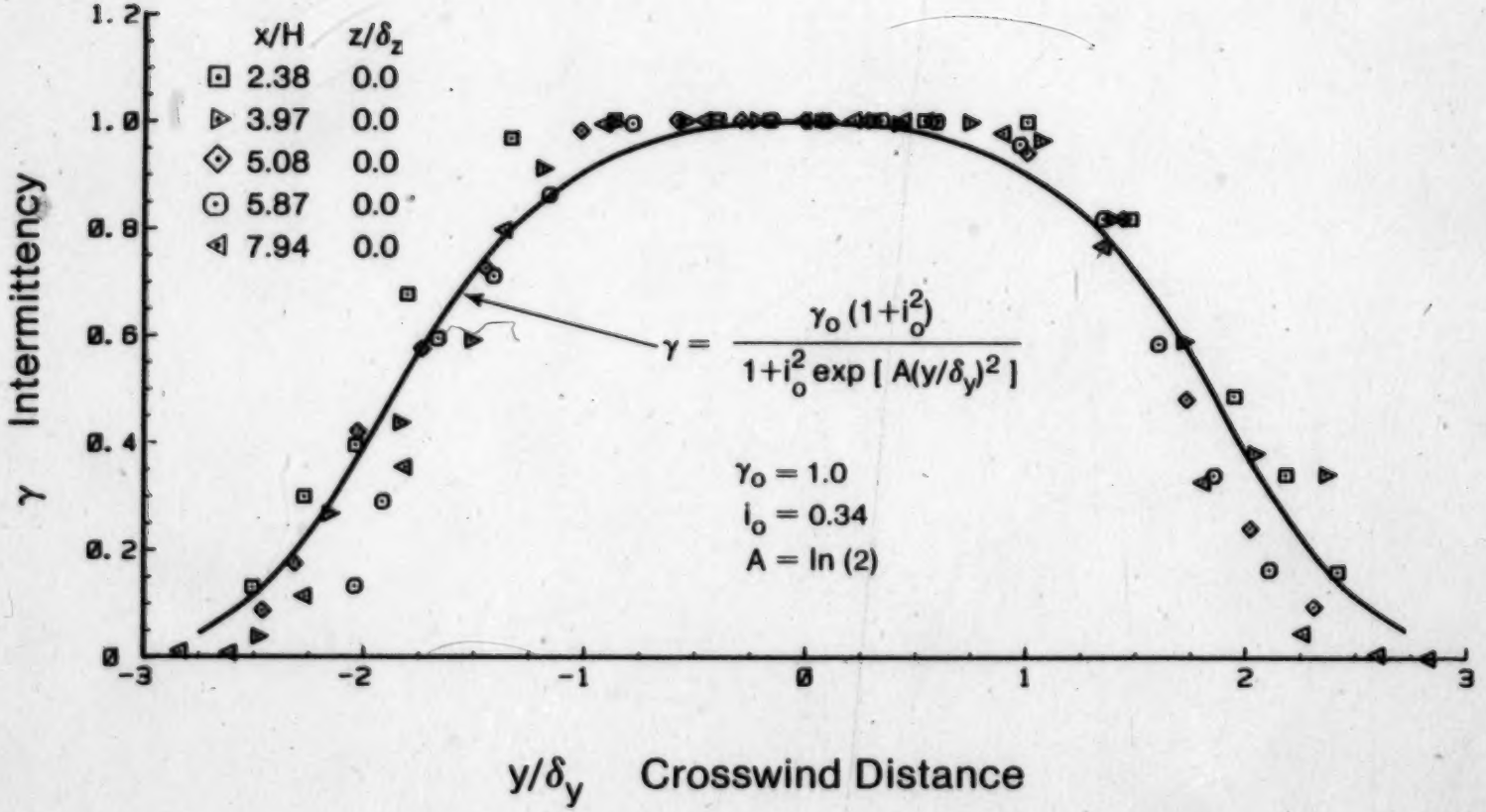

Figure 6.7 Crosswind intermittency measured at the ground surface compared to equation (6-4).

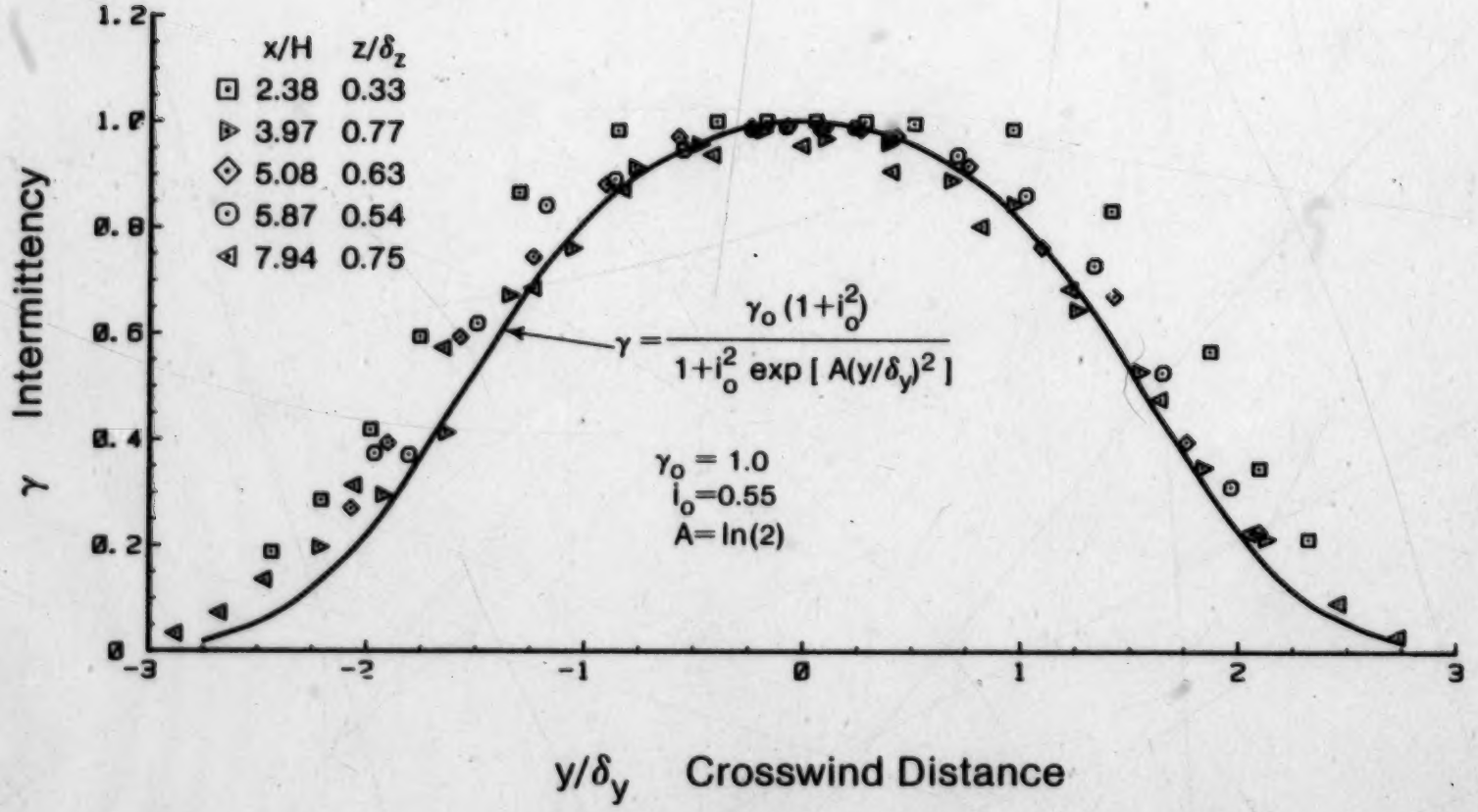

Figure 6.8 Crosswind intermittency measured above the ground compared to equation (6-4).

that equation (6-4) is not flat enough in the central region of the plume. It does fit the data at x/H=7.94 in Figure (6.8) reasonably well, but this is because the value of I_p at this location was indeed very nearly constant with y. The discrepancies that result between the other measured profiles and equation (6-4) are mainly due to the inability of the constant I_p assumption to model the actual phenomena. From a fundamental point of view the constant I_p assumption is inadequate but for practical applications, it is a satisfactory model.

6.4 Vertical Profiles of Concentration Fluctuation Statistics

Mathematical models for vertical fluctuation statistics become a little more complicated since the effect of the surface must be included. Wilson, Robins and Fackrell (1982) use the following relationship to model concentration variance, $\overline{c'^2}$, from a ground level source

$$\overline{c'^2} = \left(\frac{q}{b\, U_c \delta_y \delta_z} \right)^2 G\left(\frac{y}{\delta_y}\right) F\left(\frac{z}{\delta_z}\right) \qquad (6\text{-}5)$$

where

$$G\left(\frac{y}{\delta_y}\right) = \frac{1}{2} \exp\left[-A\left(\frac{y}{\delta_y} - \beta\right)^2\right] + \frac{1}{2} \exp\left[-A\left(\frac{y}{\delta_y} + \beta\right)^2\right]$$

$$F\left(\frac{z}{\delta_z}\right) = \exp\left[-A\left|\frac{z}{\delta_z} - \beta\right|^a\right] - \alpha \exp\left[-A\left(\frac{z}{\delta_z} + \beta\right)^a\right]$$

$$b = \frac{2\sqrt{\pi}\,\Gamma(\frac{1}{a})}{aA^{1/a + 1/2}}$$

q = combined strength of variance source pair

U_c = mean convection velocity

δ_y, δ_z = plume half widths

β = location of variance sources

α = sink strength

a = exponent in vertical mean concentraion profile

$A = \ln(2)$

This model is suited to the water channel since it is only applicable to rapid concentration fluctuations caused by turbulent mixing processes and does not include wind direction meandering effects. The model uses a pair of point variance sources located at $y=\pm\beta\delta_y$ and $z=\beta\delta_z$ where β is a constant expected to be in the range of 0.5-1.0. Wilson, Robins and Fackrell (1982) justify the use of point sources at the plume origin from the observation that most $\overline{c'^2}$ is produced near the source and its along wind distribution is dominated by diffusion and dissipation.

The reduction of variance near the surface is accounted for by an image sink with a strength of α. The physics of the model assumes that the distribution of $\overline{c'^2}$ is by diffusion alone and does not take into account any local effects of production.

A more useful form of equation (6-5) for applying to the water channel measurements is obtained by normalizing equation (6-5) by the maximum variance $\hat{c}^2$,

$$\frac{\overline{c'^2}}{\hat{c}^2} = \frac{\exp\left[-A\left|\frac{z}{\delta_z} - \beta\right|^a\right] - \alpha \exp\left[-A\left(\frac{z}{\delta_z} + \beta\right)^a\right]}{F_{max}} \qquad (6\text{-}6)$$

where

$\overline{c'^2}$ = concentration variance

$\hat{c}^2$ = maximum concentration variance

F_{max} = maximum value of $F(z/\delta_z)$ occuring at the location of $\hat{c}^2$

α = sink strength

β = location of variance sources

δ_z = vertical plume half width

a = power in vertical mean concentration profile

A = ln(2)

The value chosen for β was 0.6, the same value used by Wilson, Robins and Fackrell (1982). This is a physically realistic location for the variance sources since this is near the locations of maximum production, which occurs at y/δ_y=0.85 and for a=1.4, z/δ_z=0.53. Equation (6-6) is compared to the channel measurements in Figure (6.9) using values for α of 1.0, 0.6 and 0.0. Each experimental profile was normalized with a value which produced a "best fit" of the theoritical curve. The value of α=0 implies that any $\overline{c'^2}$

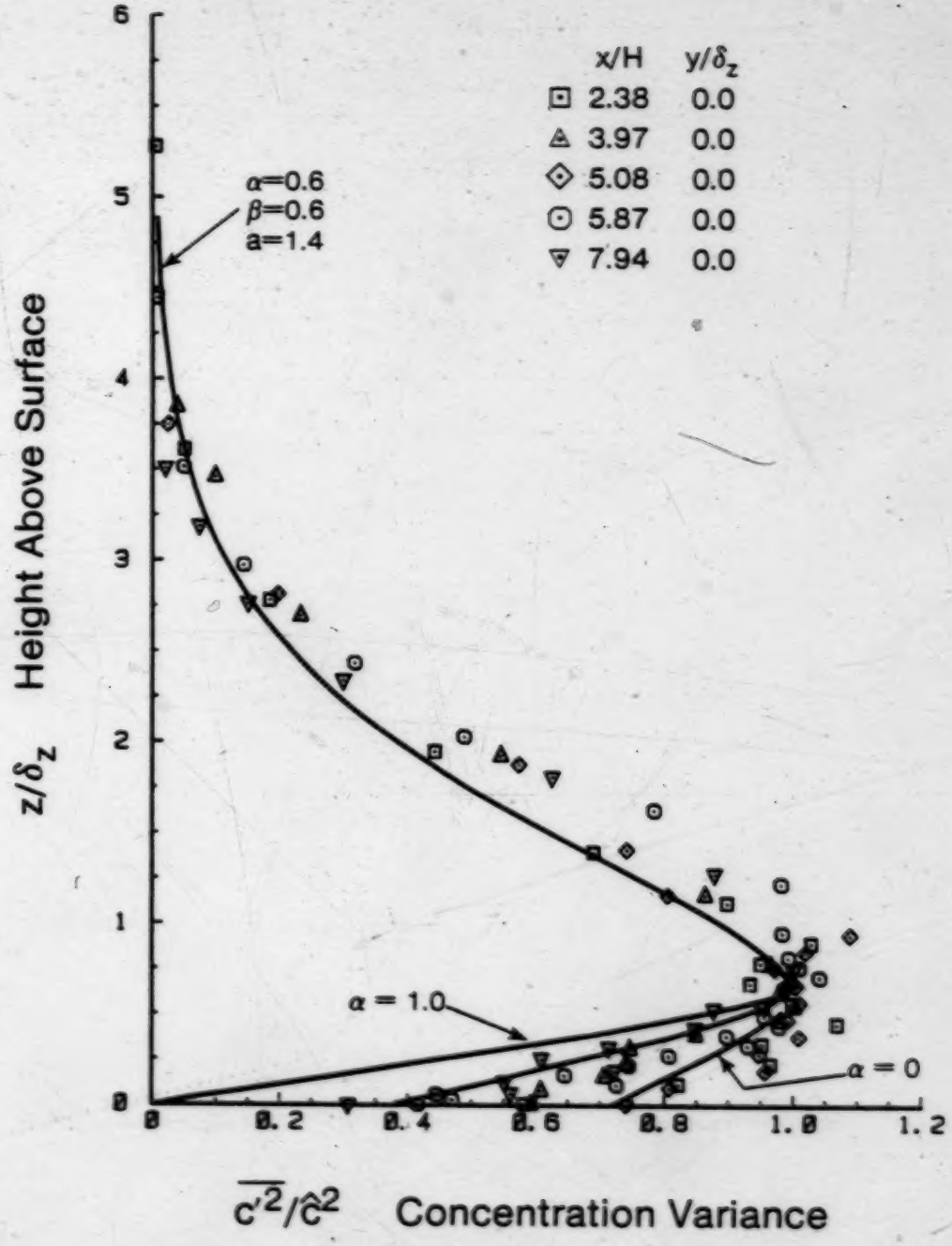

Figure 6.9 Vertical profiles of concentration variance measured at the water channel centerline compared to equation (6-6).

diffused to the surface is removed without affecting the fluctuations above the surface. A value of α=1.0 means total dissipation at the surface resulting in $\overline{c'^2}$=0 at the surface. A value of α=0.6 was used by Wilson, Robins and Fackrell (1982) which was the best fit to their wind tunnel data. The values of $\hat{c}^2$ used to normalize the water channel data were chosen to give the best fit to equation (6-6).

The water channel measurements in Figure (6.9) are subject to about ±15% to 20% scatter as discussed previously, but the general shape of the measured profiles is satisfactorily represented by equation (6-6). Surface measurements were taken at a height of approximately $5z_o$ and show that concentration fluctuations are still present. This seems to indicate that even at heights of $z=z_o$ there will still be fluctuations present.

The behaviour of the data near the surface is made clearer if an expanded vertical scale is used as shown in Figure (6.10). It is evident that, unlike equation (6-6), the measured concentration variance profiles from the channel are not self similar. There seems to be a trend for a larger reduction in $\overline{c'^2}$ near the surface as the downwind distance increases. This behaviour is likely due to local effects of variance production which the model does not take into account.

Models for vertical mean concentration and variance exist from equations (5-1) and (6-6) respectively. By dividing the square root of equation (6-6) by equation (5-1)

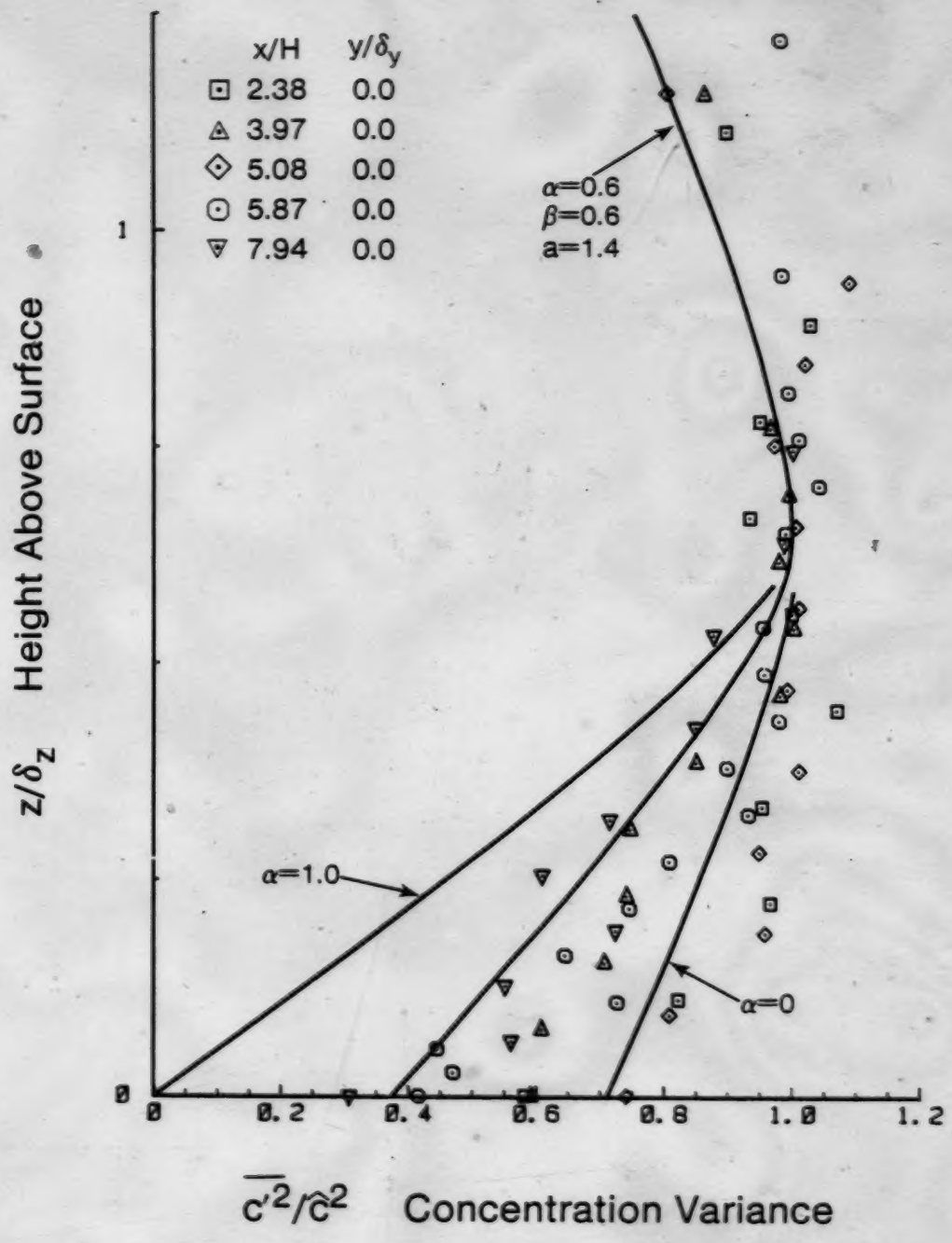

Figure 6.10 Vertical profiles of concentration variance near the ground surface on water channel centerline compared to equation (6-6).

the following expression for total fluctuation intensity, i, is obtained,

$$i = \frac{\frac{\hat{c}}{c_o}\sqrt{\exp\left[-A\left|\frac{z}{\delta_z} - \beta\right|^a\right] - \alpha \exp\left[-A\left(\frac{z}{\delta_z} + \beta\right)^a\right]}}{\sqrt{F_{max}}\ \exp\left[-A\left(\frac{z}{\delta_z}\right)^a\right]} \qquad (6\text{-}7)$$

where

$\hat{c}$ = square root of maximum concentration variance in vertical direction

c_o = mean concentration at surface

z = height above surface

β = location of variance sources

α = sink strength

δ_z = plume half width

F_{max} = value of $F(z/\delta_z)$ at location where $\hat{c}^2$ occurs

a = power in vertical mean concentration profile

A = $\ln(2)$

Using the experimentally measured values of $\hat{c}/c_o$ and β=0.6 equation (6-7) is plotted against the measurements from the water channel in Figure (6.11) with values of α=1.0,0.6 and 0.0. The curvature of equation (6-7) is proper near the surface but becomes too steep higher up in the plume. This effect is due to equation (5-1) predicting mean values smaller than the measured values at this height, see Figure (5.1). As in the case of the crosswind total fluctuation intensity, the vertical intensity is also not very sensitive

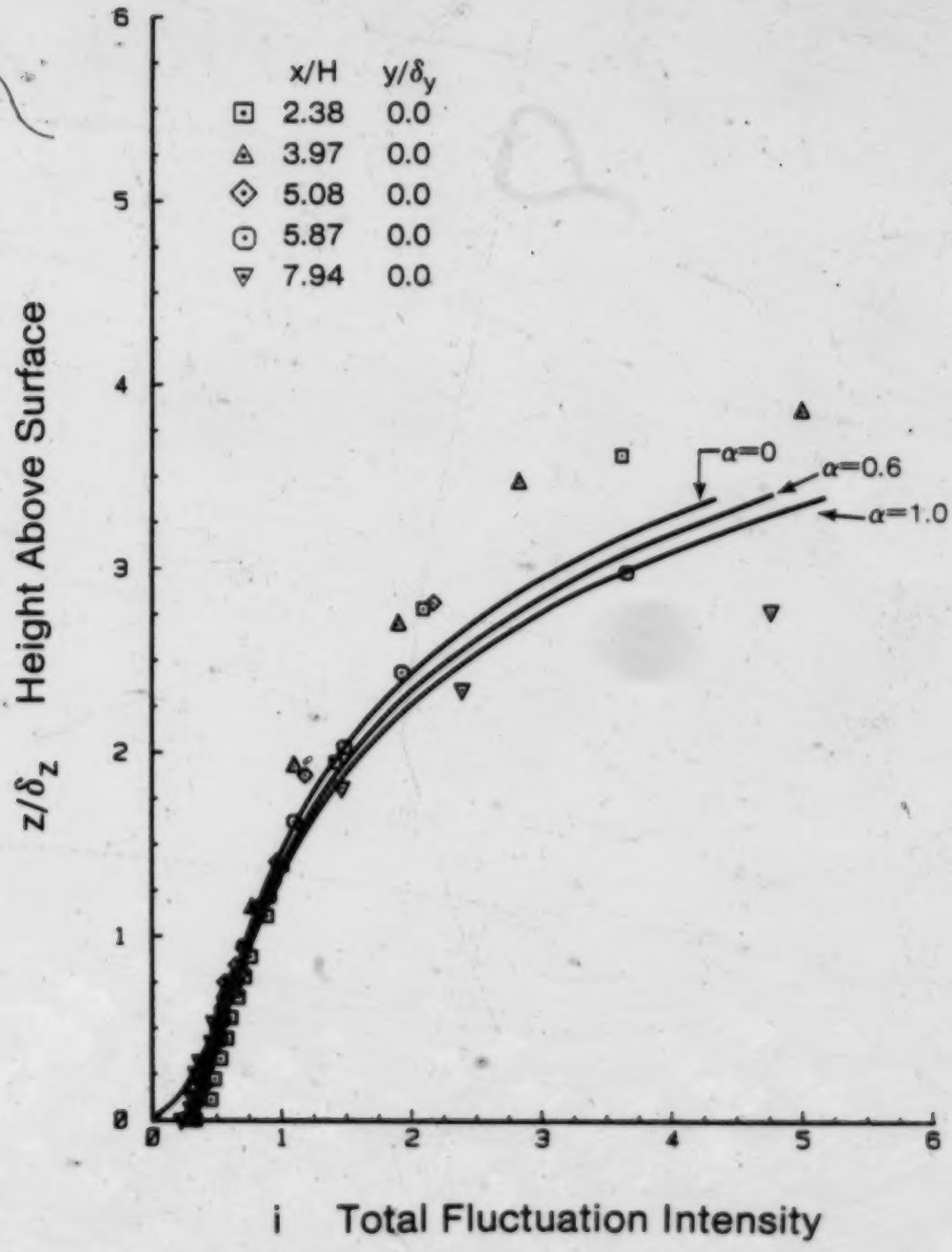

Figure 6.11 Vertical profiles of total concentration fluctuation intensity measured at the water channel centerline compared to equation (6-7).

to deviations in modeling the variance. Also, it is clear from Figure (6.11) that α=0.6 is the most representative value for the surface sink term.

The concentration integral length scale, Λ_c, as defined in equation (4-18) is a representative measure of the size of the large scale concentration eddies. Figure (6.12) shows a typical variation of the length scale in the vertical direction. The scale in the channel was evaluated by applying equations (4-19) and (4-20). Scatter in the data can be attributed to not using a long enough sample time to evaluation $E_{c,eff}(0)$ in equation (4-19).

As expected, the concentration scale increases as the surface is approached because small scale turbulence and velocity shear are acting to smear out small concentration eddies allowing only the large scale fluctuations to remain. In the upper portion of the boundary layer, outside the high velocity shear, the concentration scale levels out to a constant value. A gradual increase of scale with downwind distance, as the plume spread becomes larger, is evident from Figure (6.12) and Figures (E-2a,b,c,d) in Appendix E. In each of the vertical length scale profiles in Figures (6-12) and (E-2a,b,c,d) the scale has a maximum at about z/z_o=15 then decreases as the surface is approached. The data of Fackrell and Robins (1982) did not get close enough to the surface of their wind tunnel to observe this effect. It is not clear what is the reason for this observed phenomenon, and it would be desirable that an independent

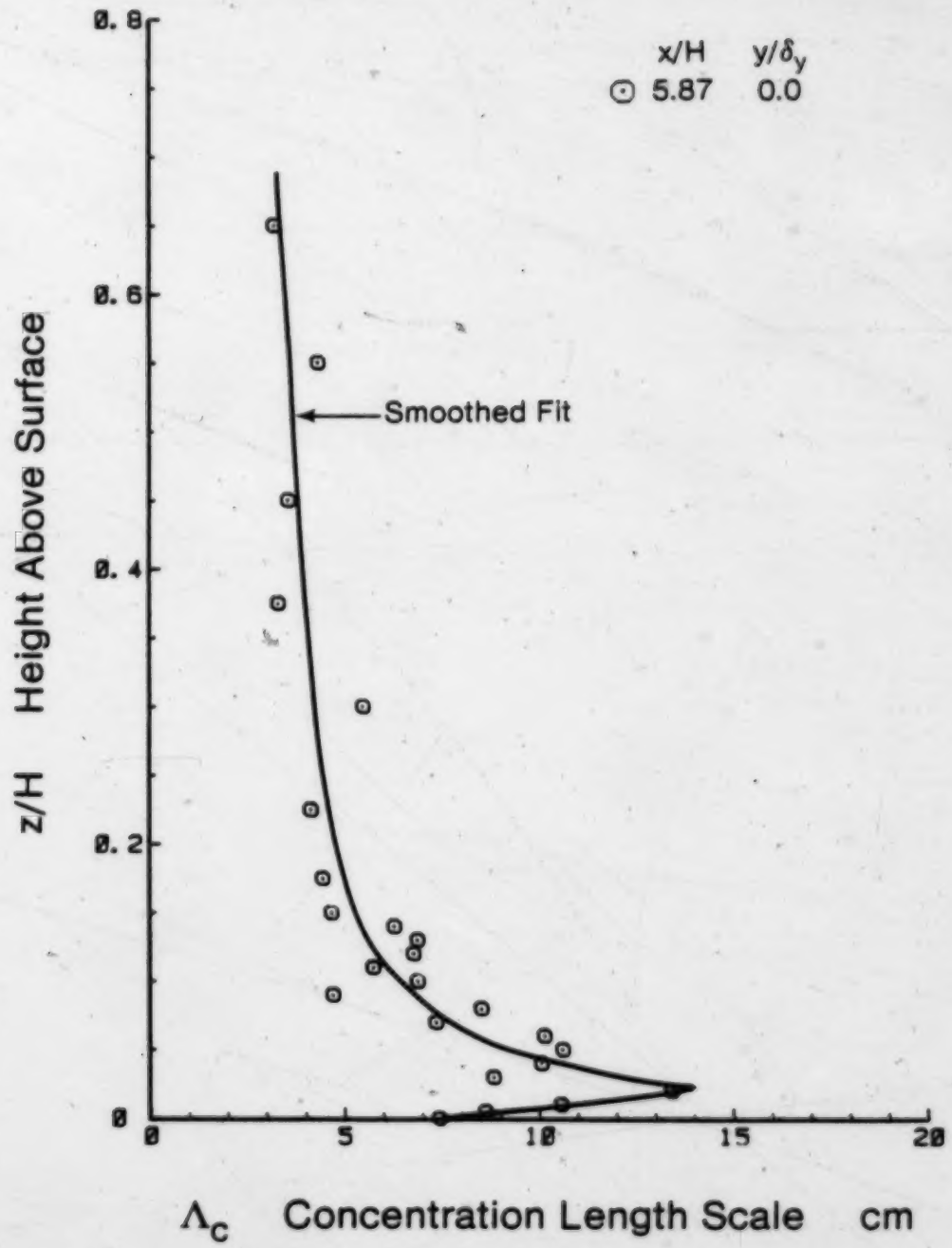

Figure 6.12 Vertical profile of concentration integral length scale measured at the water channel centerline.

set of measurements be made verifying its existence.

6.5 Deficiencies in Modeling Vertical Profiles of Conditional Fluctuation Intensity and Intermittency

From the previous section a model for i was obtained. To model intermittency it is also necessary to model the conditional fluctuation intensity i_p. This can be done by using Wilson's (1982) assumption that the small scale turbulence near the ground plane has the same relative effect on the conditional intensity i_p as it does on the total intensity i, so that

$$\frac{i_p}{i_{p\infty}} = \frac{i}{i_\infty} \tag{6-8}$$

where the subscript "∞" refers to the intensity at the same location but with the ground plane removed. Using this assumption the following expression for i_p is derived in Appendix E

$$\frac{i_p}{i_{p\infty}} = \frac{\sqrt{1 - \alpha \exp\left[A\left|\frac{z}{\delta_z} - \beta\right|^a - A\left(\frac{z}{\delta_z} + \beta\right)^a\right]}}{2} \tag{6-9}$$

where

$$i_{p\infty} = \frac{2\left(\frac{\hat{c}}{c_0}\right)\sqrt{\exp(-A\beta^a)}}{\sqrt{F_{max}}}$$

i_p = conditional fluctuation intensity

$i_{p\infty}$ = conditional fluctuation intensity at same location with effect of surface removed

α = sink strength

β = location of variance sources

z = height above surface

δ_z = plume half width

$\hat{c}$ = square root of maximum concentration variance in vertical direction

c_o = mean concentration at surface

F_{max} = maximum value of $F(z/\delta_z)$ at location where $\hat{c}$ occurs

a = power in vertical mean concentration profile

$A = \ln(2)$

The expression derived for $i_{p\infty}$ is only valid when the intermittency at the surface is 1.0. The expression is valid in this case because the intermittency was always 1.0 at z=0. Finally, using equations (6-9) and (6-7) in equation (4-21) a model for intermittency can be obtained. Equation (6-9) is compared to the measured values of i_p in the water channel in Figure (6.13) and the resulting model for intermittency, γ, is compared to measurements in Figure (6.14). The functional form of equation (6-9) is seriously deficient in modeling the actual variation of i_p in Figure (6.13). As a result, the model for intermittency in Figure (6.14) also is in poor agreement with measurements.

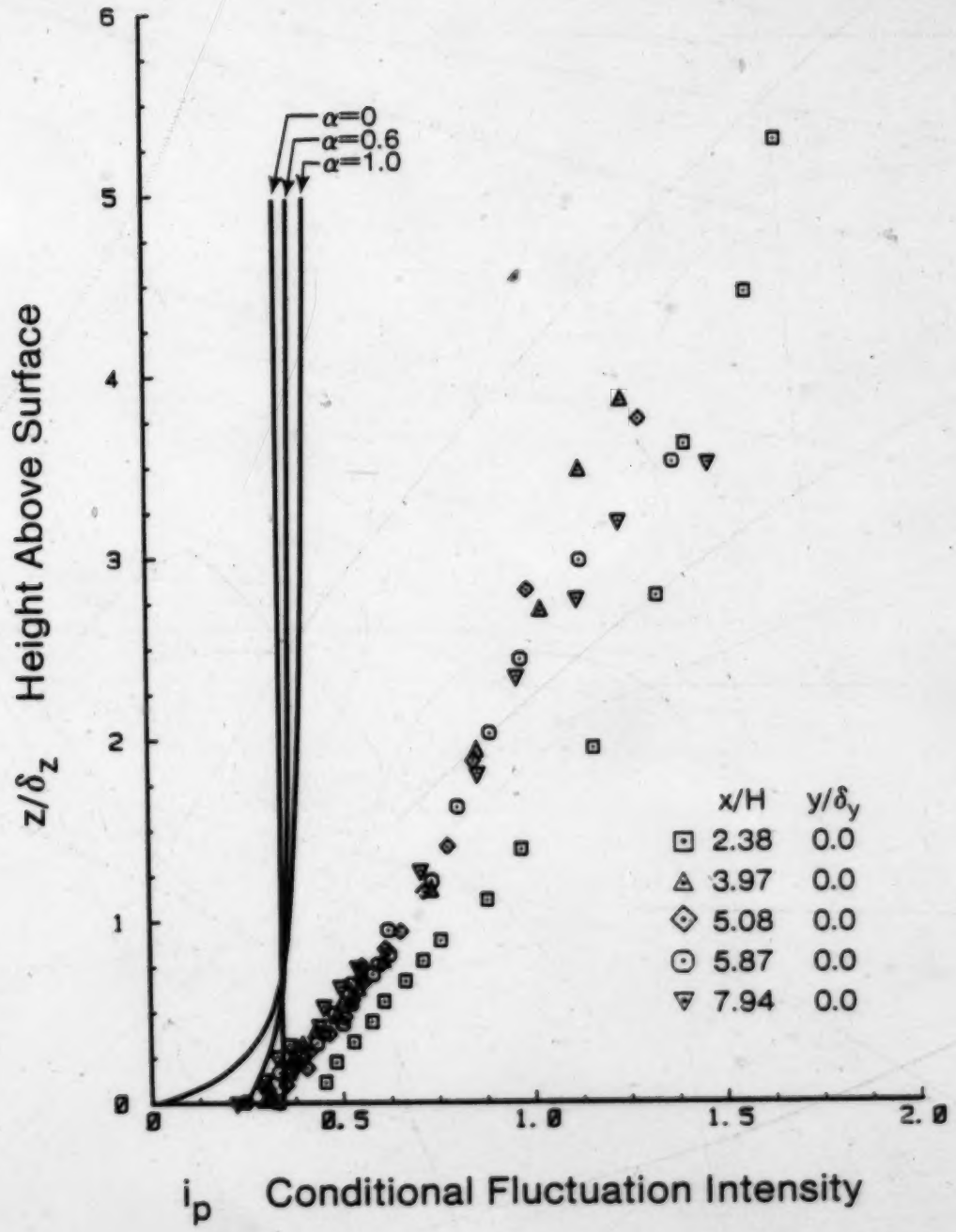

Figure 6.13 Vertical profiles of conditional fluctuation intensity measured at the water channel centerline compared to equation (6-9).

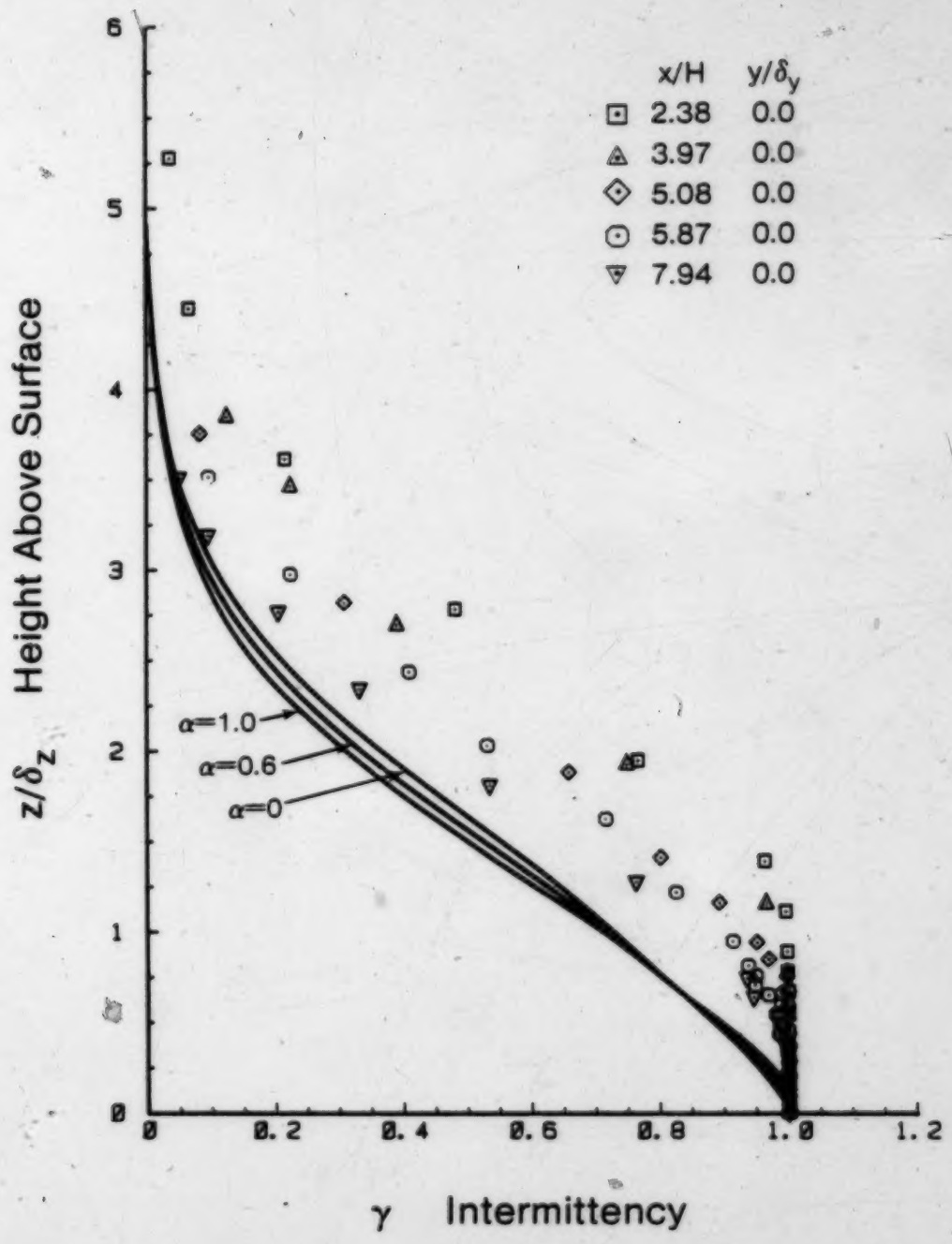

Figure 6.14 Vertical profiles of concentration intermittency measured at the water channel centerline compared to equation (4-21) with equations (6-7) and (6-9) used to model I and I_D.

There are two major deficencies in the model for conditional fluctuation intensity, i_p. The first problem with equation (6-9) is that when z is large the predicted ratio $i_p/i_{p\infty}$ tends to a value of 0.5. However, far from the surface one would expect that the value of i_p should not be affected by the presence or absence of the surface and should in fact tend to $i_p/i_{p\infty}=1.0$. The problem arises when modeling the concentration variance with and without surface effects. Removing surface effects eliminates the variance sink at the surface as well as the reflection of mass. However, in equation (6-5) there is no term that takes into account a reflection of mass back into the boundary layer. The problem in equation (6-9) arises because the mean concentration equation accounts for the change of mass when the surface is removed but equation (6-5) for the variance does not.

The second problem with the model is the assumption that $i_{p\infty}$ is a constant. It is obvious from Figure (6.13) that far from the surface (i.e. $3z/\delta_z$) i_p is not tending to a constant value but is still monotonically increasing. Looking back to Figure (6.6) the same effect is seen in the crosswind direction where i_p is still increasing monotonically at 3 half widths from the plume centerline. As seen in Wilson (1982) the constant i_p assumption works reasonably well for an elevated source. However, for a ground level source there is a strong shear layer and considerably less plume meandering so the assumption of

constant i_p is not realistic.

6.6 Summary

One of the objectives of this chapter was to examine the concentration fluctuation measurements made in the channel to determine if the experimental data produced a reasonable simulation. All the channel's measurements behaved as expected indicating that the turbulence simulation in the water channel was correct.

A second objective was to test Wilson's (1982) model for conditional statistics against a more detailed data set than was previously available. The functional forms of the equations that were fit to the data were satisfactory in modeling the measurements for all cases except the vertical conditional intensity and intermittency.

It should be emphasized that even though most of the models work in the water channel their use in the full scale atmosphere is limited. Wind direction changes with time occurring in the atmosphere are not accounted for in the fluctuation models. The models and the water channel data can only be applied to represent short times in the atmosphere when wind direction changes can be neglected.

7. CONCLUSIONS AND RECOMMENDATIONS

The major objective of this study was to set up a water channel system that was capable of modeling concentration fluctuations from a ground level source. Once the system had been set up to simulate the atmospheric wind it was desired to measure both mean and fluctuating concentrations to verify the model.

The flow field created in the water channel as described in Chapters 2 and 3 was a very good simulation of a unidirectional neutrally stable atmospheric flow. The major advantage of the water channel compared to a wind tunnel simulation is that the free water surface produces a fully developed flow that does not change with downwind distance. The mean and fluctuating concentration field described in Chapters 5 and 6, showed that the mixing processes in the water channel were correct simulations of a fully developed shear layer, thus verifying the channel's ability to model concentration fluctuations.

The ability of the water channel to model the full scale atmosphere is limited by the the inability of the channel to simulate large scale crosswind motions caused by wind direction changes. However, the mathematical models that apply to the water channel are valid for short sampling times in the atmosphere when wind direction changes with time can be neglected. Most toxic gas risk calculations are for accidential releases which last a short time, so the water channel model for the fluctuations are quite useful.

As was seen in Chapter 6, the only deficiency in Wilson's (1982) theory was in the predicted values of the vertical variation of conditional concentration variance and intermittency. Improvements for these models as pointed out in Chapter 6 require more details of spatial variations to be considered when theoretically modeling the variance in the vertical direction.

Improvements in the measurement techniques and instrumentation used in this study can be made. The technique used to calculate velocity length scale was prone to produce scatter in the data as seen in Figure (3.2). A larger sampling interval, on the order of 500 to 1000 seconds, should be used to reduce the variability in the estimates of the zero frequency intercept, $E_u(0)$. The concentration measurements made in the channel could use a larger sampling time to reduce the scatter in the variance and length scale measurements. A sample time of 122.88 seconds was used, but a time of about 500 seconds would be more appropriate to obtain steady values. The conductivity probe used in this study did a satisfactory job but a faster response probe would reduce the error in the variance measurements and better define the short intermittent periods when the concentration decreases to zero. A very valuable technique was developed in this study to allow probe response to be tested, and this should make it possible to optimize a probe design for faster time response. The method used to calculate intermittency could

be improved by using an adjustable voltage threshold level so that it is certain that small concentrations peaks in the fringes of the plume are not below the threshold value.

References

Brigham, E. O. *The Fast Fourier Transform*, Prentice-Hall, Inc., Englewood Cliffs, New Jersey, 1974

Counihan, J. "Adiabatic Atmospheric Boundary Layers: A Review and Analysis of Data from the Period 1880-1972", Atmospheric Environment, Vol. 9, pp. 871-905, 1975

Csanady G. T. *Turbulent Diffusion in the Environment*, D. Reidel Publishing Company, Boston, 1973

Eidsvik, K. J. "Estimates of Concentration Fluctuations in an Instantaneous Plume", Atmospheric Environment, Vol. 14, pp. 1365-1369, 1980

Fackrell, J. E. and Robins, A. G. "The Effects of Source Size on Concentration Fluctuations in Plumes", Boundary Layer Meteorology, Vol. 22, pp. 335-350, 1981

Fackrell, J. E. and Robins, A. G. "Concentration Fluctuations and Fluxes in Plumes from Point Sources in a Turbulent Boundary Layer", Journal of Fluid Mechanics, Vol. 117, pp. 1-26, 1982

Gaster, M. and Roberts, J. B. "The Spectral Analysis of Randomly Sampled Records by a Direct Transform", Proceedings of the Royal Society of London A, Vol. 354, pp. 27-58, 1977

Gibson, C. H. and Schwarz, W. H. "Detection of Conductivity Fluctuations in a Turbulent Flow Field", Journal of Fluid Mechanics, Vol. 16, pp. 357-364, 1963

Hanna, S. R. "Concentration Fluctuations in a Smoke Plume", Atmospheric Environment, Vol. 18, No. 6, pp. 1091-1106, 1984

Hinze, J. O. *Turbulence*, 2nd edition, McGraw-Hill, New York, 1975

Myers, G. E. *Analytical Methods in Conduction Heat Transfer*, McGraw-Hill, New York, 1971

Netterville, D. D. J. "Concentration Fluctuations in Plumes", Environmental Research Monograph 1979-4, Syncrude Canada Ltd., 10030-107 Street, Edmonton, Alberta, Canada T5J3E5

Pasquill, F. and Smith, F. B. *Atmospheric Diffusion*, 3rd edition, Ellis Horwood Ltd., John Wiley and Sons, New York, 1983

Robins, A. G. "Plume Dispersion from Ground Level Sources in Simulated Atmospheric Boundary Layers", Atmospheric Environment, Vol. 12, pp. 1033-1044, 1978

Schlichting, H. *Boundary Layer Theory*, 7th edition, McGraw-Hill, New York, 1979

Smith, R. J. *Circuits Devices and Systems*, 3rd edition, John Wiley and Sons, New York, 1976

Tennekes, H. and Lumley, J. L. *A First Course in Turbulence*, MIT Press, Cambridge, Massachusetts, 1972

Thomson, W. T. *Theory of Vibration with Applications*, 2nd edition, Prentice-Hall, Englewood Cliffs, New Jersey, 1981

United States Atomic Energy Commission, "Meteorology and Atomic Energy 1968", USAEC Division of Technical Information Extension, Oak Ridge, Tennessee, 1968

Wilson, D. J. "Wind Tunnel Simulation of Plume Dispersion at Syncrude Mildred Lake Site", Environmental Research Monograph 1979-1, Syncrude Canada Ltd., 10030-107 Street, Edmonton, Alberta, Canada T5J3E5

Wilson, D. J., Robins, A. G. and Fackrell, J. E., "Predicting the Spatial Distribution of Concentration Fluctuations from a Ground Level Source", Atmospheric Environment, Vol. 16, No. 3, pp. 497-504, 1982

Wilson D. J. "Predicting Risk of Exposure to Peak Concentrations in Fluctuating Plumes", Alberta Environment Technical Report, December 1982, 90 pp.

Wilson D. J. and Simms, B. W. "Exposure Time Effects on Concentration Fluctuations in Plumes", Alberta Environment Technical Report, 1985

APPENDIX A: LDV System and Data Analysis Procedure

A LDV measures particle velocities at the intersection of two laser beams which are crossed in the flow to producce interference fringes. Discrete samples of the flow velocity are obtained only when particles pass, randomly in time, through the sample volume at the beam intersection. As a particle passes through the sample volume it scatters light which is collected and focused into a photomultiplier. The frequency or doppler shift in the scattered light is directly proportional to the velocity of the particle. The signal from the photomultiplier is then fed to a signal processor which determines the velocity of the particle from the doppler shift.

The LDV system used in this study was a one-component helium-neon system used in backscatter mode with a 50mW laser source. The signal from the photo multiplier was processed by a T.S.I. model 1090 tracker processor. The tracker processor produces an analog voltage output directly proportional to velocity each time a valid sample is verified from particles crossing the sample volume. However, in the interval between the time that the latest valid reading was taken until the time that a new sample is verified the voltage output of the tracker processor remains at the same value of the latest valid sample. This is a result of the sample and hold circuitry used in the tracker processor. Figure (A.1) gives a graphic illustration of how the output of the tracker can compare to the true velocity

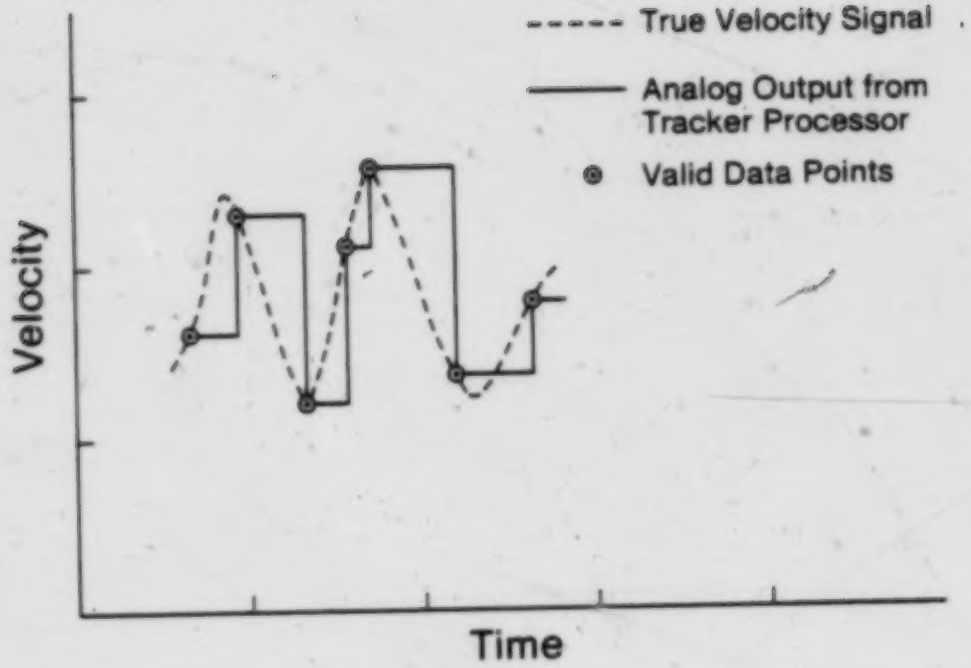

Figure A.1 Comparison of true velocity signal to indicated tracker processor output.

signal. This type of output from the tracker usually results when there is a low number of samples being verified. The number of samples that qualify as "verified" is related to the number of particles in the flow plus, to a greater extent, the intensity of scattered light that returns from the sample volume. The intensity of light that the photomultiplier receieves depends on the amount of energy that the laser optics can concentrate at the beam crossing, plus the medium and distance through which the scattered light must return. In measuring the water channel velocity at the centerline, there was 35cm of water from the centerline to the channel sidewall that the scattered light had to travel through. This combined with the fact that a 50mW low power laser was being used meant that the number of verified samples were often low. The number of samples were not low enough to cause loss of frequency information but it was low enough to cause the effect illustrated in Figure (A.1).

The analog output signal of the tracker processor, illustrated in Figure (A.1), could be averaged using a D.C. voltmeter to give the correct mean velocity. However, because the shape of the signal is quite distorted from the true velocity signal, RMS velocities and power spectrum analysis on the analog tracker output often give erroneous results. Due to this inherent shortcoming of the tracker processor, it is for the most part ineffective for measuring turbulence quantities. The tracker processor used in this

study was used for measuring the RMS velocities and frequency spectra by utilizing the sync pulse output of the tracker. A voltage pulse appears at the sync terminal every time a valid data point is processed. Feeding this pulse into the Schmidt trigger of a Digital LSI 11/23 minicomputer, the A/D was triggered to sample the analog output of the tracker. A schematic of this is shown in Figure (A.2) Sampling the tracker output like this resulted in a discrete set of samples of the true velocity signal. The RMS of the signal could then be calculated by a standard algorithm. The power spectrum of the signal was also calculated using a standard FFT algorithm. The only problem that arises with the FFT is that it requires equally spaced time intervals of the sampled data which a LDV does not provide. However, as pointed out by Gaster and Roberts (1976), an FFT can be used on the randomly sampled data points of the LDV to give a reliable estimate of the true spectrum provided the sample rate is sufficient.

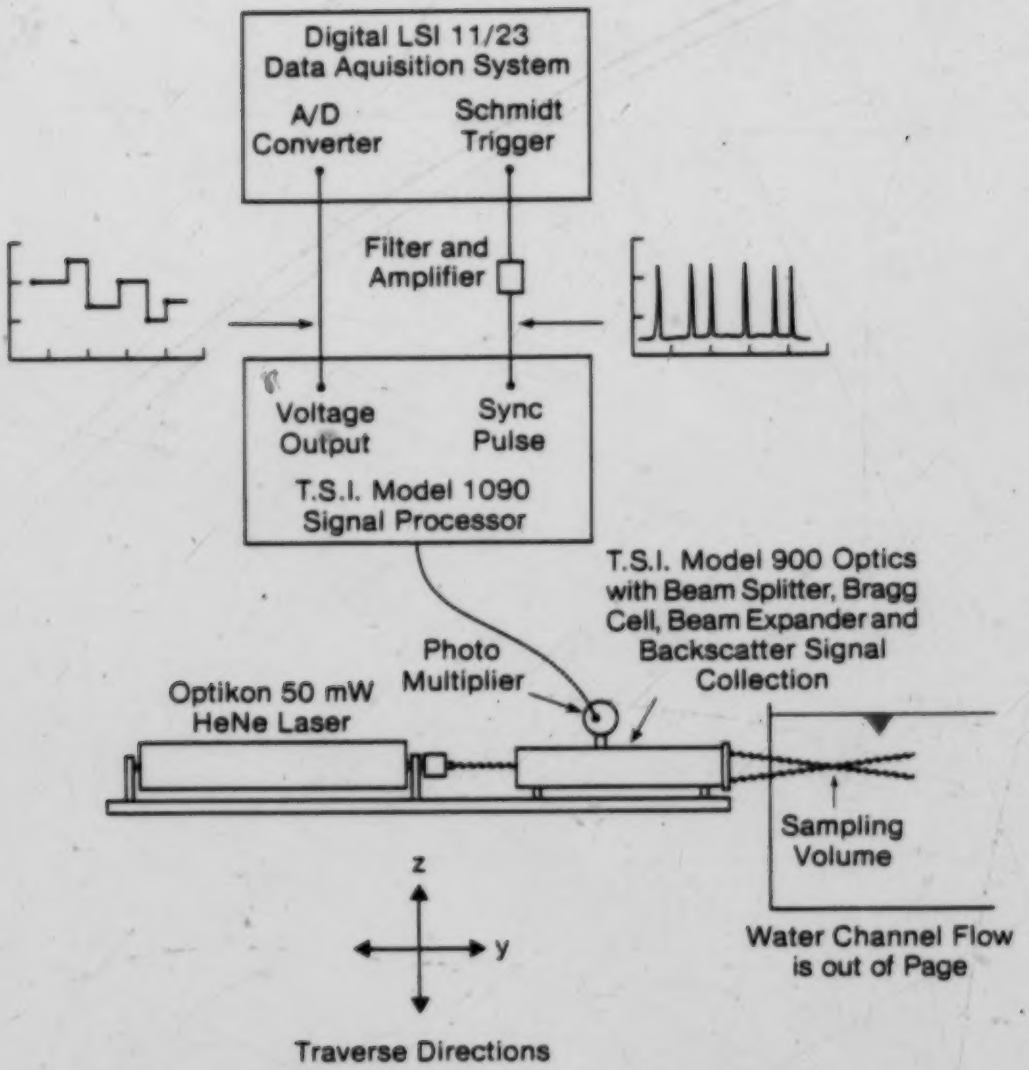

Figure A.2 Schematic of LDV system used for measuring velocities in water channel.

APPENDIX B: Measuring Water Velocity with a Pressure Transducer Operating With Air

The pitot-static system used to measure mean velocities incorporated a pressure transducer operating with air to measure the dynamic head of the water channel flow. The transducer was operated with air to eliminate the possibility of overpressuring, and the need to bleed the transducer. Also, operating with air instead of water avoids corrosion and increases the service life of the transducer.

A Validyne DP-45 pressure transducer with 0-2.5cm water ΔP range was operated with air by using a cell which isolated the water filled lines of the pitot tube from the transducer. Figure (B.1) shows a schematic of the isolation cell incorporated into the system. The cell consisted of a plexiglass block with two 3/4" diameter holes bored through it. The lines of the pitot tube were filled with deaerated water and attached to the bottom of the bored holes. The height of the block was adjusted relative to the free surface in the water channel to create the air-water interface near the top of the cell. This action minimized the volume of air in the system. With no flow past the pitot tube, the equalization valve was opened to equalize the pressure in both bores thus allowing the transducer to be zeroed. With the equalization valve closed a flow past the pitot tube creates a pressure difference between the two air volumes in the bores which was measured by the transducer. Due to the compressibility of the air in the system, the

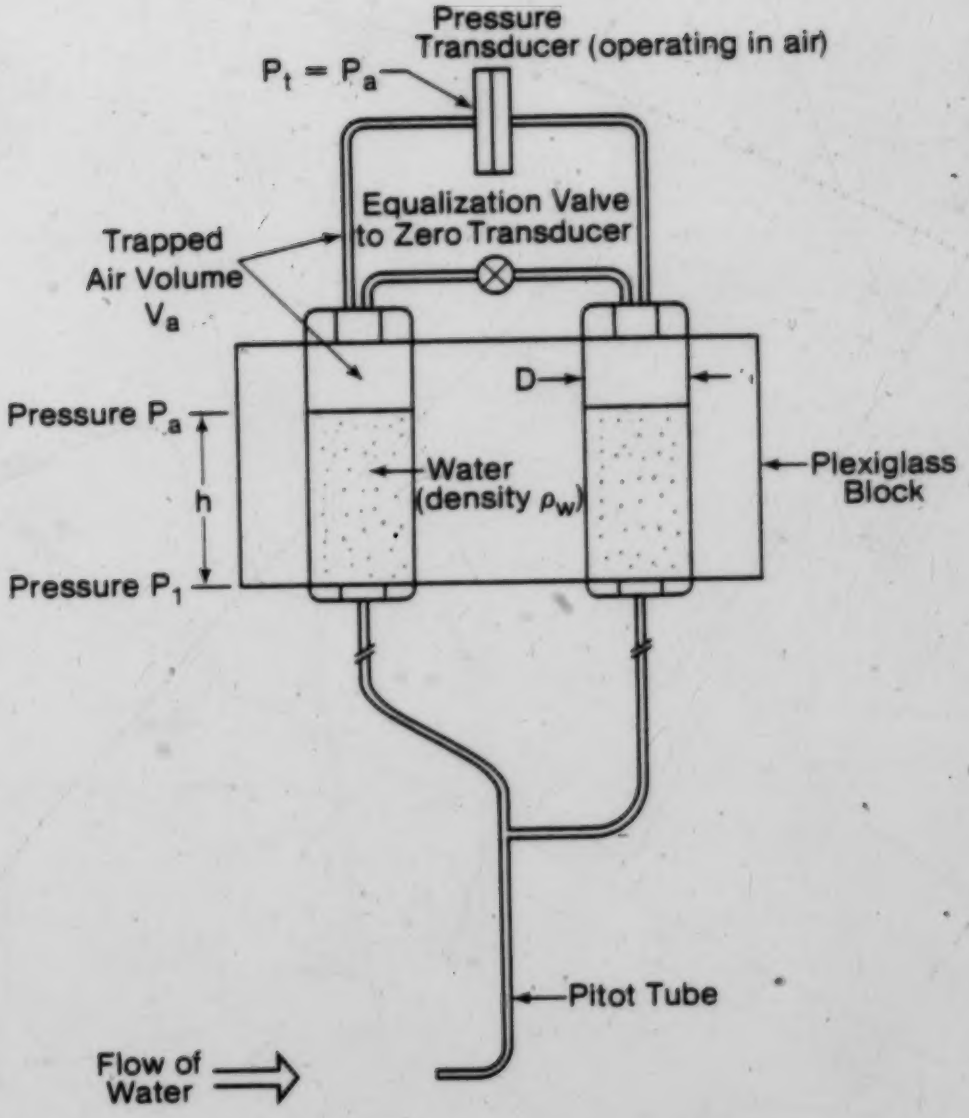

Figure B.1 Schematic of pitot tube system with isolation cell.

pressure difference measured by the transducer was not the true pressure difference caused by the dynamic head of the flow. Therefore, a correction is required to obtain the pressure difference occuring at the pitot tube.

A correction for the pressure difference measured by the transducer can be derived using the nomenclature in Figure (B.1). The use of a differential pressure transducer allows the pressure variation through the columns of trapped air to be neglected resulting in the pressure at the transducer, P_1, to be the uniform air pressure, P_a. Using hydrostatics, the pressure, P_1, can be expressed as

$$P_1 = P_a + \rho_\omega gh \qquad \text{(B-1)}$$

If P_1, is increased by ΔP_1 to $P_1+\Delta P_1$ then the water column rises by Δh to $h+\Delta h$ and P_a increases to $P_a+\Delta P_a$ Again, using hydrostatics

$$P_1 + \Delta P_1 = P_a + \Delta P_a + \rho_\omega g\,(h + \Delta h) \qquad \text{(B-2)}$$

If (B-1) is subtracted from (B-2), an expression for ΔP_1 is obtained

$$\Delta P_l = \Delta P_a + \rho_\omega g \, \Delta h \qquad \text{(B-3)}$$

The constant mass, m_a, of air in the system is compressed isothermally, so by assuming the ideal gas law for the volume of air, V_a

$$P_a V_a = m_a R T_a$$

it is seen that $P_a V_a$ is a constant. This implies that

$$d(P_a V_a) = 0$$

$$P_a dV_a + V_a dP_a = 0$$

or for small changes

$$\Delta P_a = \frac{-P_a \Delta V_a}{V_a} \qquad \text{(B-4)}$$

With a bored hole of diameter, D, the volume change ΔV_a is simply

$$\Delta V_a = \frac{\pi D^2}{4} \Delta h \qquad \text{(B-5)}$$

Substituting (B-5) into (B-4) results in

$$\Delta h = \frac{-4\ \Delta P_a\ V_a}{\pi\ D^2\ P_a} \qquad \text{(B-6)}$$

Finally, substituting (B-6) back into (B-3), the fractional error in ΔP_a can be expressed as

$$\frac{\Delta P_a - \Delta P_1}{\Delta P_a} = \frac{4\ g\ \rho_\omega\ V_a}{\pi\ D^2\ P_a} \qquad \text{(B-7)}$$

ΔP_a is the pressure difference measured by the transducer and ΔP_1 is the true pressure difference. It is seen that by having D as large as possible and the volume of air, V_a, in the system as small as possible, the error can be minimized.

APPENDIX C: Evaluation of Integral for the Ratio of Effective to True Variance

The ratio of the effective variance, (i.e. measured variance), to the true variance is given by

$$\frac{\overline{c'^2_{eff}}}{\overline{c'^2}} = \int_0^\infty \left[\frac{1}{1 + (2\pi f\tau)^2}\right]\left[\frac{4\,T_c}{1 + (2\pi f T_c)^2}\right] df \qquad (C\text{-}1)$$

Defining

$$a = \frac{1}{2\,\pi\,\tau} \qquad (C\text{-}2)$$

$$b = \frac{1}{2\,\pi\,T_c} \qquad (C\text{-}3)$$

And removing constants from the integrand, equation (C-1) can be written as

$$\frac{\overline{c'^2_{eff}}}{\overline{c'^2}} = 4\,T_c\,a^2b^2\int_0^\infty \frac{df}{(a^2 + f^2)(b^2 + f^2)} \qquad (C\text{-}4)$$

The key to solving the integral in equation (C-4) is to break the integral into two parts by using partial fractions

$$\frac{1}{(a^2 + f^2)(b^2 + f^2)} = \frac{A}{a^2 + f^2} + \frac{B}{b^2 + f^2} \qquad (C\text{-}5)$$

From equation (C-5) we obtain

$$Ab^2 + Af^2 + Ba^2 + Bf^2 = 1$$

Rearranging

$$(Ab^2 + Ba^2) + (A + B)f^2 = 1$$

To satisfy the above relation requires that

$$(A + B) = 0$$

and

$$(Ab^2 + Ba^2) = 1$$

The solution for A and B is

$$A = \frac{1}{b^2 - a^2}$$

$$B = \frac{1}{a^2 - b^2}$$

Equation (C-4) now becomes

$$\frac{\overline{c'^2}_{eff}}{\overline{c'^2}} = \frac{4\,T_c\,a^2b^2}{b^2 - a^2}\int_0^\infty \frac{df}{a^2 + f^2} + \frac{4\,T_c\,a^2b^2}{a^2 - b^2}\int_0^\infty \frac{df}{b^2 + f^2} \qquad (C\text{-}6)$$

The first integral in equation (C-6) can be solved by letting

$$f = a\tan\theta$$

This results in

$$\int_0^\infty \frac{df}{a^2 + f^2} = \int_0^{\pi/2} \frac{\sec^2\theta\, d\theta}{a(1+\tan^2\theta)} = \frac{\pi}{2a}$$

Similarily, the solution to the second integral in (C-6) is

$$\int_0^\infty \frac{df}{b^2 + f^2} = \frac{\pi}{2b}$$

Substituing this back into equation (C-6) results in

$$\frac{\overline{c'^2}_{eff}}{\overline{c'^2}} = 2\,\pi\,T_c a^2b^2\left[\frac{1}{a(b^2 - a^2)} + \frac{1}{b(a^2 - b^2)}\right]$$

Using a common denominator

$$\frac{\overline{c'^2}_{eff}}{\overline{c'^2}} = 2\,\pi\,T_c a^2b^2\left[\frac{(b - a)(a^2 - b^2)}{ab(a + b)(a - b)(a^2 - b^2)}\right]$$

$$= 2\pi T_c a^2 b^2 \left[\frac{1}{ab(a+b)}\right]$$

From the definition in (C-3), $2\pi T_c = 1/b$, so the equation reduces to

$$\frac{\overline{c'^2}_{eff}}{\overline{c'^2}} = \frac{a}{a+b}$$

or

$$\overline{c'^2} = \left[1 + \frac{b}{a}\right] \overline{c'^2}_{eff}$$

Substituting the definition from (C-2) and (C-3) results in the final expression

$$\overline{c'^2} = \left[1 + \frac{\tau}{T_c}\right] \overline{c'^2}_{eff} \qquad \text{(C-7)}$$

APPENDIX D: Measurements of Concentration Fluctuation Statistics at Various Downwind Distances

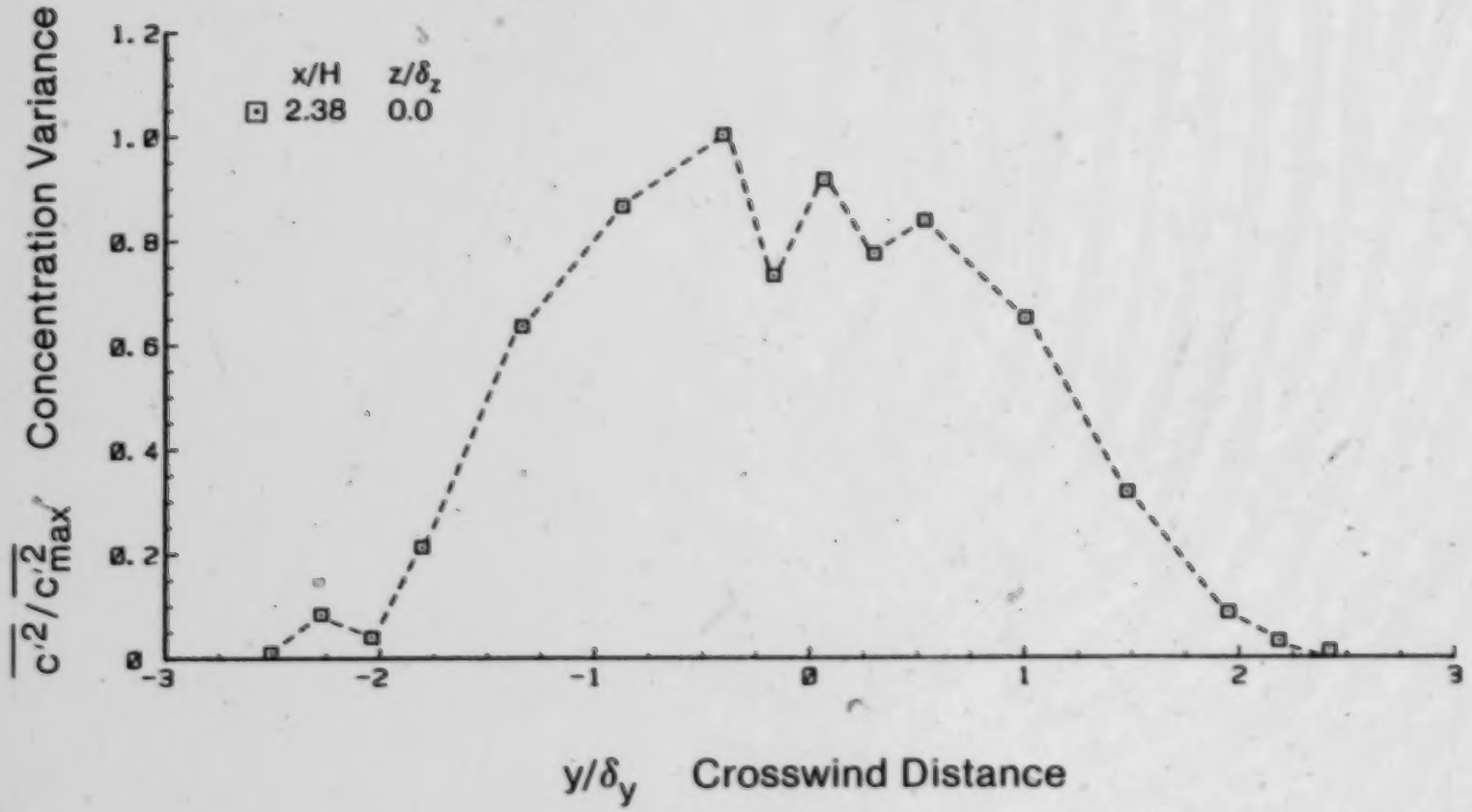

Figure E.1a Crosswind concentration variance profile measured at the ground surface at a downwind distance of x/H=2.38.

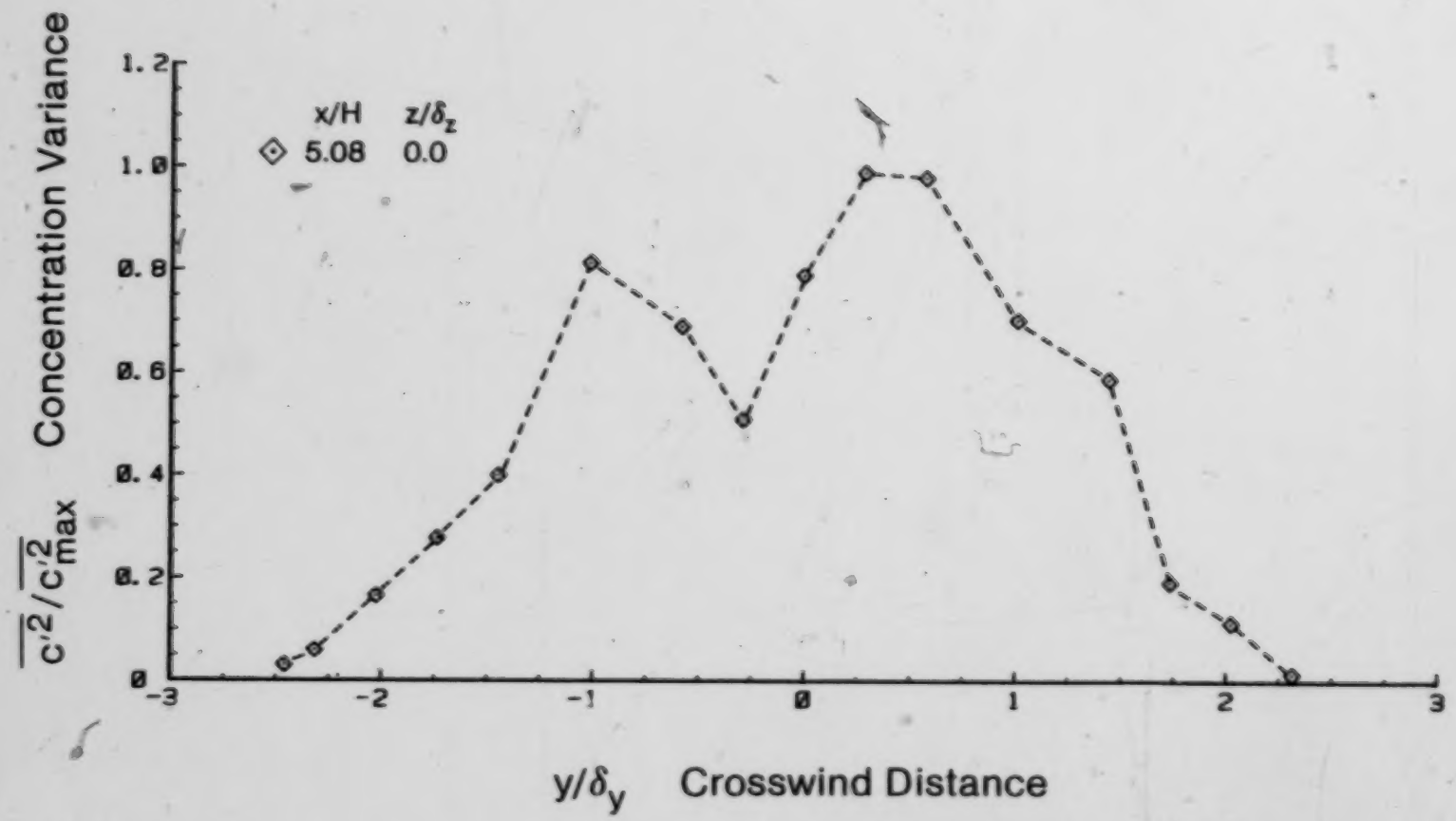

Figure E.1b Crosswind concentration variance profile measured at the ground surface at a downwind distance of x/H=5.08.

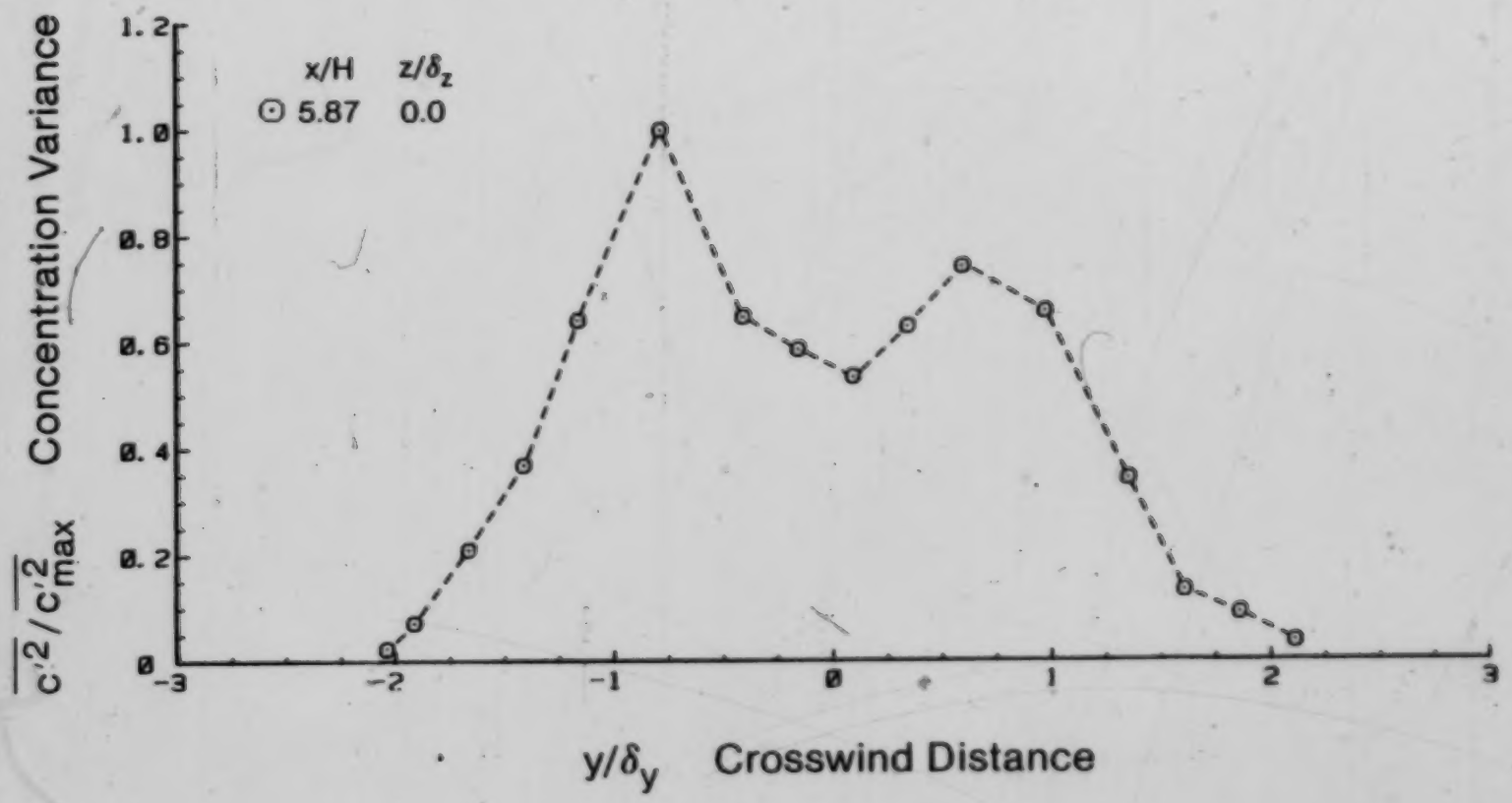

Figure E.1c Crosswind concentration variance profile measured at the ground surface at a downwind distance of x/H=5.87.

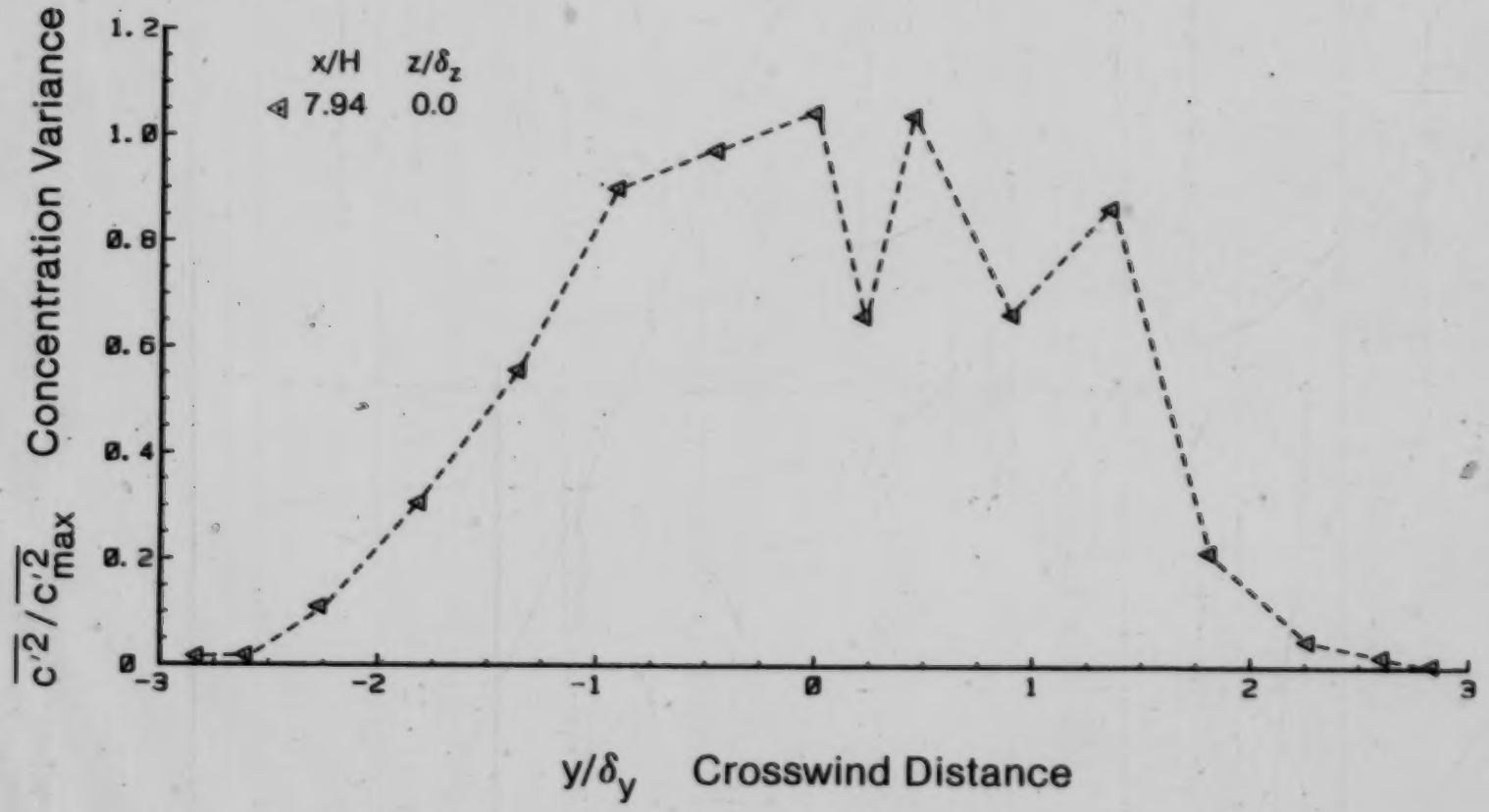

Figure E.1d Crosswind concentration variance profile measured at the ground surface at a downwind distance of x/H=7.94.

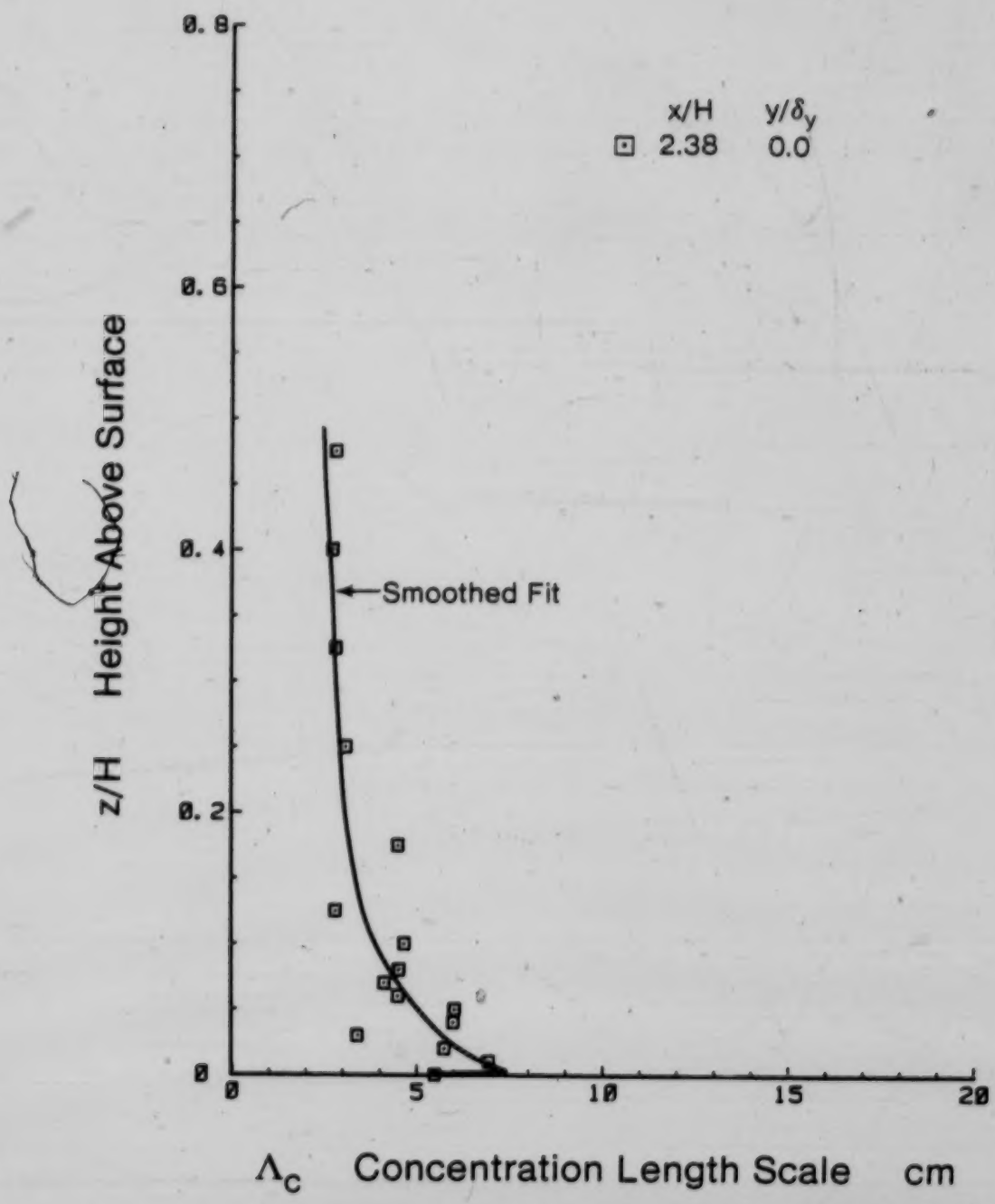

Figure E.2a Vertical profile of concentration integral length scale measured at the water channel centerline.

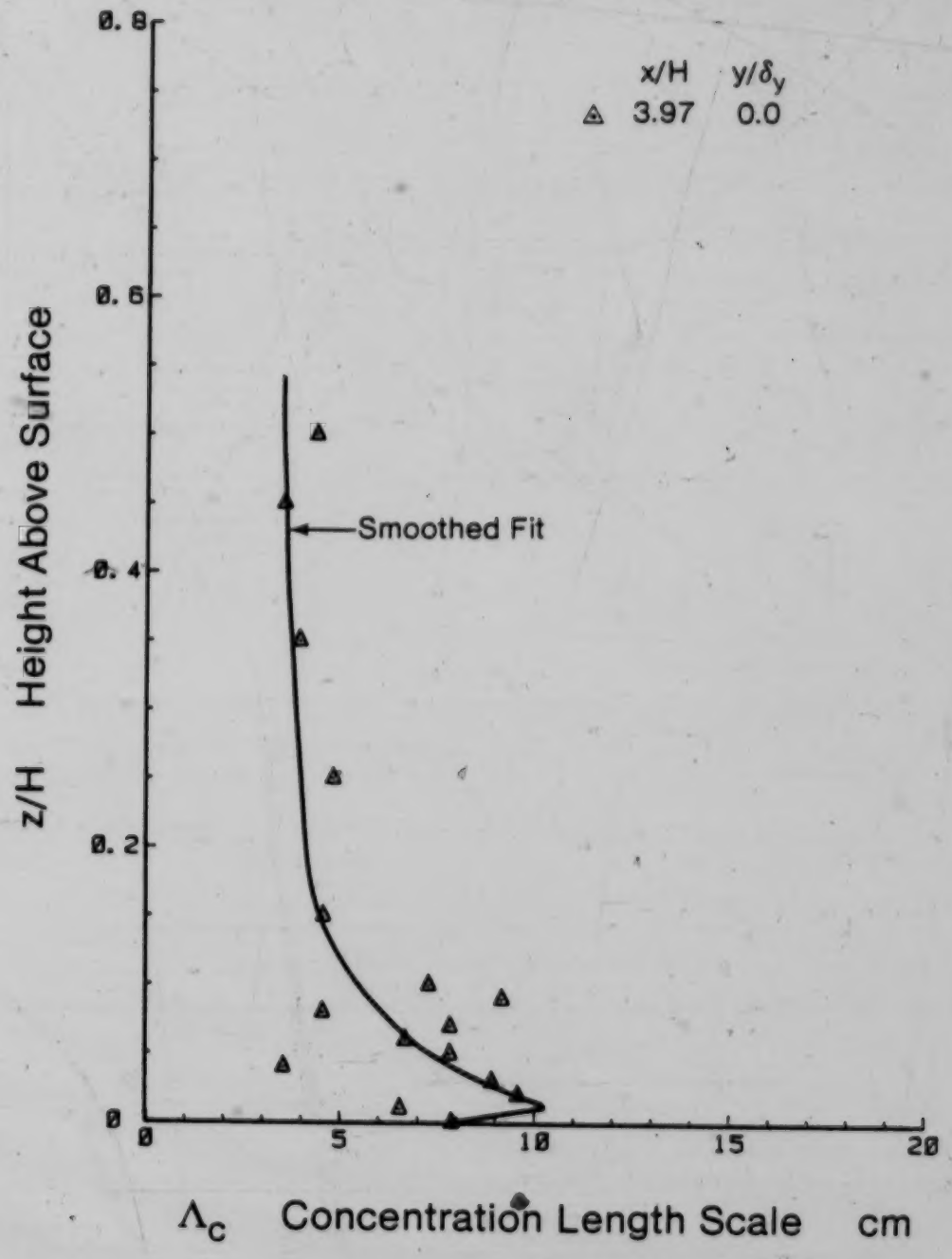

Figure E.2b Vertical profile of concentration integral length scale measured at the water channel centerline.

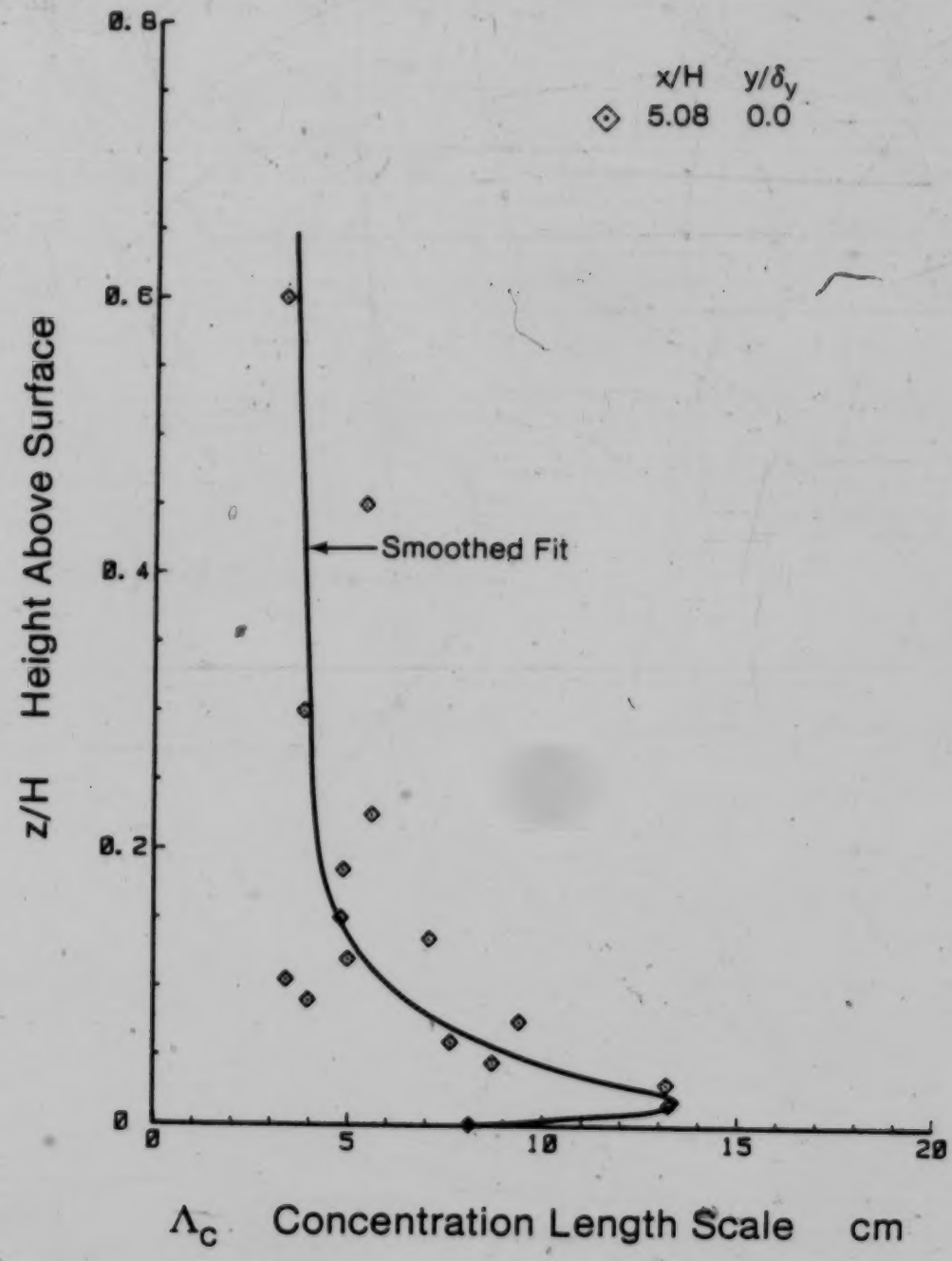

Figure E.2c Vertical profile of concentration integral length scale measured at the water channel centerline.

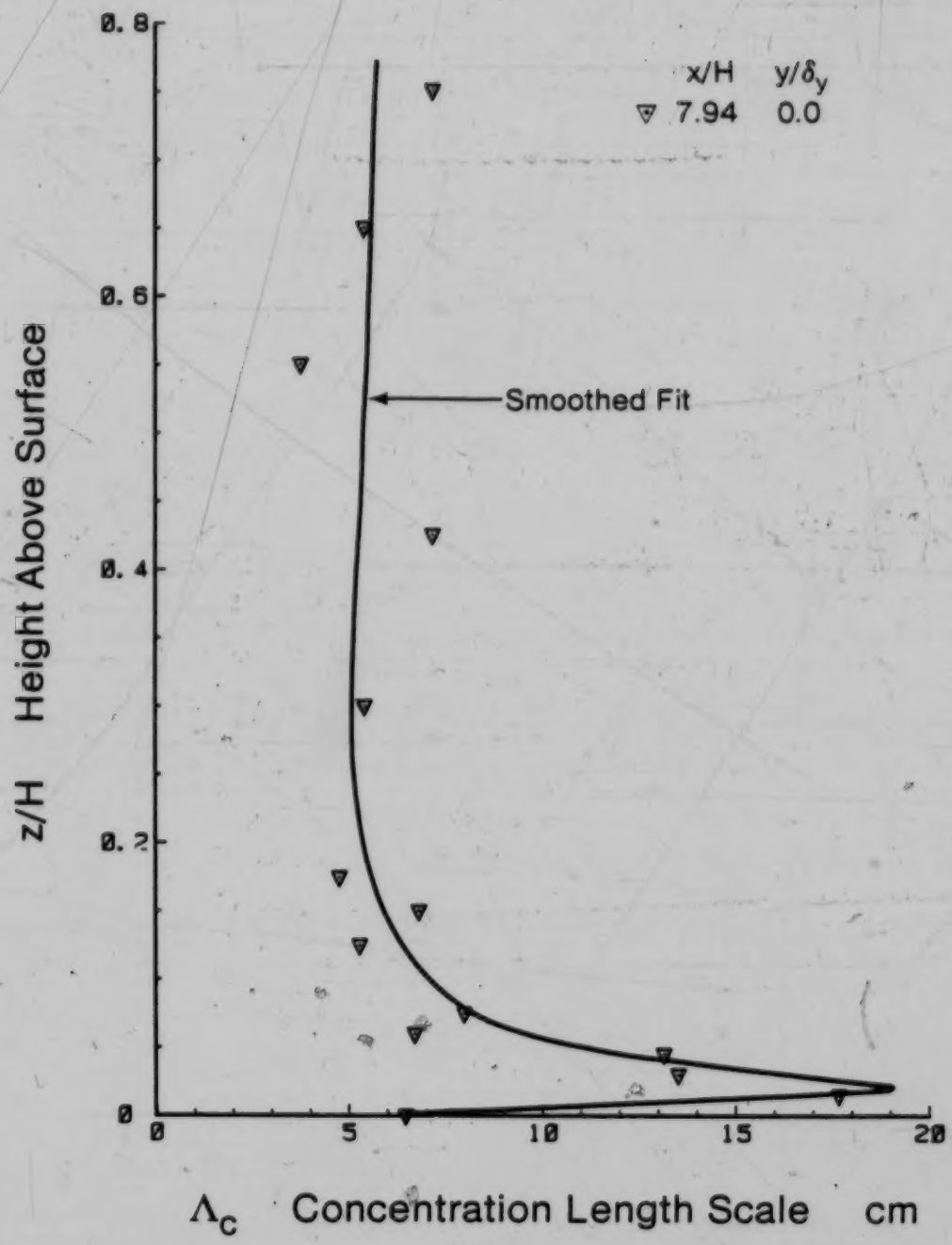

Figure E.2d Vertical profile of concentration integral length scale measured at the water channel centerline.

APPENDIX E: Derivation of an Expression for Conditional Fluctuation Intensity in Vertical Direction

An expression for the vertical variation if i_p can be derived using Wilson's (1982) assumption of

$$\frac{i_p}{i_{p\infty}} = \frac{i}{i_\infty} \qquad \text{(E-1)}$$

The vertical variation of i/i_∞ can be determined by using equation (6-5) for $\overline{c'^2}$ and the following equation for the mean concentration, c, from Wilson, Robins and Fackrell (1982)

$$c = \frac{2Q}{b\, U_c \delta_y \delta_z} \exp\left[-A\left(\frac{y}{\delta_y}\right)^2\right] \exp\left[-A\left(\frac{z}{\delta_z}\right)^a\right] \qquad \text{(E-2)}$$

where

$$b = \frac{2\sqrt{\pi}\,\Gamma\left(\frac{1}{a}\right)}{aA^{1/a + 1/2}}$$

c = mean concentration

Q = emission rate

U_c = mean convection velocity

δ_y, δ_z = plume half widths

z = height above surface

y = crosswind distance

A = ln(2)

The term 2Q is a result of complete reflection for a ground level source. Taking equation (6-5) and dividing by equation (E-2) squared, results in the following expression for i^2,

$$i^2 = \left(\frac{q}{Q}\right)^2 \frac{G\left(\frac{y}{\delta_y}\right) F\left(\frac{z}{\delta_z}\right)}{4 \exp\left[-2A\left(\frac{z}{\delta_z}\right)^a\right]} \qquad \text{(E-3)}$$

The expression for i_∞ is obtained by removing the effect of the ground surface in equations (6-5) and (E-2). The ground surface effect for the mean, c, in equation (E-2) is removed by changing 2Q to Q which in effect removes the complete reflection of mass. The effect of the ground surface is removed in equation (6-5) for $\overline{c'^2}$ by leaving out the sink term in $F(z/\delta_z)$. With ground effects removed i_∞^2 becomes,

$$i_\infty^2 = \left(\frac{q}{Q}\right)^2 \frac{G\left(\frac{y}{\delta_y}\right) \exp\left[-A\left|\frac{z}{\delta_z} - \beta\right|^a\right]}{\exp\left[-2A\left(\frac{z}{\delta_z}\right)^a\right]} \qquad \text{(E-4)}$$

An expression can now be obtained for $i_p/i_{p\infty}$ by taking the square root of equation (E-3) divided by the square root of equation (E-4) resulting in,

$$\frac{i_p}{i_{p\infty}} = \frac{\sqrt{1 - \alpha \exp\left[A\left|\frac{z}{\delta_z} - \beta\right|^a - A\left(\frac{z}{\delta_z} + \beta\right)^a\right]}}{2} \qquad \text{(E-5)}$$

Inserting z=0 into equation (E-5) results in

$$\frac{i_{p,z=0}}{i_{p\infty,z=0}} = \frac{(1 - \alpha)}{2} \qquad \text{(E-6)}$$

In the water channel the intermittency was always 1.0 at the surface, therefore $i_{p,z=0} = i_{z=0}$. Using this relationship in equation (6-7) results in an expression for $i_{p,z=0}$

$$i_{p,z=0} = \frac{\frac{\hat{c}}{c_0}\sqrt{(1 - \alpha)\exp(-A\beta^2)}}{\sqrt{F_{max}}} \qquad \text{(E-7)}$$

Using Wilson's (1982) theory, $i_{p\infty}$ is assumed to be constant across a plume cross section, therefore it is possible to insert equation (E-7) into equation into equation (E-6) to obtain

$$i_{p\infty} = \frac{2\left(\frac{\hat{c}}{c_0}\right)\sqrt{\exp(-A\beta^2)}}{\sqrt{F_{max}}} \qquad \text{(E-8)}$$

Equations (E-5) and (E-8) now make up the model for the vertical variation of i_p in the water channel when the intermittency is 1.0 at the surface.